

DOI: 10.31891/2079-1372

THE INTERNATIONAL SCIENTIFIC JOURNAL

***PROBLEMS
OF
TRIBOLOGY***

Volume 29

No 4/114-2024

МІЖНАРОДНИЙ НАУКОВИЙ ЖУРНАЛ

ПРОБЛЕМИ ТРИБОЛОГІЇ

PROBLEMS OF TRIBOLOGY

INTERNATIONAL SCIENTIFIC JOURNAL

Published since 1996, four time a year

Volume 29 No 4/114-2024

Establishers:

Khmelnyskyi National University (Ukraine)
Lublin University of Technology (Poland)

Associated establisher:

Vytautas Magnus University (Lithuania)

Editors:

O. Dykha (Ukraine, Khmelnytskyi), **M. Pashechko** (Poland, Lublin), **J. Padgurskas** (Lithuania, Kaunas)

Editorial board:

V. Aulin (Ukraine, Kropivnitskiy),
B. Bhushan (USA, Ohio),
V. Voitov (Ukraine, Kharkiv),
Hong Liang (USA, Texas),
E. Ciulli (Italy, Pisa),
V. Dvoruk (Ukraine, Kiev),
M. Dzimko (Slovakia, Zilina),
M. Dmitrichenko (Ukraine, Kiev),
L. Dobzhansky (Poland, Gliwice),
G. Kalda (Ukraine, Khmelnytskyi),
T. Kalaczynski (Poland, Bydgoszcz),
M. Kindrachuk (Ukraine, Kiev),
Jeng-Haur Horng (Taiwan),
L. Klimenko (Ukraine, Mykolaiv),
K. Lenik (Poland, Lublin),

O. Mikosianchyk (Ukraine, Kiev),
R. Mnatsakanov (Ukraine, Kiev),
J. Musial (Poland, Bydgoszcz),
V. Oleksandrenko (Ukraine, Khmelnytskyi),
M. Opielak (Poland, Lublin),
G. Purcek (Turkey, Karadeniz),
V. Popov (Germany, Berlin),
V. Savulyak (Ukraine, Vinnytsya),
A. Segall (USA, Vancouver),
M. Stechyshyn (Ukraine, Khmelnytskyi),
M. Chernets (Poland, Lublin),
V. Shevelya (Ukraine, Khmelnytskyi),
Zhang Hao (China, Peking),
M. Śniadkowski (Poland, Lublin),
D. Wójcicka-Migasiuk (Poland, Lublin)

Executive secretary: O. Dytyniuk

Editorial board address:

International scientific journal "Problems of Tribology",
Khmelnyskyi National University,
Instytutska str. 11, Khmelnytskyi, 29016, Ukraine
phone +380975546925

Indexed: CrossRef, DOAJ, Ulrichsweb, ASCI, Google Scholar, Index Copernicus

E-mail: tribology@khmnu.edu.ua

Internet: <http://tribology.khnu.km.ua>

ПРОБЛЕМИ ТРИБОЛОГІЇ

МІЖНАРОДНИЙ НАУКОВИЙ ЖУРНАЛ

Видається з 1996 р.

Виходить 4 рази на рік

Том 29

№ 4/114-2024

Співзасновники:

Хмельницький національний університет (Україна)
Університет Люблінська Політехніка (Польща)

Асоційований співзасновник:

Університет Вітовта Великого (Литва)

Редактори:

О. Диха (Хмельницький, Україна), М. Пашечко (Люблін, Польща),
Ю. Падгурскас (Каунас, Литва)

Редакційна колегія:

В. Аулін (Україна, Кропивницький),
Б. Бхушан (США, Огайо),
В. Войтов (Україна, Харків),
Хонг Лян (США, Техас),
Е. Чіуллі (Італія, Піза),
В. Дворук (Україна, Київ),
М. Дзимко (Словакія, Жиліна)
М. Дмитриченко (Україна, Київ),
Л. Добжанський (Польща, Глівіце),
Г. Калда (Україна, Хмельницький),
Т. Калачинські (Польща, Бидгощ),
М. Кіндрачук (Україна, Київ),
Дженг-Хаур Хорнг (Тайвань),
Л. Клименко (Україна, Миколаїв),
К. Ленік (Польща, Люблін),

О. Микосянчик (Україна, Київ),
Р. Мнацаканов (Україна, Київ),
Я. Мушял (Польща, Бидгощ),
В. Олександренко (Україна, Хмельницький),
М. Опеляк (Польща, Люблін),
Г. Парсек (Турція, Караденіз),
В. Попов (Германія, Берлін),
В. Савуляк (Україна, Вінниця),
А. Сігал (США, Ванкувер),
М. Стечишин (Україна, Хмельницький),
М. Чернець (Польща, Люблін),
В. Шевеля (Україна, Хмельницький)
Чжан Хао (Китай, Пекин),
М. Шнядковський (Польща, Люблін),
Д. Войцицька-Мігасюк (Польща, Люблін),

Відповідальний секретар: О.П. Дитинюк

Адреса редакції:

Україна, 29016, м. Хмельницький, вул. Інститутська 11, к. 4-401
Хмельницький національний університет, редакція журналу "Проблеми трибології"
тел. +380975546925, E-mail: tribology@khmnu.edu.ua

Internet: <http://tribology.khnu.km.ua>

Зареєстровано Міністерством юстиції України

Свідоцтво про держреєстрацію друкованого ЗМІ: Серія КВ № 1917 від 14.03. 1996 р.
(перереєстрація № 24271-14111ПР від 22.10.2019 року)

Входить до переліку наукових фахових видань України
(Наказ Міністерства освіти і науки України № 612/07.05.19. Категорія Б.)

Індексується в МНБ: CrossRef, DOAJ, Ulrichsweb, ASCI, Google Scholar, Index Copernicus

Рекомендовано до друку рішенням вченої ради ХНУ, протокол № 5 від 28.11.2024 р.

© Редакція журналу "Проблеми трибології (Problems of Tribology)", 2024



Problems of Tribology, V. 29, No 4/114-2024

Problems of Tribology

Website: <http://tribology.khnu.km.ua/index.php/ProbTrib>

E-mail: tribosensor@gmail.com

CONTENTS

V.I. Dvoruk. Influence of the shape of abrasive soil particles on the regularities of destruction of structural steels during wear.....	6
V. Izemenko, A. Zahorulko, Yu. Zahorulko. Leakage and rotordynamic coefficients of labyrinth-scallop seals.....	14
D.D. Marchenko, K.S. Matvyeyeva, V.M. Kurepinrskyi. Increasing the wear resistance of plunger pairs of high-pressure fuel pumps using extreme pressure additives.....	24
O.V. Dykha, A.A. Vychavka, M.O. Dykha. Wear resistance and lubricity of the spiral oil distribution profile of the valve guide sleeves of an internal combustion engine.....	32
O.V. Bereziuk, V.I. Savulyak, V.O. Kharzhevsky, A.Ye. Alekseiev. Dependence of wear intensity on the coating material of the hydraulic cylinder of the garbage truck's sealing plate.....	40
V.A. Honchar. Research on the wear resistance of the material cylinder of an automatic injection molding machine during plastics processing.....	47
K.E. Holenko, A.A. Vychavka, M.O. Dykha, V.O. Dytyniuk. Modeling of contact stresses and evaluation of wear life of a valve mechanism guide with lubricating grooves.....	54
M. Pashechko, V. Holubets, J. Zubrzycki, O. Tisov. Cavitation-erosion resistance of eutectic coatings in sodium chloride solution.....	63
Rules of the publication	68



ЗМІСТ

Дворук В.І. Вплив форми абразивних частинок ґрунту на закономірності руйнування низьколегованих сталей при зношуванні	6
В. Іземенко, А. Загорулько, Ю. Загорулько. Витоки і ротородинамічні коефіцієнти лабіринтно-лункових ущільнень.....	14
Марченко Д.Д., Матвєєва К.С., Курепін В.М. Підвищення зносостійкості плунжерних пар паливних насосів високого тиску за допомогою протизадирних присадок.....	24
Диха О.В., Вичавка А.А., Диха М.О. Зносостійкість і мастильна здатність спірального маслорозподільного профілю напрямних втулок клапанів двигуна внутрішнього згоряння.....	32
Березюк О.В., Савуляк В.І., Харжевський В.О., Алексеєв А.Є. Залежність інтенсивності зносу від матеріалу покриття гідроциліндра ущільнюючої плити сміттєвоза.....	40
Гончар В.А. Дослідження зносостійкості матеріального циліндра термопластавтомата при переробці пластмас.....	47
Голенко К.Є. Вичавка А.А., Диха М.О., Дитинюк В.О. Моделювання напружень в контакті і оцінка ресурсу по зносу прямої клапанного механізму із змащувальними канавками.....	54
Пашечко М., Голубець В., Зубжицький Я., Тісов О. Кавітаційно-ерозійна стійкість евтектичних покриттів в розчині хлориду натрію.....	63
Вимоги до публікацій	68



Influence of the shape of abrasive soil particles on the regularities of destruction of structural steels during wear

V.I. Dvoruk

State University "Kyiv Aviation University", Kyiv, Ukraine

E-mail: vidvoruk@gmail.com

Received: 05 September 2024; Revised: 25 September 2024; Accept: 05 October 2024

Abstract

The article presents the results of studying the patterns of destruction and their influence on the wear resistance of structural steels: steel 45, steel 65G and steel 28MnB5 when moving in soils with different abrasive particle shape factors. The phenomenon of the presence of a critical abrasive particle shape factor (CPSF) was established, up to which the wear resistance of steels decreases. In the supercritical region, wear resistance is stabilized, and the differences between its values of the studied steels are significantly reduced. When forming wear resistance, the role of the particle shape factor is to regulate active deformation and fatigue phenomena by means of the level of external force action on the working surface and is realized through the rheological-fatigue parameter, which is controlled by the cyclic viscosity of steel deformation. In this regard, the choice of structural steel grade for the manufacture of machine parts intended for use in soils with different abrasive particle shape factors must be made based on its ranking by the rheological-fatigue parameter. It is shown that in the strength basis of the steel wear mechanism under sliding friction in soils with different particle shape factors, in addition to the resistance to the propagation of axial and radial fatigue cracks in the destructive deformation layer, an important role is played by the resistance to the initiation and propagation of lateral fatigue cracks at its boundary with the plastic-destructive deformation layer, and the mechanical component of the contact interaction is decisive. It is established that under wear in soils with different particle shape factors, the action of the softening process is more effective than the hardening process. In the supercritical region, the intensity of steel softening is significantly reduced due to the increase in the effectiveness of the hardening action due to the dispersion hardening of steel. However, no qualitative changes in the metal wear process are observed.

Key words: abrasive wear, soil, abrasive particle shape factor, fatigue, destructive deformation, plastic-destructive deformation, fatigue crack, wear resistance, rheological parameter, rheological-fatigue parameter, fracture toughness, size of the region of nonlinear effects, cyclic deformation toughness, softening, hardening, dispersion hardening.

Introduction

When machine parts and tools move in a soil environment containing an abrasive, intensive wear of the metal occurs, accompanied by a rapid change in their geometric dimensions and shape.

The reason for the high aggressiveness of this type of wear is the specific process of contacting the abrasive, in which not every particle on the friction surface is capable of interacting with the metal, and the speed of relative movement of the particles is significantly less than the translational speed of the part. In addition, most of them have a rounded shape and, making a complex movement, can not only slide at high speed, but also rotate or roll along the friction surface until they take a more stable position in relation to it, as well as to each other. In this regard, it is advisable to consider the soil environment as a solid body with a very rough surface (where the role of irregularities is played by abrasive particles) and a mobile active layer [1]. Experiments have shown that when interacting with the friction surface, the abrasive particles of the active layer of such a body are pressed into the metal with a certain force and move progressively along its surface. Particular attention should be paid to the fact that both of these stages of interaction of the abrasive with the surface occur simultaneously, which significantly



complicates its nature. The destruction of the surface is carried out both by the micro-cutting and deforming action of the particles. Micro-cutting particles directly produce wear, but there are relatively few of them (0.07 - 7% of the total). Deforming particles, the pressure of which on the contact area brings the worn metal to the yield point, are significantly more numerous. They do not directly produce wear, but multiple deformation of the same surface areas contributes to their fatigue destruction. Based on this, the leading form of abrasive wear of the friction surface when moving in the soil is mechanical fatigue by the mechanism of low-cycle and high-cycle fatigue [2]. The process of destruction from fatigue, which precedes the formation and separation of wear particles, includes the stages of nucleation and propagation of fatigue cracks in microvolumes of the deformed surface layer of the metal. Therefore, it should be considered as a kinetic process that predetermines the formation of two qualitatively different zones in the area of each crack: the zone of the inner surface of the crack and the zone of nonlinear effects in the vicinity of its tip. Based on the change in the stress-strain state with distance from the surface, the structure of the surface layer of the metal has a layered structure, including the following layers: a layer of destructive deformation, consisting of an outer (cracked) sublayer and an adjacent sublayer of nonlinear effects in the vicinity of the crack tips; a layer of plastic-destructive deformation; a layer of plastic deformation; a layer of elastic deformation, passing into undeformed metal [2]. The cracked sublayer contains the largest defects in the form of axial and radial microcracks, as well as the centers of their origin, i.e. the connection between individual microvolumes in it is weakened due to the violation of the continuity of the metal. The sublayer of nonlinear effects is a plastically deformed metal localized in the areas of crack propagation. Thus, the destructive deformation layer obeys not the laws of continuum mechanics, but the laws of solid-body fracture mechanics and, due to its "looseness", has the lowest strength. Inside the adjacent layer of plastic-destructive deformation, a rotational fragmented structure and rare microcracks, reflecting the disclination nature of deformation, predominate. In the deformation mechanism located below the layer of plastic deformation, the leading role is played by linear and point defects of the crystalline structure, forming a structure of predominantly dislocation type. In terms of its structure, the elastically deformed layer is practically no different from the undeformed metal bordering it. Such a structure indicates the simultaneous occurrence of two independent processes in each of the layers - deformation and destruction [3]. These processes are realized in dialectical unity: deformation does not happen without destruction, and destruction - without deformation. The relationship between them changes with an increase in the depth of the layer from the surface. Thus, in the layer of destructive deformation, destruction processes predominate, plastic-destructive deformation - large plastic deformations, plastic deformation - moderate plastic deformations, and elastic deformation - elastic deformations. The specified relationship is controlled by changes in the level of acting stresses as they penetrate deeper into the surface layer and depends on the physical characteristics of the metal, in particular the rheological-fatigue parameter [2]. Among the factors determining the destruction of the metal surface layer during wear in the soil, an important role is played by the shape acquired by the abrasive particles during the natural formation of sand. For the quantitative assessment of this factor, various variants of the shape coefficient K_F have been proposed [4-6] - a criterion whose values vary from 11 for rounded particles to 100 for acute-angled particles measuring 0.2 - 2 mm. The value of K_F , on the one hand, determines the probability of particle contact with the wear surface along a protrusion of a small radius of curvature, and on the other hand, the degree of deviation of its shape from spherical (the latter affects the degree of particle fixation in the mass of particles - its temporary retention in a motionless state with respect to the surrounding particles). The level of contact stresses and, consequently, the type of surface destruction depend on these indicators. Thus, at $K_F \leq 11.25$ direct destruction of the material does not occur. With further increase of K_F a gradual transition from plastic deformation to direct destruction of the material occurs, which occurs at $K_F \geq 45$. It has been established [4-6] that with increase of K_F the intensity of wear of metal in the soil environment increases. The initiation and propagation of fatigue cracks in metallic materials is caused by plastic deformation, the quantitative measure of which can be the width of the hysteresis loop (cyclic viscosity of deformation) per cycle of change of load at a given level of stresses [7]. The regularities of change of cyclic viscosity of deformation allow us to come to the conclusion that cyclically repeating alternating stresses during wear cause in each of the layers of the surface layer of metal two simultaneously proceeding opposite processes: strengthening and softening.

Materials and research methods

The objects of the study were structural steels: steel 45, steel 65G and steel 28MnB5, the chemical composition of which is presented in Table 1.

Table 1

Chemical composition of the investigated steel

Steel grade	Content, %									
	C	Mn	Si	P	S	Cr	Ni	Cu	B	As
65G	0,65	1,11	0,27	0,035	0,035	0,25	0,25	0,22	-	-
28MnB5	0,272	1,26	0,234	0,020	0,035	0,22	-	-	0,0023	-
45	0,46	0,65	0,27	0,035	0,04	0,25	0,25	0,25	-	0,08

Samples from the specified steels were made in the form of plates with dimensions of (70×70×6) mm and subjected to strengthening by heat treatment in the modes specified in Table 2.

The heating source during maintenance was an electric muffle furnace SNOL7.2/1300 (NPP Termoizhenering, Kharkov).

Table 2

Mode of heat treatment of investigated steels

Steel grade	Hardening			Tempering	
	Heating temperature, °C	Holding time, min	Hardening environment	Heating temperature, °C	Holding time, min
65G	820	30	Oil	470	60
28MnB5	900	30	Oil	500	60
45	850	30	Water	550	60

The hardened samples were subjected to indentation and wear tests by friction in the soil.

Indentation tests were carried out using a universal hardness tester "NOVOTEST T-UD2" (OOO NTC "Industrial Equipment and Technologies", Novomoskovsk). As a result, the Rockwell hardness of steel in the initial state was determined.

Wear tests of steel by friction in the soil were carried out using a modernized "impeller" method on a test rig [8], the diagram of which is shown in Fig. 1

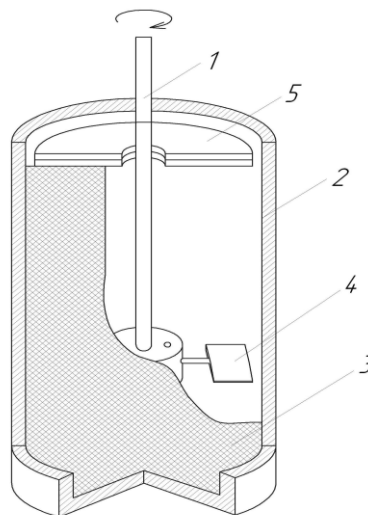


Fig. 1. Diagram of a setup for testing steel for wear when friction in soil: 1 - sample holder shaft; 2 - cylinder; 3 - soil; 4 - samples; 5 - mogosection disk

The essence of the tests consisted in rotating a steel sample immersed in the specified soil. The test mode is as follows: soil pressure on the sample $P = 122.6$ kPa, sample rotation speed $V = 125.28$ m/min, sample friction path $L = 500$ km. During wear, the friction force F_{tr} of the sample was measured. Sample wear G was measured by weighing on an electronic analytical scale CP 34001 S (Sartorius (Germany)). The measure of wear resistance ε was the reciprocal of wear G .

Quartz sand from three deposits in the Zhytomyr region of Ukraine - Tarasovskoye, Ignatpolsky and Irshansky - was used as soil, from which particles of a fraction of 0.5 - 1.0 mm were isolated by sifting through a sieve. The hardness of the particles was 1000 - 1300 kg / mm². The particle shape coefficient K_F was calculated using the formula [6]. The geometric parameters of the particle required for this are shown in the diagram (Fig.2).

Для оценки указанных параметров частицы помещали под микроскоп «SIGETA CAM-03, фотографировали, после чего производили требуемые измерения с привлечением программы «КОМПАС-3D».

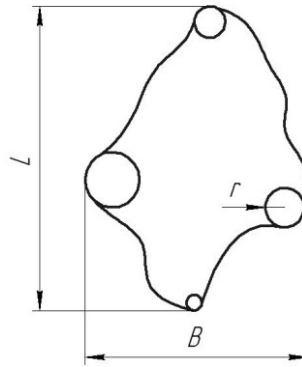


Fig. 2. Geometric parameters of the abrasive particle: L – the largest value of the longitudinal size; B – the largest value of the transverse size; r – protrusion

The analysis of the process of steel destruction during wear in soil was carried out using the following criteria: critical stress intensity factor (fracture viscosity) K_{Ic} , size of the region of nonlinear effects in the vicinity of crack tips h_p , rheological parameter $R = K_{Ic} / h_p$, cyclic deformation viscosity $\Delta\varepsilon$, as well as true deformation ε_{true} , which were determined by the methods [3, 9]. Using the specified characteristics, the rheological-fatigue parameter of the studied steels $R_f = R (\varepsilon_{true} / 2 \Delta\varepsilon)^2$ [10] was determined. The obtained experimental results were processed using the methods of mathematical statistics.

Research results and their discussion

The values of the shape coefficient of abrasive particles of the studied soils are presented in Table 3.

Table 3

Shape coefficient of abrasive soil particles

Sand deposit	Irshanskoe	Tarasovskoye	Ignatpolskoe
Shape coefficient	98,71	114,18	153,72

Data on changes in the tribomechanical and rheological properties of the studied steels in soils with different shape factors of abrasive particles are presented in Table 4.

Table 4

. Dependence of tribomechanical and rheological properties of steels on the shape factor of abrasive particles

Steel grade	Sand deposit	Shape coefficient, K_F	Tribomechanical properties		Rheological properties	
			Hardness, HRC	Wear resistance, ε , kg^{-1}	Rheological parameter R , GPa	Rheological-fatigue parameter R_f , TPa
45	Irshanskoe	98,71	8	58,8	1,82	20,5
	Tarasovskoye	114,18	8	46,5	1,82	16,27
	Ignatpolskoe	163,72	8	35,1	1,82	12,3
65G	Irshanskoe	98,71	40	133,3	4,94	126,5
	Tarasovskoye	114,18	40	71,4	4,94	67,63
	Ignatpolskoe	163,72	40	42,6	4,94	40,12
28MnB5	Irshanskoe	98,71	50	200	6,9	265,24
	Tarasovskoye	114,18	50	100	6,9	132,37
	Ignatpolskoe	163,72	50	55	6,9	74,23

By comparing the shape factor K_F and wear resistance ε , the following inversely proportional correlation dependence was established (Fig. 3): with an increase in the particle shape factor, the wear resistance of the steels under study decreases. Moreover, in stronger steels (steel 28MnB5, steel 65G) this occurs much more intensively than in the less strong steel 45

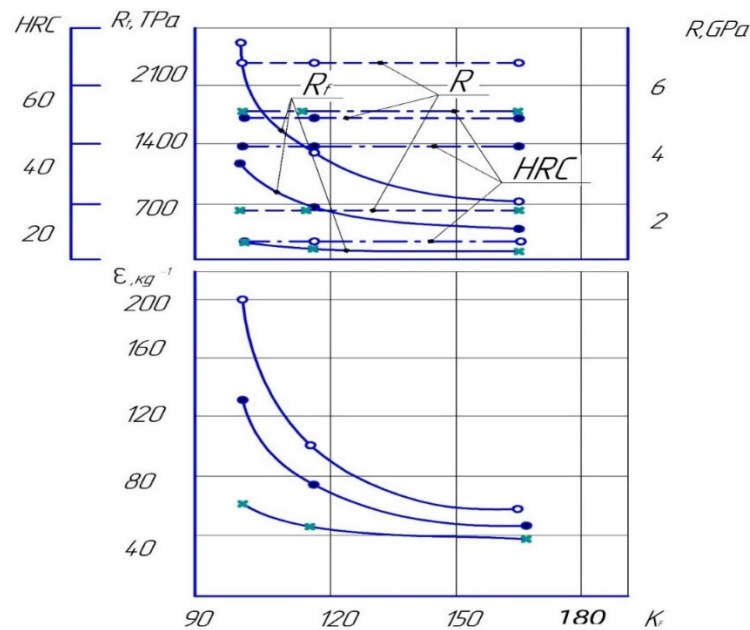


Fig. 3. Comparison of wear resistance (ϵ) with hardness (HRC), rheological parameter (R) and rheological-fatigue parameter (R_f) of steels after wear in soils with different shape coefficients of abrasive particles (K_F): \times - steel 45; \bullet - steel 65 G; \circ - steel 28MnB5

A significant decrease in wear resistance is observed until the shape factor reaches a value of the order of $K_F \approx 140-150$, after which a clear tendency towards stabilization of the indicated pattern is observed. In addition, with an increase in the particle shape factor, a gradual convergence of the wear resistance of steels takes place. For example, if at $K_F = 98.71$ the wear resistance of steel 28MnB5 was 3.4 times higher than that of steel 45, then at $K_F = 153.72$ - 1.6 times. Consequently, during wear in soils with different shape factors of abrasive particles on the working surfaces of steels, the phenomenon of the presence of a critical shape factor of abrasive particles (CPSF) is realized, the value of which is 140 - 150.

Analysis of the obtained results showed that the characteristics of resistance to deformation (hardness HRC) and destruction (rheological parameter R) under static loading do not show sensitivity to the formation of wear resistance of steels when moving in soils with different shape factors of particles. At the same time, between the characteristic of resistance to destruction under fatigue loading - the rheological-fatigue parameter R_f and wear resistance ϵ as K_F of particles increases, the following correlation is established: the higher the particle shape factor, the lower the rheological-fatigue parameter and wear resistance of steel. Consequently, the wear resistance of steels when moving in soils with different shape factors of abrasive particles is controlled by the rheological-fatigue parameter.

Based on the above, it can be stated that in the strength basis of the mechanism of steel wear under sliding friction in soils with different shape factors of abrasive particles, in addition to the resistance to the propagation of axial and radial fatigue cracks in the destructive deformation layer (see above), an important role is played by the resistance to the initiation and propagation of lateral fatigue cracks on its boundary with the layer of plastic-destructive deformation. In this case, the mechanical component of the contact interaction is decisive.

Lateral cracks originate from the boundary of these layers and then grow towards the surface. Their intersection with radial cracks leads to the formation of wear particles [11].

Along with lateral cracks, axial and radial cracks originate at the same boundary, which propagate in the opposite direction - towards the layer of plastic-destructive deformation, thereby gradually transforming it into a destructive layer. It finally becomes destructive after the complete destruction of the layer preceding it. In this way, layer-by-layer destruction of the metal occurs, the result of which is its wear. The immediate cause of localization of the origin of the system of lateral, axial and radial fatigue cracks at the boundary of the destructive and plastic-destructive layers is the state of plane deformation, which occurs here during contact interaction with the abrasive and contributes to an increase in the effective maximum stresses to a level three times greater than at the boundary of the cracked sublayer with the sublayer of nonlinear effects in the vicinity of the cracks [10]. Along with the maximum, residual stresses simultaneously arise and act in the metal due to the unevenness of its deformation. The superposition of these stresses under cyclic action determines the actual load level at the specified boundary. Consequently, the stress distribution curve from the boundary of the cracked sublayer along the depth of the surface layer has a non-monotonic character with a maximum at the boundary of the destructive and plastic-destructive layers.

Based on the proposed mechanism of destruction, it is advisable to rank the wear resistance of structural steels under the conditions under consideration by the rheological-fatigue parameter.

Since the rheological-fatigue parameter includes a number of physical quantities, the patterns of their change during wear, as well as the role of each of them in the formation of steel wear resistance with varying the shape factor of abrasive soil particles, are of scientific and practical interest.

Fig. 4 and 5 show the patterns of true deformation ϵ_{true} and cyclic viscosity of deformation $\Delta\epsilon$ (Fig. 4), fracture toughness K_{1c} and the size of the region of nonlinear effects in the vicinity of crack tips h_p (Fig. 5) of steels with a change in the particle shape factor K_F .

From this it is evident that the true deformation ϵ_{true} (Fig. 4), fracture toughness K_{1c} (Fig. 5) and the size of the region of nonlinear effects h_p (Fig. 5) of the studied steels are insensitive to changes in the particle shape factor K_F , while the cyclic deformation viscosity $\Delta\epsilon$ (Fig. 4) increased with the latter.

Comparison of the cyclic deformation viscosity $\Delta\epsilon$ (Fig. 4) with the rheological-fatigue parameter R_f and wear resistance ϵ (Fig. 3) of steels with variations in the particle shape factor K_F shows the presence of an inversely proportional correlative relationship between them: with an increase in the cyclic deformation viscosity, the rheological-fatigue parameter and wear resistance decrease.

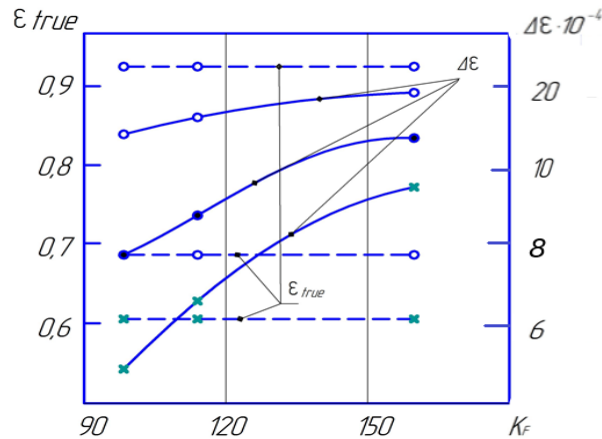


Fig. 4. Change true deformation (ϵ_{true}) and cyclic deformation viscosity ($\Delta\epsilon$) of steels after wear in soils with different shape coefficients of abrasive particles (K_F): \times - steel 45; \bullet - steel 65 G; \circ - steel 28MnB5

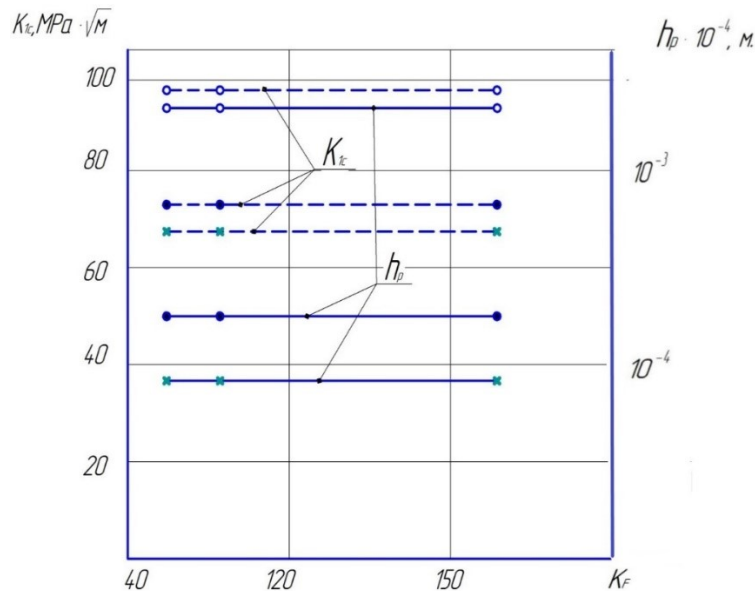


Fig. 5. Change in fracture toughness (K_{1c}) and the size of the area of nonlinear effects in the vicinity of the crack (h_p) steels after wear in soils with different shape coefficients of abrasive particles (K_F): \times - steel 45; \bullet - steel 65 G; \circ - steel 28MnB5

Consequently, the leading role in the formation of the rheological-fatigue parameter and wear resistance of steels when moving in soils with different shape factors is played by the cyclic viscosity of deformation, which characterizes the ability of the metal to absorb the supplied energy in an irreversible form and is determined by the parameters of the hysteresis loop, in particular, its width $\Delta\epsilon$.

Cyclically repeating stresses during abrasive wear cause two simultaneously occurring opposite phenomena in the metal: strengthening and softening. From the established pattern of change in the cyclic viscosity of deformation (Fig. 4), it is evident that with an increase in the shape factor of the abrasive, the value of $\Delta\epsilon$

continuously increases. This allows us to consider the effect of softening during wear to be more effective than strengthening. The softening process, in this case, occurs as a result of cyclic deformation of the surface layer, leading to the occurrence and development of structural defects, embrittlement of the material, an increase in internal stresses and the opening of microcracks, while hardening is associated with the work hardening factor - the formation of obstacles in the metal that slow down the movement of dislocations.

Noteworthy is the noticeable decrease in the intensity of softening of the metal after reaching the value of the form factor of the order of $K_F \approx 140-150$. This effect is especially clearly manifested in strong steels 28MnB5 and 65G. It is explained by an increase in the effectiveness of the hardening action due to factors that complement the work hardening. For steel 45, such a factor is most likely dynamic strain aging (DSA) - blocking of dislocations due to diffusion of carbon and nitrogen atoms to them, and for steels 28MnB5 and 65G - dispersion hardening (DH), caused by partial decomposition of martensite, as well as white layers of thermomechanical origin, consisting of martensite and its decomposition products, residual austenite, carbides, nitrides, oxides.

Due to the high hardness of the martensite base, plastic deformation of strong steels during wear cannot be significant, as a result of which, it is not capable of causing significant strain hardening and dynamic strain aging. Therefore, the main type of strengthening of steels 28MnB5 and 65G, in all likelihood, is dispersion hardening. Despite the decrease in the intensity of destruction under the influence of the indicated factors of additional strengthening, qualitative changes in the wear process of steels are not observed (Fig.3).

Conclusions

1. When worn in soils with different abrasive particle shape factors on the working surfaces of low-alloy steels, the phenomenon of the presence of a critical abrasive particle shape factor (CPSF) is realized, up to which the wear resistance of steels decreases. With a further increase in the particle shape factor, the wear resistance stabilizes, and the differences between its values of the studied steels are significantly reduced.

2. The role of the particle shape factor in the formation of wear resistance lies in the regulation of active deformation and fatigue phenomena in the surface layer by changing the level of external force action on the working surface.

3. The influence of the soil particle shape factor on wear resistance is carried out through the rheological-fatigue parameter in the following relationship: the higher the rheological-fatigue parameter, the higher the wear resistance of the steel.

4. In the strength basis of the steel wear mechanism under sliding friction in soils with different particle shape factors, in addition to the resistance to the propagation of axial and radial fatigue cracks in the destructive deformation layer, an important role is played by the resistance to the initiation and propagation of lateral fatigue cracks at its boundary with the plastic-destructive deformation layer, and the mechanical component of the contact interaction is decisive.

5. When selecting a grade of structural steel for the manufacture of machine parts operated in soils with different abrasive particle shape factors, it is necessary to be guided by its ranking by the rheological-fatigue parameter.

6. The role of the particle shape factor in the formation of the rheological-fatigue parameter is carried out mainly through the cyclic viscosity of deformation in the following relationship: the higher the cyclic viscosity, the lower the rheological-fatigue parameter of steel. The effect of the softening process during wear in soils with different particle shape factors is more effective than the hardening process. In the supercritical region of the abrasive shape factor, the intensity of softening of steels is significantly reduced due to the increase in the effectiveness of the hardening action due to the dispersion hardening of steel. However, no qualitative changes in the process of metal wear are observed.

References

1. Dvoruk V. I., Borak K. V., Buchko I. A. Destruction of Steel, by the Work-Hardened Speed Electrothermal Treatment at Wear by Friction of Skidding at the Non-Rigid Envisaged Abrasive // *Journal of Friction and Wear*, 2022, Vol. 43, No. 3, pp. 255–264
2. Dvoruk V. I., Borak K. V., Buchko I. A., and N. A. Kirienko N. A. Influence of Soil Type on Breaking of Low-Alloy Steels during Wear // *Journal of Friction and Wear*, 2022, Vol. 43, No. 6, pp. 383–390
3. Dvoruk V. I. Scientific bases for increasing abrasive resistance of machine parts. — Kyiv: KМУHA, 1997. 101 p.
4. Tadolder Yu.F. Influence of the geometry of the abrasive grain on the intensity of metal extraction in the flow of abrasive particles. *Proceedings of the Tallinn Polytechnic Institute, Ser. A.* 1966. 237. P.15-22.
5. Tenenbaum M.M. Resistance to abrasive wear, 1976. 271 s.
6. Bernshtein D.B., Kyssetova N.Y., Sorkyna E.M., Sheko Y.B. Macrogeometry and wearing capacity of soil abrasive particles. *Friction and wear*. 1992.13, No2. P. 333-339.
7. Ivanova V.S. Fatigue failure of metals. 1963. 272 p.

8. V.I. Dvoruk. A method for examining materials and rotating them for wear resistance and determining the coefficient of wear and tear of an abrasive mass.: pat. 142596 Ukraine, G01N 3/00; № u2019 02358; publ. 25.06.2020. Biul. № 12
9. Dvoruk, V. I. (2018). A method of abrasive wear is for determination of superfical energy of crystals. Problems of Tribology, 90(4), 22–31. <https://tribology.khnu.km.ua/index.php/ProbTrib/article/view/686>
10. Dvoruk, V. (2015). Modeling of metals wear when driving in abrasive mass. Problems of Tribology, 75(1), 77–85. <https://tribology.khnu.km.ua/index.php/ProbTrib/article/view/449>
11. Lown B.R. A model for the wear of brittle solids under fixed abrasive conditions // Wear, 1975, Vol.33, No.2, pp. 309-372

Дворук В.І. Вплив форми абразивних частинок ґрунту на закономірності руйнування низьколегованих сталей при зношуванні

Наведено результати вивчення закономірностей руйнування та їх впливу на зносостійкість конструкційних сталей - сталі 45, сталі 65Г і сталі 28MnB5 при русі в ґрунтах з різним коефіцієнтом форми абразивних частинок. Встановлено явище критичного коефіцієнта форми абразивних частинок (CPSF), аж до якого зносостійкість сталей знижується. При формуванні зносостійкості роль коефіцієнта форми частинок полягає в регулюванні активних деформаційних та утомних явищ за допомогою рівня зовнішнього силового впливу на робочу поверхню та реалізується через реолого-утомний параметр, який контролюється циклічною в'язкістю деформування сталі. У зв'язку з цим вибір марки конструкційної сталі для виготовлення деталей машин, призначених для експлуатації в ґрунтах з різним коефіцієнтом форми абразивних частинок необхідно проводити, виходячи з її ранжування за реолого-утомним параметром. Показано, що в міцністному підґрунті механізму зношування сталі при терті ковзання в ґрунтах з різним коефіцієнтом форми частинок, крім опору поширенню осьових та радіальних утомних тріщин в шарі деструкційного деформування, важливу роль відіграє опір зародженню і поширенню бічних втомних тріщин на його кордоні з шаром деструкційного деформування, а механічний компонент контактної взаємодії є визначальним. Встановлено, що при зношуванні в ґрунтах з різним коефіцієнтом форми частинок дія процесу знеміцнення є більш ефективною, ніж процесу зміцнення. В закритичній області коефіцієнта форми абразивних частинок інтенсивність знеміцнення істотно зменшується через зростання інтенсивності зміцнення внаслідок дисперсійного тверднення сталей.

Ключові слова: абразивне зношування, ґрунт, коефіцієнт форми абразивних частинок, утома, деструкційна деформація, пластично-деструкційна деформація, утомна тріщина, зносостійкість, реологічний параметр, реолого-утомний параметр, в'язкість руйнування, розмір області нелінійних ефектів в околі тріщин, циклічна в'язкість деформування, знеміцнення, зміцнення, дисперсійне твердіння



Leakage and rotordynamic coefficients of labyrinth-scallop seals

V. Izemenko, A. Zahorulko*, Yu. Zahorulko

Sumy State University, Ukraine

*E-mail: a.zagorulko@cm.sumdu.edu.ua

Received: 15 September 2024; Revised: 30 September 2024; Accept: 15 October 2024

Abstract

Reducing leakages and improving the rotor-dynamic damping characteristics of annular seals is an essential problem of sealing technology. A whole range of damping seals are used to seal the shafts of turbomachines, such as honeycomb, hole pattern, pocket, and scallop seals. To reduce the cost and production time, the scallop seals are increasingly used. They showed quite good dynamic and leakage characteristics in the modernization of compressors in the chemical industry. Some designs of scallop seals are able not only to increase dynamic performance (additional use of swirl brakes in the form of semi-open scallops at the inlet) but also thanks to the hybrid design of the scallop and labyrinth seal made of PEEK material, which ensures a minimum clearance between the seal and the shaft, reduce leakages of pumped fluid.

This paper presents the results of calculating the rotordynamic and flow rate characteristics of scallop and labyrinth-scallop seals depending on the operating parameters using computational fluid dynamics (CFD) methods. The CFD was used to calculate the hydrodynamic and rotordynamic characteristics of the seal with shaft whirl. The rotordynamic coefficients were obtained using the frequency excitation method. The obtained characteristics were compared with experimental data available from the literature for annular and labyrinth seals. The study confirmed the relatively low leakages, the high dynamic characteristics of the labyrinth-scallop seals, and the frequency dependence of the stiffness and damping coefficients. It has been confirmed that sickle-shaped scallops create obstacles to the circumferential flow of the working medium. Reducing the circumferential gas flow increases the hydraulic resistance in the grooves and simultaneously minimizes the circulation forces that create shaft whirl, increasing vibration.

Keywords: leakage, rotordynamic coefficients, labyrinth and scallop seal, damping seal, swirl brakes

Introduction

As is known, leakages in the seals of high-pressure centrifugal compressors are limited due to the use of potential pressure energy to overcome local resistances, frictional resistance along the channel length, and sometimes inertial resistance. The larger leakage, the smaller part of potential energy is transferred to the kinetic energy of the flow, as well as the lower values of the average velocity of the liquid in the channel and its mass flow rate. Thus, annular seals are not completely eliminated, but only limit flow rates.

Labyrinth seals, in which local resistances prevail, can be attributed to seals with throttling channels. The main function of labyrinth seals is to ensure minimal leakage through the sealing surfaces, taking into account minimal aerodynamic effects on the compressor rotor. However, in labyrinth seals, due to the fluid flow in the circumferential direction, while the flow is carried by the rotating shaft, circulating aerodynamic forces arise. Therefore, in practice, a number of annular seals have been proposed, which can reduce circulating forces that cause an increase in rotor whirl and, accordingly, vibration. These basic seals include honeycomb, hole-pattern, pocket and scallop seals. If the sealing mechanism and dynamic characteristics of the first three types of seals are well studied [1-6], a rather limited number of studies and publications are devoted to the last type of seals [7-10].

Scallop seals (Fig. 1. a) are widely used and have proven themselves in the process of modernization of compressors for the chemical industry [8]. There are a number of designs of scallop seals that are able not only to improve dynamic characteristics (Fig. 1. a), but also to reduce leakages of the pumped medium (Fig. 1. b) [8].



The first patent for the scallop seal design (Fig. 2. a, b shows the longitudinal section and the isometric view of the seal) [11,12] was obtained in 1984. And it has a sleeve 1 on the inner surface of which there is scallops 2. In the axial direction, the rows of scallops are separated by ridges 4, and in the circumferential direction, adjacent scallops are separated by bridges 3. The ridges perform the same role as the ridges in conventional labyrinth seals, and the bridges slow down the circumferential flow.

The role of bridges is particularly important because, by slowing down the circumferential flow, they thereby reduce the circulating force, the existence of which is the main reason for the loss of dynamic stability of the rotor in the seals. In addition, the scallops are semi-closed chambers that slow down the expansion flow and, accordingly, increase the damping force [13].

In the research work of A. Gulyi [7] presents the experimentally obtained characteristics of flow rate and stiffness for three types of liquid seals, namely: labyrinth with overlapping ribs, scallop and honeycomb seals. All characteristics were compared with the characteristics of standard annular seals. Flow rates, amplitudes, and phases of forced rotor oscillations were measured at four pressure drop values of 0.2; 0.5; 1.0; 2.0 MPa at rotational speeds from 0 to 1000 s⁻¹ in steps of 50 s⁻¹. Leakage rate characteristics of all types of seals, with an averaged rotational frequency, show that the minimum flow rates were obtained for a labyrinth seal with a small axial gap between the ridges. Flow rates throughout scallop, honeycomb and labyrinth seals with central location of ridges are almost the same and about 20% less compared to flow rates due to standard annular seal. Numerical values of hydrostatic stiffness are determined by evaluating parameters based on phase and amplitude-frequency characteristics. The latter applies to all types of seals with a pressure drop value of 1 MPa. The type of characteristic corresponds to the model of the dynamic system of the rotor seal as a linear oscillating system of the second order. The honeycomb seal has more dominant dynamic properties, and the scallop seal is closer to the standard one. If the tasks of reducing vibration and leakage are equally important for a particular pump, then scallop seals should be used. In terms of hydraulic resistance, they are not inferior to labyrinth and honeycomb seals, and in terms of damping and stiffness properties, they significantly exceed them. At the same time, they are less prone to scoring than conventional annular and labyrinth seals. However, it should be remembered that the coefficient of hydrostatic stiffness of scallop seals is approximately two times lower than that of conventional annular seals [13].

Gocha Chochua [9] investigated the flow between the surface of the stator with scallops made by a disk cutter and the smooth surface of the rotor in a scallop seal with sloping sidewalls developed by Dresser-Rand using the Computational Fluid Dynamics (CFD) method. The main direction in the calculation of the scallop seal was the study of the turbulent compression flow under the action of the pressure drop for the periodic region, the assessment of the effect of the rotor rotation and the swirl at the inlet on the physics of the flow, the extrapolation of the results for the periodic region on the full geometry of the seal and determination of friction coefficients due to pressure losses and shear stress.

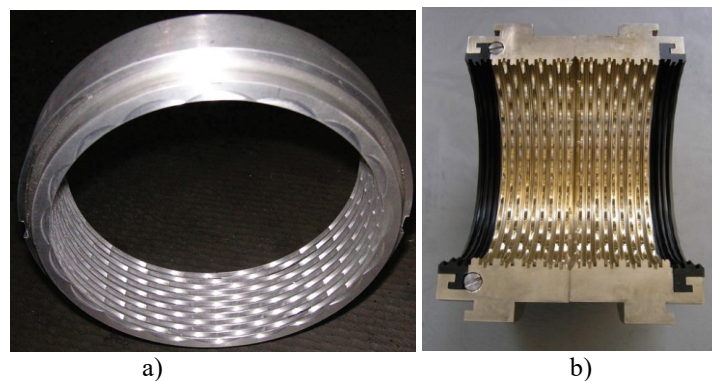


Fig. 1. Designs of scallop seals [8]

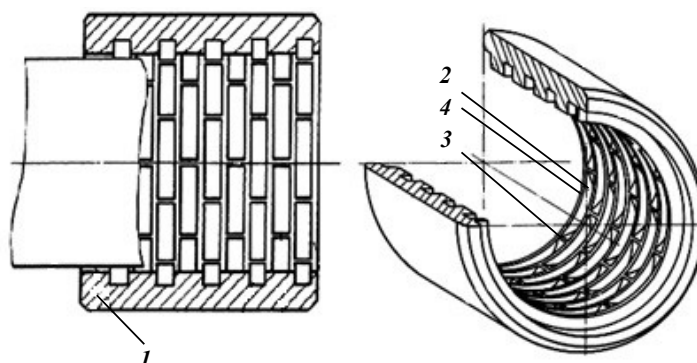


Fig. 2. The first patented design of scallop seal [14]

In his paper, Naohiko Takahashi et al. (Hitachi, Ltd. Company) [10] presented an evaluation of the rotordynamic coefficients of a scallop seal that has elongated ridges and sloping sidewalls with narrow ribs, as in labyrinth seals. The results of the experiment showed that the new seal had improved damping, which is in good agreement with the calculation results based on the bulk flow and CFD analysis by the excitation method. In the analysis by the excitation method, the whirl motion was considered as a stationary problem using a rotating frame of reference. The friction coefficients for the rotor surface, the stator surface, and the surface between the two control volumes for the bulk flow model were determined using steady-state CFD analysis.

The scallop seal can also be made in a stepped configuration, which is used in the unloading piston seals to change the diameter in the axial direction [8,10].

Based on the analysis of previous studies, we can draw the following conclusions and formulate the purpose of this study. Scallop seals showed quite good dynamic and flow rate characteristics during the modernization of compressors in the chemical industry. There are a number of designs of scallop seals that are able not only to increase dynamic performance (additional use of swirl brakes in the form of semi-open scallops at the inlet), but also thanks to the hybrid design of the scallop and labyrinth seal made of PEEK material (Fig. 1. b), which ensures a minimum clearance between the seal and the shaft, leakages of the pumped liquid are reduced. However, a number of studies and publications [7-10] are dedicated to scallop seals and are mainly related to the study of flow physics and the friction coefficient for the analysis of losses in scallop seals with inclined side walls [9], as well as obtaining dynamic coefficients using CFD analysis by the frequency excitation method and the bulk flow method for seal with elongated scallops and inclined sides walls [10]. For scallop seal, there are results regarding leakages and stiffness characteristics only for liquid media [7]. There is no comparison of leakage and dynamic coefficients of scallop seals with other types of labyrinth and annular seals for gas mediums. There is no information about the frequency-dependent dynamic coefficients of labyrinth-scallop seal. Due to the fact that the labyrinth-scallop seal is a damping type of seal, therefore, to obtain frequency-dependent rotordynamic stiffness and damping coefficients, it is advisable to use the calculation method of trajectories, which simulates the gas flow and the movement of the shaft along a given orbit.

1. Geometrical parameters, working and boundary conditions of the labyrinth-scallop seal

The calculation of the leakages in the labyrinth-scallop seal can be performed using CFD modeling in the Ansys CFX software [15]. In Fig. 3 a, an example of a geometry sector created in the Ansys Design Modeler software module is shown, in fig. 3 b mesh of the seal sector with imposed boundary conditions, in Fig. 3 c the complete geometry of the labyrinth-scallop seal. The sector geometry is 1/20 of the full geometry. The geometry of the seal consists of inlet and outlet chambers, periodically repeated along the length of the seal of scallop rows, annular channels, and four labyrinths made of PEEK material. The Ansys Meshing software was used to generate a computationally structured hexa mesh for the generated labyrinth-scallop seal geometry. The number of elements in the clearance was equal to 10 elements. The total size of the mesh was equal to 460,000 elements. The analysis of mesh independence of the model was carried out for four different mesh sizes - 137470, 331860, 460000, 653640 cells. The mesh thickened near the walls to obtain the necessary parameter $y^+=30-300$ for the corresponding $k-\varepsilon$ turbulence model.

Table 1 shows the geometrical dimensions and operating conditions obtained for the shaft diameter, length, clearance, and boundary conditions in the experiment for the hole-pattern seal performed in [14].

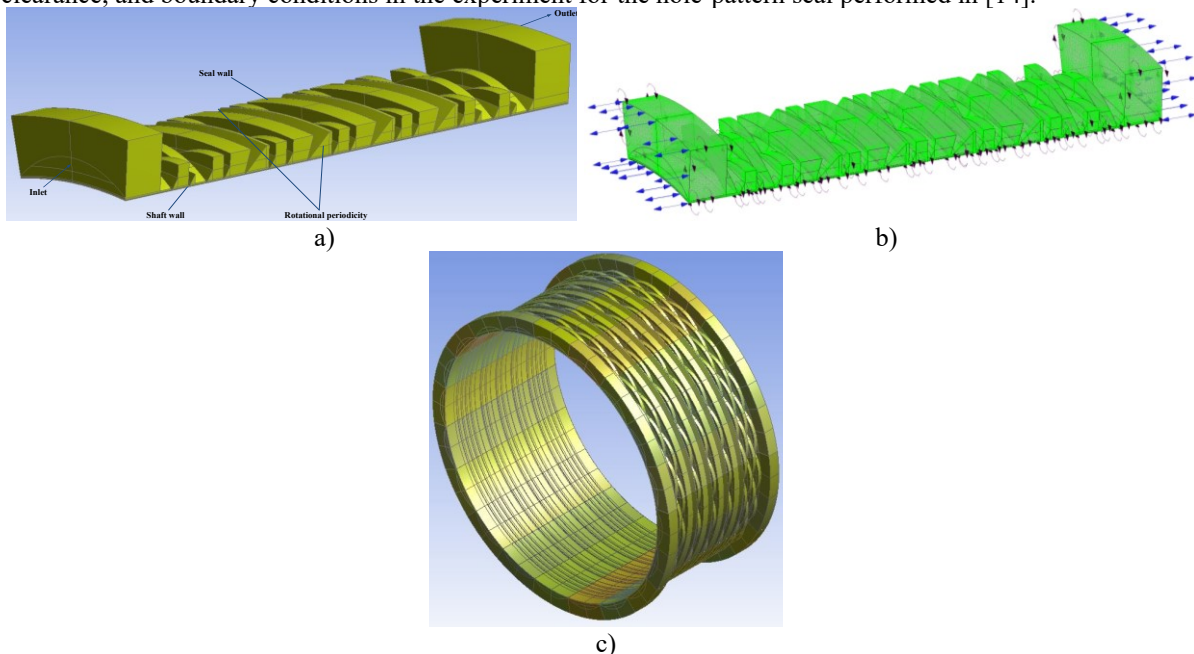


Fig. 3. Geometry and boundary conditions of labyrinth-scallop seal

Table 1

Geometrical parameters and operating conditions for scallop seal in CFD modeling

Parameter	Value
Inlet pressure	7.00 MPa
Outlet pressure	3.15 MPa
Inlet temperature	17.4 °C
Shaft rotation speed	20200 rpm
Clearance	0.2 mm
Shaft radius	57.37 mm
Seal length	85.7 mm
Fluid	Air (Ideal gas)
Scallops number in the circumferential direction	20, 30

Calculations were performed using Ansys CFX software which uses a hybrid finite volume method with shape functions from the finite element method to discretize the equations (Reynolds Averaged Navier–Stokes Equations). The k-ε model of turbulence with a standard wall function was used to describe the turbulent flow. The compressibility of a gaseous medium is represented by air as the ideal gas, the total energy equation, and the mass flow balance equation. To check the convergence during the calculation, the mass flow rates at the entrance and exit were monitored. The inlet and outlet boundary conditions were static pressures (Table 1). To take into account the centrifugal and inertial Coriolis forces, the computational domain of the seal was considered in a rotating frame of reference. The shaft wall is in a rotating coordinate system, while the seal wall has a counter-rotating wall boundary condition. This is necessary to create zero velocity with a no-slip wall boundary condition. A static temperature was also set at the seal inlet (Table 1).

3. Mathematical formulation of liquid flow

The averaged Reynolds equations for unsteady simulations, called URANS (Unsteady Reynolds Averaged Navier-Stokes Equations), are given below [15]. In the following equations, the upper underscore is omitted for the averaged values, with the exception of pulsation values

$$\frac{\partial \rho U_i}{\partial t} + \frac{\partial}{\partial x_j} (\rho U_i U_j) = -\frac{\partial p}{\partial x_i} + \frac{\partial}{\partial x_j} (\tau_{ij} - \rho \overline{u_i u_j}) + S_M$$

where τ is the molecular stress tensor (which includes both normal and shear stress components). Reynolds stresses $\rho \overline{u_i u_j}$, flow velocities U_i, U_j consist of averaged and pulsational components, ρ is density, S_M is source.

Reynolds-averaged energy equation:

$$\frac{\partial \rho h_{tot}}{\partial t} - \frac{\partial \rho}{\partial t} + \frac{\partial}{\partial x_j} (\rho U_j h_{tot}) = \frac{\partial}{\partial x_j} \left(\lambda \frac{\partial T}{\partial x_j} - \rho \overline{u_j h} \right) + \frac{\partial}{\partial x_j} [U_i (\tau_{ij} - \rho \overline{u_i u_j})] + S_E$$

The average total enthalpy is given by:

$$h_{tot} = h + \frac{1}{2} U_i U_i + k$$

where h is the specific static enthalpy.

The total enthalpy contains a contribution from the turbulent kinetic energy k :

$$k = \frac{1}{2} \overline{u_i^2}$$

Turbulence models close the averaged Reynolds equations providing the models for calculation, Reynolds stress, and Reynolds fluctuation.

The k-ε model assumes that turbulent viscosity is related to turbulent kinetic energy and turbulent dissipation by the ratio:

$$\mu_t = C_\mu \rho \frac{k^2}{\varepsilon}$$

where C_μ is a constant.

The turbulent kinetic energy k and its dissipation rate ε are derived directly from the differential equations of transfer.

For the ideal gas, the main dependence and equation of state are:

$$dh = c_p(T)dT$$

$$\rho = \frac{p}{RT}$$

where T, p – static temperature and pressure, respectively, c_p – specific heat capacity at constant pressure, R – universal gas constant.

A mixed method of discretization of equations is used. The solution of the system of discretized equations is carried out on the basis of a coupled approach. The pressure and velocity components are determined simultaneously in one cycle.

The most important of the calculations is the calculation of seal mass flow rate. The mass flow through the seal is determined by calculating the following integral on the outlet surface

$$M = \rho U \int_S dA$$

where U is the component of the velocity vector perpendicular to the outlet surface S .

The components of the sealing reaction forces are determined by integrating the pressure field of the sealing medium over the entire shaft surface [14]

$$F_x = -R \int_0^L \int_0^{2\pi} p(\theta, z) \cos\theta \, d\theta \, dz, \quad F_y = -R \int_0^L \int_0^{2\pi} p(\theta, z) \sin\theta \, d\theta \, dz,$$

where R is the shaft radius, L is the seal length.

4. Results of calculations and comparison of leakages of the labyrinth-scallop seal

As a result of the calculations, the dependences of the mass flow rate through the labyrinth-scallop seal on the pressure ratio $P_r = P_{out} / P_{in}$ and the shaft rotational speed was obtained (Fig. 4). It can be seen from the graphs that with a decrease in the pressure drop and an increase in the rotational speed, the mass flow rate through seal decreases.

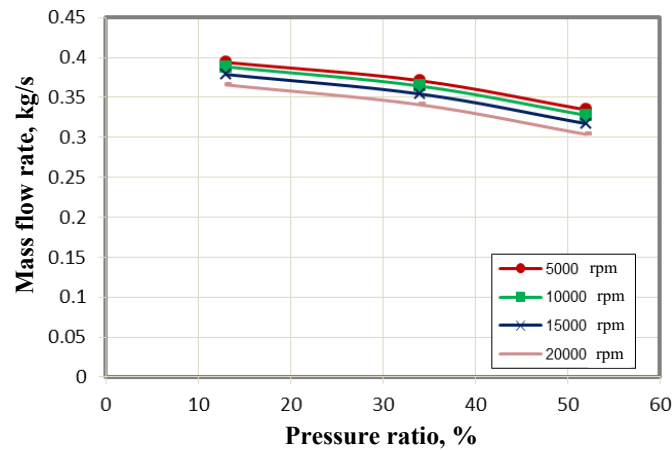


Fig. 4. Dependence of the mass flow rate on the pressure ratio

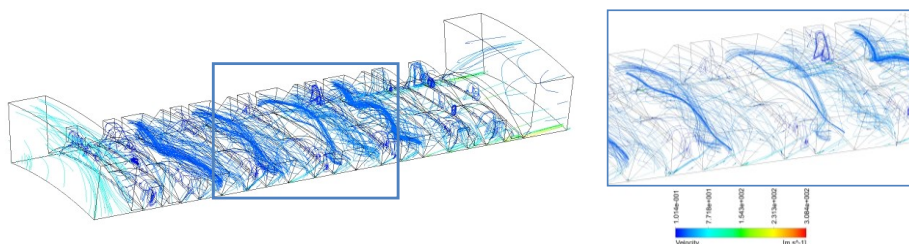


Fig. 5. 3D flow in a labyrinth-scallop seal

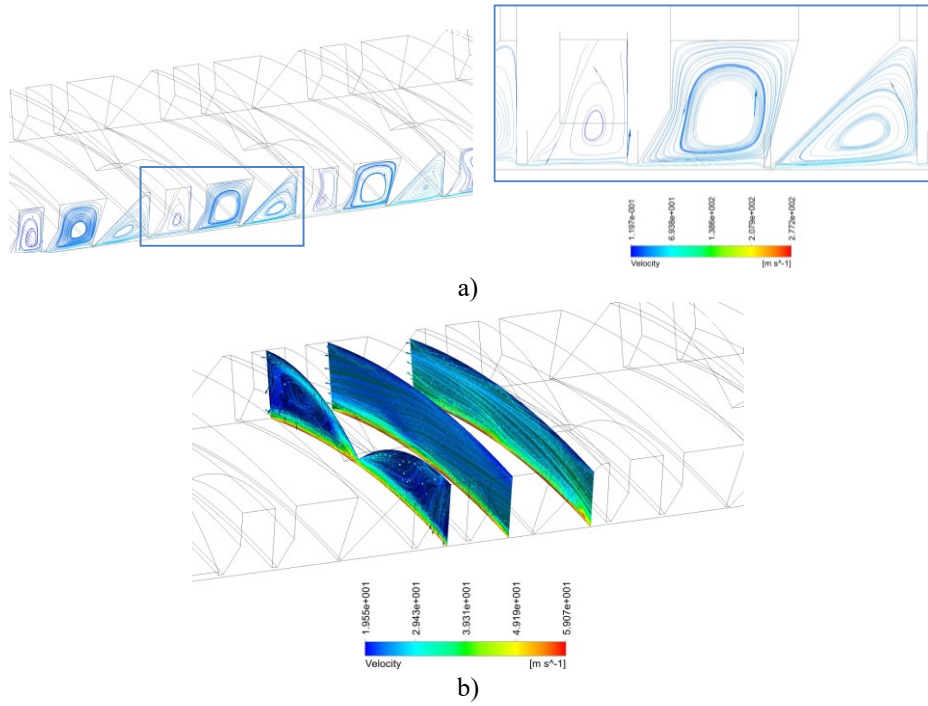


Fig. 6. Vortex flow in the axial (a) and circumferential directions (b)

3D flow in a labyrinth-scallop seal is presented in Figure 5. It has a complex three-dimensional structure with three types of vortex flow, such as circumferential flow in the clearance between the seal and the shaft, vortex flow inside the scallops in the circumferential and axial directions, and vortex flow in the labyrinth annular channel (Fig. 6 a,b).

Fig. 7 a,b shows the field of velocities and pressure in a labyrinth-scallop seal. The distribution of static pressure along the length of the seal (Fig. 8) shows that the largest pressure drop occurs on four labyrinths made of PEEK material with the smallest radial clearance between the seal and the shaft. Moreover, the amplitude of the pressure drop on each subsequent labyrinth increases.

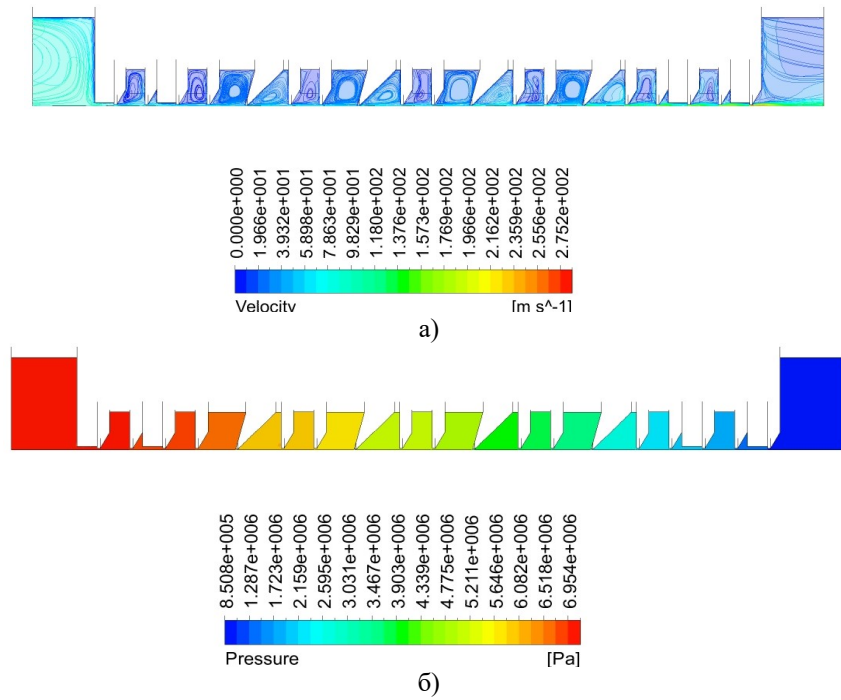


Fig. 7. The velocities (a) and pressure (b) fields

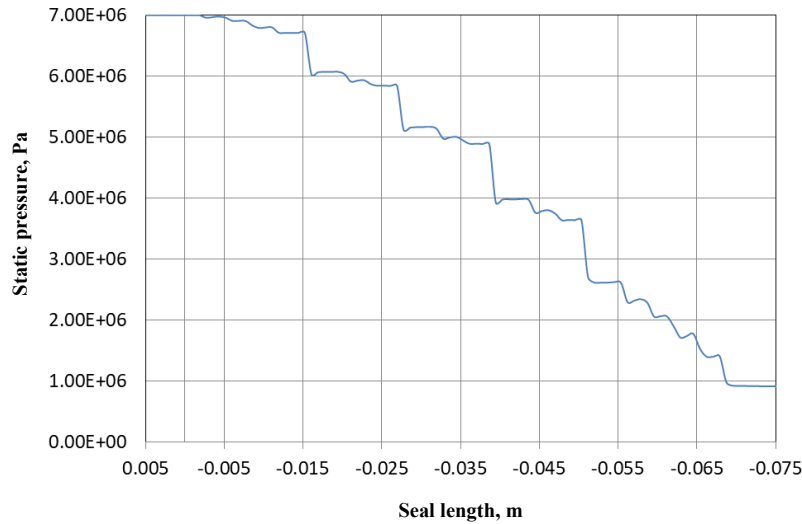


Fig. 8. The static pressure distribution along the seal length

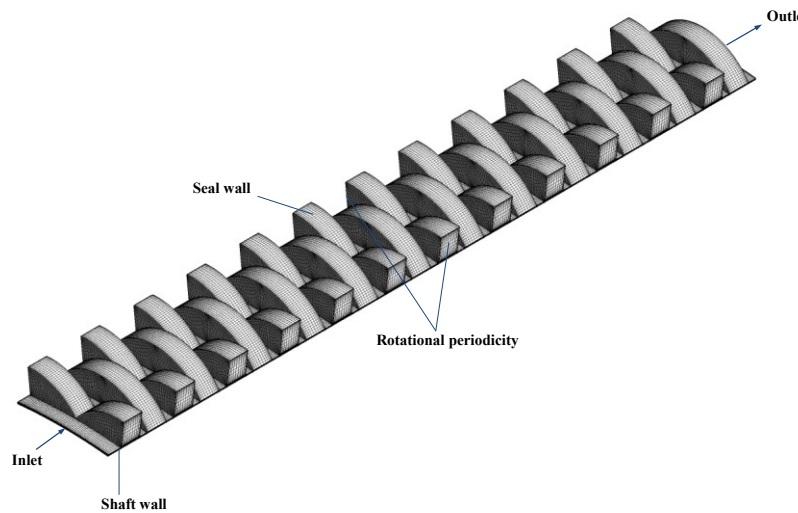


Fig. 9. Calculation mesh and boundary conditions of scallop seal

To compare flow coefficients for annular, labyrinth, scallop, and labyrinth-scallop seals calculations were performed with three different pressure coefficients: $P_r = P_{out} / P_{in} = 0.13, 0.34, 0.52$. As a scallop seal design, a seal design with 30 crossed rows of scallops was used. An example of the calculation mesh for the scallop seal sector is shown in Fig. 9. The calculation results are presented in a dimensionless form in the form of a flow coefficient [6,16]:

$$\Phi = \frac{M \sqrt{\frac{R_c T_{in}}{2 \Delta P P_{in}}}}{\pi D C_r}$$

where M - mass flow rate, R_c - gas constant, P_{in} , T_{in} - pressure and temperature at the inlet, respectively, ΔP - pressure drop at the seal, C_r - radial clearance, D - shaft diameter.

The calculated values were added to the graph obtained by Childs [16] for annular and labyrinth seals (Fig. 1.10). All results are presented at a rotational speed of 10,200 rpm, as this minimizes the effect of rotational speed on the comparison procedure.

It can be seen from Figure 10 that the largest values of the flow coefficient belong to the annular seal, the scallop seal has slightly lower values of the flow coefficient than the traditional labyrinth seal, and the smallest value of the flow coefficient has the labyrinth-scallop seal. Thus, at a pressure ratio of 0.3, the flow coefficient of the labyrinth-scallop seal is 41.7% less than that of the annular seal and 19% less than that of the labyrinth seal.

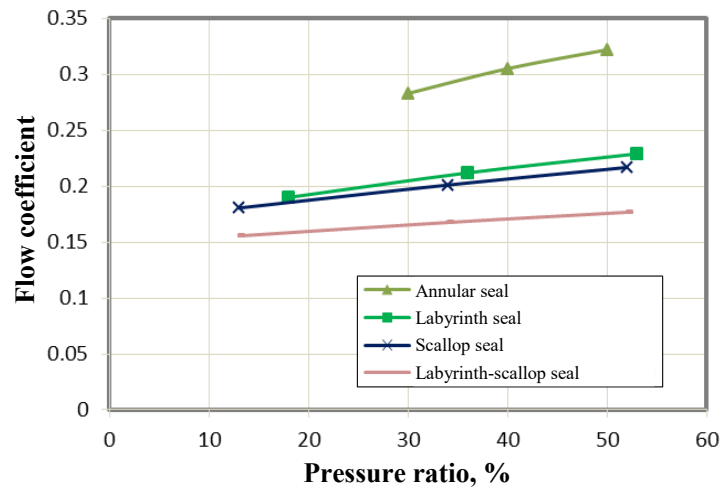


Fig. 10. Dependence of the flow coefficient on the pressure ratio [6,16]

5. Results of comparing the rotordynamic stiffness and damping coefficients of the scallop seal

To calculate the rotordynamic coefficients, a full model of the geometry and mesh of the scallop seal was used. The mesh deformation technology was used to model the shaft uniaxial excitation by the trajectory method. Unsteady calculations were performed for six different frequencies with physical time steps. Depending on the time, the radial and tangential forces of the shaft reaction were obtained, according to which the rotordynamic force coefficients of stiffness and damping were estimated. The amplitude of the shaft movement was 10% of the radial clearance and was equal to 0.02 mm.

To analyze the effectiveness of the scallop seal, it is quite important to compare its rotordynamic force coefficients with the coefficients for other annular seals.

For a more reliable comparison of rotordynamic coefficients, stiffness K and damping C for each seal design, they are presented in the form of normalized coefficients determined by the Childs equation [16]:

$$C^* = \frac{C}{\left(\frac{LD\Delta P}{C_r}\right)}$$

$$K^* = \frac{K}{\left(\frac{LD\Delta P}{C_r}\right)}$$

where L is the seal length, D is the shaft diameter, ΔP is the pressure drop across the seal, and C_r is the radial clearance.

The result of these equations is the normalized damping C^* in seconds, and the normalized stiffness K^* , which is dimensionless (in the graphs presented below, the normalized damping and stiffness values are multiplied by 10^6).

The effective damping coefficient C_{eff} relates the cross-stiffness coefficient k and the direct damping coefficient C and is defined

$$C_{eff} = C(\Omega) - k(\Omega)/\Omega$$

The comparison is made for experimental data obtained for annular and labyrinth seals, which were studied at an inlet pressure of 68.9 bar and various pressure drops. The graphs are taken from the work [6], and the calculated data for the scallop seal are plotted on these graphs (Fig. 11). The graphs (Fig. 11 a,b) show normalized data of effective damping and direct stiffness for labyrinth, annular and scallop seals.

The given dependences show that the traditional labyrinth seal has a negative direct stiffness and very low values of effective damping in the entire range of excitation frequencies. The scallop seal has significantly higher values of direct stiffness and effective damping than the labyrinth seal. However, in the low-frequency range of 40-70 Hz, the effective damping of the scallop seal can take negative values, which can cause loss of shaft stability at these frequencies. The annular seal has more effective damping and comparable stiffness at higher frequencies of 225-300 Hz. Therefore, if the combination of sealing and dynamic stability is important, then a scallop seal should be chosen among the considered types of seals.

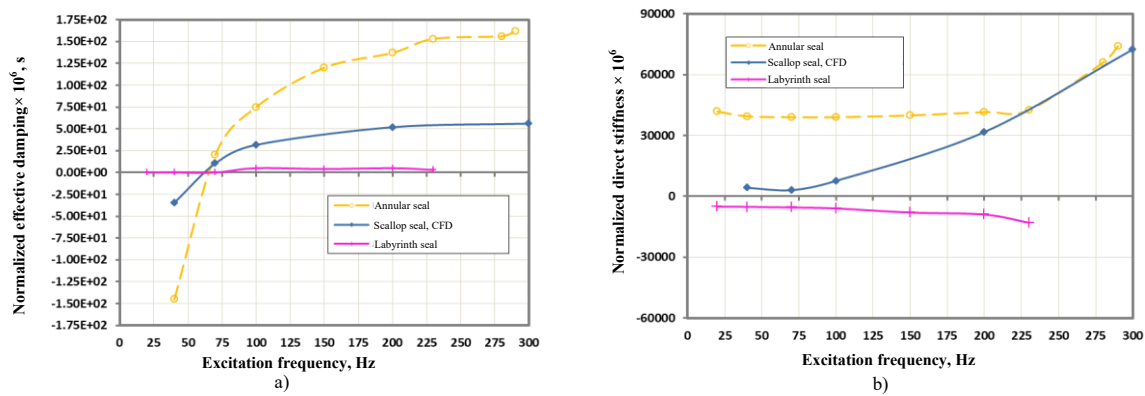


Fig. 11. Comparison of normalized coefficients of effective damping (a) and direct stiffness (b) [6]

Conclusions

Using the repeatedly tested CFD methods for modeling the gas flow in the seal, the values of the labyrinth-scallop leakages and the dynamic characteristics of the scallop seals were obtained. A comparison of the obtained characteristics with experimental data available from the literature for annular and labyrinth seals is given. The study confirmed the rather low values of the labyrinth-scallop leakages and the high dynamic characteristics of the scallop seals, as well as the frequency dependence of the stiffness and damping coefficients.

The study of labyrinth-scallop and scallop seals showed that to improve dynamic characteristics, especially effective damping at low excitation frequencies, it is necessary to use swirl brakes in the form of semi-open scallops at the seal entrance. To reduce leakages, it is advisable to use stepped and hybrid designs of scallop seals, i.e. labyrinth-scallop seals, in which the values of leakages are reduced with sufficiently high dynamic characteristics.

Studies have confirmed that scallops create obstacles to the circumferential flow of the working medium. Reducing the circumferential gas flow increases the hydraulic resistance in the grooves and at the same time reduces the circulation forces that create shaft whirl, increasing vibration. Rows of scallops are characterized by increased strength and rigidity. Scallop seals have good damping properties.

Acknowledgments

This paper was supported by the Sumy State University Projects: Researches on the -Increasing the bearing capacity, sealing and dynamic stability of rotor systems of turbomachines (0123U101853) and -Problems of dynamics and designing of sealing units for centrifugal machines (pumps, compressors) in terms of 4.0 industry (0123U103299) funded by the Ministry of Education and Science of Ukraine.

This research work has been carried out within the project "Fulfillment of tasks of the perspective plan of development of a scientific direction "Technical sciences" Sumy State University" (State Reg. No. 0121U112684) funded by the Ministry of Education and Science of Ukraine.

References

1. Z. Yu, D.W. Childs, A comparison of experimental rotordynamic coefficients and leakage characteristics between hole-pattern gas damper seals and a honeycomb seal, *J. Eng. Gas Turb. Power* 120 (1998) 778-783.
2. D.W. Childs, J. Wade, Rotordynamic-coefficient and leakage characteristics for hole-pattern-stator annular gas seals-measurements versus predictions, *J. Tribol.* 126 (2004) 326-333.
3. M. Vannarsdall, D.W. Childs, Static and rotordynamic characteristics for a new hole-pattern annular gas seal design incorporating larger diameter holes, *J. Eng. Gas Turb. Power* 136 (2014) 022507.
4. B.H. Ertas, Rotordynamic force coefficients of pocket damper seals, Ph.D Dissertation, Texas A&M University, 2005.
5. B. Ertas, A. Gamal, J. Vance, Rotordynamic force coefficients of pocket damper seals, *J. Turbomach.* 128 (2006) 725-737.
6. A.M.G. Eldin, Leakage and rotordynamic effects of pocket damper seals and see-through labyrinth seals, Ph.D Dissertation, Texas A&M University, 2007.
7. A.N. Guliy, Hydrodynamic stiffness of non-contact seals, *Newsl. Mech. Eng.* 2 (1987) 21-25.
8. V. Martsinkovsky, V. Yurko, Economic efficiency of synthesis-gas turbocompressor modernization, *Proc. Eng.* 39 (2012) 339-365.
9. G. Chochua, Computations of gas annular damper seal flows, Ph.D Dissertation, University of Florida, 2002.
10. N. Takahashi, H. Miura, M. Narita, N. Nishijima, Y. Magara, Development of scallop cut type damper seal for centrifugal compressors, *J. Eng. Gas Turb. Power* 137 (2015) 032509.

11. V.V. Usenko, V.A. Martsynkovskyy, I.S. Bereghnoy, A.N. Guliy, Labyrinth seal, Patent SU 1118827 A, 1984.
12. V. Martsynkovskyy, I. Ovseyko, I. Kukharev, Labyrinth seal, Patent UA 20521 U, 2007.
13. V.A. Martsynkovskyy, Rotordynamics of centrifugal machines, SumSU, Sumy, 2012.
14. A. Untaroiu, C. Liu, P.J. Migliorini, H.G. Wood, C.D. Untaroiu, Hole-pattern seals performance evaluation using computational fluid dynamics and design of experiment techniques, *J. Eng. Gas Turb. Power* 136 (2014) 102501.
15. Ansys CFX-Solver Theory Guide, Release 12.1, ANSYS Inc., 2009.
16. D.W. Childs, Bearings+Gas Seals, MEEN 688 Course Presentation, Texas A&M University, 2007.

В. Ізменко, А. Загорулько, Ю. Загорулько. Витоки і ротородинамічні коефіцієнти лабіринтно-лункових ущільнень.

Зменшення витоків і покращення роторно-динамічних демпфуючих характеристик шпаринних ущільнень є важливою задачею ущільнювальної техніки. Для герметизації валів турбомашин використовується цілий ряд демпферних ущільнень, таких як стільникові, з сіткою отворів, кишенькові і лункові ущільнення. Для зменшення вартості і часу виробництва, все частіше використовуються лункові ущільнення. Вони показали досить гарні динамічні та ущільнювальні характеристики при модернізації компресорів хімічної промисловості. Деякі конструкції лункових ущільнень здатні не тільки підвищити динамічні характеристики (додаткове використання вихрових гальм у вигляді напіввідкритих лунок на вході), але й завдяки гібридній конструкції лункового та лабіринтного ущільнень з матеріалу РЕЕК, яка забезпечує мінімальний зазор між ущільненням і валом, зменшують витoki перекачуваної рідини.

У цій статті наведено результати розрахунку роторно-динамічних і витратних характеристик лункових і лабіринтно-лункових ущільнень в залежності від робочих параметрів за допомогою методів обчислювальної гідродинаміки (ОГД). ОГД методи використовувалися для розрахунку гідродинамічних і ротородинамічних характеристик ущільнення з прецесією вала. Ротородинамічні коефіцієнти отримано методом частотного збудження. Отримані характеристики порівнювали з експериментальними даними, наявними в літературі для шпаринних і лабіринтних ущільнень. Дослідження підтвердило відносно низькі витoki, високі динамічні характеристики лабіринтно-лункових ущільнень, частотну залежність коефіцієнтів жорсткості та демпфування. Підтверджено, що лунки створюють перешкоди для окружного потоку робочого середовища. Зменшення окружного потоку газу збільшує гідравлічний опір у канавках і одночасно мінімізує циркуляційні сили, які створюють прецесію валу, посилюючи вібрацію.

Ключові слова: витoki, ротородинамічні коефіцієнти, лабіринтне та лункове ущільнення, демпферне ущільнення, вихрові гальма



Increasing the wear resistance of plunger pairs of high-pressure fuel pumps using extreme pressure additives

D.D. Marchenko*, K.S. Matvyeyeva, V.M. Kurepin

**Mykolayiv National Agrarian University, Mykolayiv, Ukraine*

E-mail: marchenkodd@mnau.edu.ua

Received: 22 September 2024; Revised: 05 October 2024; Accept: 19 October 2024

Abstract

The paper presents studies and substantiates extreme pressure additives that are in demand in almost all areas where heavy equipment and machines operate: in heavy industry, metallurgy and metalworking, machine tool manufacturing, aircraft and shipbuilding, automotive production, construction, and power engineering. At the same time, the development and use of this type of additives in energy facilities of the agro-industrial complex is very difficult due to their relative high cost, and the lack of a complete scientific study of the problem does not contribute to the widespread use of extreme pressure additives in agricultural tractor engines. Therefore, there was a need to conduct scientific research to assess the effect of extreme pressure additives on the performance of high-pressure fuel pumps and, based on the information obtained, to develop production recommendations. In the course of the research, a functional model of the plunger pair performance indicator was obtained, taking into account the performance properties of summer diesel fuel with extreme pressure additives. The results of experimental studies are presented, taking into account the performance properties of summer diesel fuel with extreme pressure additives. The results of production tests of plunger pairs of high-pressure fuel pumps using summer diesel fuel with an extreme pressure additive have been obtained. The use of summer diesel fuel with an extreme pressure additive allows increasing the service life of plunger pairs of high-pressure fuel pumps from 1230 to 2214 hours; recommendations for using fuel for 14 kN traction class engines have been developed. The friction coefficient decreases from 0.005 to 0.001 when plunger pairs operate on summer diesel fuel with an extreme pressure additive. The results have been obtained for selecting the component composition of the additive in diesel fuel and recommendations for using the extreme pressure additive in diesel fuel have been developed.

Key words: wear resistance, coefficient of friction, fuel pump, friction steam, diesel fuel, anti-seize additive, resource tests.

Introduction

The main type of motor fuel used in modern internal combustion engines (ICEs) used in agriculture is diesel fuel. In an internal combustion engine, motor fuel is not only a source of thermal energy, it performs a number of other functions that are directly related to ensuring the longevity and economy of the engine. In particular, motor fuel in diesel fuel equipment is used as a working fluid and as a lubricating medium for fuel equipment pairs that rub, etc. Insufficient lubricity of diesel fuel is the reason for the failure of the working elements of diesel fuel equipment of internal combustion engines, namely piston pairs high pressure fuel pumps (HPFP). HPFP plunger pair failures account for 20 to 35% of all engine failures. The failure of the plunger pairs occurs due to wear, galling and seizing of the materials of the parts of the precision pairs.

One of the ways to ensure the serviceable condition and resource of piston pairs of diesel equipment is the use of an anti-seize additive in diesel fuel. Currently, such additives are not used in diesel fuel. However, in the domestic and foreign literature, there is no information about the chemotological composition of the anti-caking additive. In this regard, the thesis proposes the use of an anti-caking additive based on ethylene triglyceride hydrogen hydroxide. Such an additive consists of a lubricating component, an oxidizer and a fuel combustion stabilizer. The use of an anti-seize additive contributes to the adsorption of boundary films on the rubbing surfaces of precision pairs. The anti-seize additive for diesel fuel, consisting of polar molecules of a chain structure, has



high compressive strength, elasticity and, in the presence of normal pressure, provides the possibility of sliding as a result of shifting along the planes formed by the end groups of molecules. The strength of the structured film increases with increasing pressure, which helps prevent contact between rubbing surfaces [1].

Additive components have both a high lubricating capacity and the ability to increase the energy capacity of diesel fuel.

The research in the article, aimed at ensuring the working condition of the plunger pairs of the high-pressure fuel pump by using an anti-seize additive in diesel fuel, is relevant.

Literature review

It is known from the practice of operating diesel fuel equipment that failures of plunger pairs account for about 65...80% of all HPFP failures (depending on the HPFP brand).

Failures of plunger pairs are mainly caused by natural mechanical wear of materials on the surfaces of plunger pairs.

The cause of mechanical wear of the materials of the plunger pair is metal contact, which occurs as a result of the contact pressure between the parts and is a consequence of the displacement of the lubricating liquid (namely, diesel fuel) from the gap. Moreover, the magnitude of the contact voltage is subject to Hertz's law and increases depending on the movement of the plunger in accordance with the law of motion of the camshaft cam (the law of motion of the plunger).

Numerous studies have established that fuel equipment, being one of the main elements of a diesel engine, in a number of cases does not ensure its required reliability in operating conditions and causes 25...30% of all engine failures [2].

Conducted studies on determining the average working life in real operating conditions show a significant reduction in the resource of pumps. With a confidence probability of 0.9, the average operating time of the pumps before their replacement was from 2.94 to 4.24 thousand. motorcycle watch

As research by V.E. Gorbanevsky showed, in the vast majority of cases, deterioration of fuel injection parameters is associated with problems of friction and wear of friction pairs of fuel equipment. Parts of friction pairs are made of steel, have high hardness (about 60 HRC) and low roughness (R_a up to 0.04 μm for precision and up to 0.32 μm for precise surfaces). The diametric gaps are 1...2 μm in precision and 10...40 μm in precise sliding pairs.

In works on ensuring the durability of friction steel pairs of fuel equipment, the most profound generalizing works are taken as a basis, such as, for example, the domestic structural and energy theory of friction by B.I. Kostecki.

From [3] studies of natural of fuel equipment friction pairs, data on plunger pairs are of particular interest. Gorbanevskiy V.E. and Kyslov V.G. it was found that the wear of the precision surface of the plunger is more often observed on the head on the side opposite to the working cutting spiral, i.e. in the zone where the influence of the maximum pressing forces (created by the pressure of 50...80 MPa) of an impact nature (the period of pressure build-up) is observed, it is superimposed on the effect of the maximum (2...4 m/s) movement speed of the plunger in each working cycle.

Our studies of the jamming of the plunger pairs of 36 in-line pumps of the MW type of combine diesel engines (the pump's service life 746...2740 engine hours) showed that, as a rule, in in-line pumps, jamming of one, rarely - two pairs of plungers occurs. At the same time, a similar jamming pattern was observed. It should be noted that the other pump plunger pairs had good surface condition, without visible damage or stains. An element-by-element analysis of the injection line of the failed sections revealed that when the nozzles of the nozzles of the nozzles coked in the high-pressure line, the effect of water hammer was observed. Since HPFPs of the MW type have a high injection pressure and the plunger is unbalanced (there is no symmetrical groove in relation to the cut-off groove), as a result, jamming of the plunger pair occurs [4].

Antipov V.V., Bakhtiyarov N.I., Zagorodskikh B.P. and others note that the working surfaces of the plungers and bushings are worn by abrasive particles contained in the fuel.

Research conducted by TsNITA showed that the wear of the plunger pair is local, in the area of the inlet and outlet windows. The total value of the worn friction surface does not exceed 5%, and the nature of the micro-uniformities on it indicates wear from abrasive particles that, together with the fuel, enter the super-plunger space during suction of the plunger. During the injection stroke, part of the fuel flows back into the filler, and the fuel flow is throttled along the plunger stroke, which is accompanied by an increase in pressure in the space above the plunger and a sharp increase in flow rates [5].

The resource of precision pairs increases with a decrease to certain limits of their initial clearances and an increase in hydraulic density [6]. The rational limit of reducing the gap in pairs is determined by the amount of installation and working deformations of the bushings, as well as the fineness of fuel filtration. As the pairs wear, their gap increases, and larger particles begin to have a sharp effect on wear. A change in the gap within 0.6...2.5 μm does not significantly affect the rate of wear, so it is impractical to further reduce the gap. In ND distribution pumps, this gap varies within 0.6...1.6 μm .

With small gaps in pairs, the issue of reducing the probability of the plunger sticking in the bushing becomes particularly important, which is achieved, in particular, by reducing the mounting deformations of the bushing by

reducing the tightening force of the pump fitting, increasing the stiffness of the bushing and improving its design. Research in the State found that when the pressure fitting of the TN type fuel pump is tightened with a torque of 120 Nm, the bushing in the section below the windows is deformed by up to 3 microns. These data were confirmed by studies of the deformation of the parts of the plunger pair during the assembly of the UTN-5 pumps, which were carried out at the IMESH [7, 8].

Gorbanevsky V.E. and Vashchenko O.M. found that with high-quality fuel filtration (cardboard or paper fuel), the filters retain up to 99.5% or more of mechanical particles 2 μm in size and larger, abrasive wear cannot be decisive. The working medium for precision friction pairs is diesel fuel, for precise ones (inside the HPFP) it is a mixture of oil from the diesel oil system with fuel that seeped into the pump crankcase through the gaps of the precision plunger friction pairs.

The use of fuels containing rapeseed oil, FAME - fatty acid methyl ethers, etc., leads to the appearance of deposits, resin formation on parts and assemblies of HPFP, loosening and destruction of non-metallic seals. In HPFP with electronic control, such deposits can cause a change in the characteristics of the control of the fuel supply process and the appearance of numerous diesel malfunctions in general.

The failure of fuel pumps is due to the wear of parts and, as a result, the main adjustment characteristics change. The processing of data obtained by TsNITA during operational tests of UTN-5 pumps showed that 29% of all failures are due to wear of camshaft bearings, 12.5% to violations of the tightness of seals, 29.2% to increased unevenness of fuel distribution and reduced cyclic supply (wear of plunger pairs and injection valves) and 8.5% - to reduce the rotation frequency of the start of the regulator [9].

In fuel-lubricated VE and VP pumps, when low-quality fuel is used or the drive belt is improperly tensioned (in diesels with a belt drive), the drive shaft and its bushings wear out, a gap appears between the drive shaft, the cross and the cam washer, which reaches 0.35 mm. The permissible radial gap between the sleeve and the shaft is 0.25 mm.

Due to the decrease in stiffness of the springs of the mechanical regulators of the HPFP during operation, the rotation frequency of the start of its operation will significantly decrease. Of the parts of the regulator, the following are mainly worn out: legs and axles of loads, bearing brackets, control lever, adjusting bolts, etc. work is 0.127 mm.

In the process of routine work, 32 MW-type pumps were checked for RSV-type all-mode regulators (the regulator unit could not be disassembled). The analysis of the control parameters of 18 HPFPs of the MW type of Cummins 6CTA diesels of Case 2366 combines and 4 VE pumps with all-mode regulators of 4T390 diesels of Case 8825HP self-propelled mowers showed the stability of the regulator parameters set at the factory. In particular, for MW pumps, the value of the rail position differed from the one specified by the manufacturer at the nominal frequency of rotation of the camshaft by 2%, at the regulator start-up mode - by 3%.

At the same time, the volumetric supply of 8 pumps did not satisfy the regulation value due to the low hydraulic density of the plunger pairs. A feature of the operating conditions of distribution pump regulators (types VE, VP) is that fuel is fed into the superplunger space through the regulator cavity. If the fuel is not cleaned satisfactorily, deposits accumulate on the internal walls and parts of the regulator, which later peel off and enter the injection line, disrupting the operation of the plunger pair and the nozzle. In addition, the reduction of the passage section of the jet in the drain fitting due to its clogging negatively affects both the size and the uniformity of cyclic feeds [10].

Along with model mixtures of individual hydrocarbons, naphthenic and aromatic hydrocarbons isolated from kerosene fractions of oil were studied [11].

The tests were carried out in the following mode: sliding speed 1.18 m/s; axial load 100 N; test duration 30 min. The material of the parts of the friction unit is ShKh15 steel.

During sliding friction, the maximum wear is observed in the environment of H-paraffin hydrocarbons. Allowable wear in naphthenic and isoparaffinic hydrocarbons. In aromatic hydrocarbons, the wear regime corresponds to the standard one. The mixture of naphthenic hydrocarbons isolated from kerosene fractions is optimal in terms of lubricating properties. The addition of 10% of aromatic hydrocarbons to the mixture of naphthenic hydrocarbons significantly improves their lubricating properties, while bicyclic aromatic hydrocarbons are more effective [12].

Mineral liquid (DP) [7] (DSTU 2511) is used as a fuel in ground machinery. Under the operating conditions, the DP is in the system and repeatedly passes through friction pairs, being exposed to high temperatures and pressures. During operation, accumulation of oxidation products can occur in the DP during operation, as well as due to long periods of time, the formation of insoluble solid wear products of the system's frictional elements.

For some non-hydrocarbon liquids (synthetic), the wear of ShX15 steel is significantly dependent on the sliding speed (compared to hydrocarbon liquids), which indicates that more complex processes than in hydrocarbons occur in the friction zone.

Purpose

The purpose of the research is to ensure the operational condition and increase the wear resistance of the plunger pairs of the high-pressure fuel pump using an anti-seize additive based on ethylene triglyceride hydrogen hydroxide diesel fuel.

Research methodology

The research stages included:

- selection and justification of the components of the anti-seize additive for summer diesel fuel;
 - conducting laboratory comparative resource tests on commercial diesel fuel and diesel fuel with an anti-seize additive;
 - estimation of hydraulic density of plunger pairs;
 - conducting operational production tests of plunger pairs with an anti-seize additive in diesel fuel.
- The experimental research program included the development and improvement of the following methods:
- methods of selection of anti-seize additive components and the process of obtaining finished motor fuel;
 - methods of assessing the stability of additive components in diesel fuel;
 - methods of evaluating the operational properties of diesel fuel with an anti-seize additive;
 - methods of comparative resource tests of plunger pairs of a high-pressure fuel pump;
 - methods of estimating the hydraulic density of plunger pairs of a high-pressure fuel pump;
 - methods of operational and motor tests of plunger pairs in the high-pressure fuel pump of the D-240 engine.

The method of selecting anti-seize additive components in summer commercial diesel fuel was based on a cluster analysis of existing components of numerical modeling. Numerical modeling involved modeling the density of multicomponent hydrocarbon liquids and the calorific value of fuel with an anti-seize additive.

For numerical modeling, optimization methods were used taking into account vector algebra.

The stability of the additive in diesel fuel was evaluated in static and dynamic mode. Static mode provided evaluation of the delamination of the components of the anti-seize additive in diesel fuel without mechanical influence under the conditions of natural settling of diesel fuel.

In the dynamic mode, the diesel fuel was affected by forced mechanical oscillations with a frequency and amplitude equal to the operating frequency and amplitude of the tractor.

The evaluation of operational properties was carried out according to the methodology outlined in [8] and involved determining the viscosity and density of diesel fuel with an anti-seize additive.

Bench comparative resource tests of plunger pairs were carried out on HPFP type UTN-5 on commercial summer diesel fuel L-40 (DSTU 2511) and commercial summer diesel fuel L-40 (DSTU 2511) with an anti-seize additive.

Research was conducted on serial and specially manufactured equipment.

Diesel fuel of operational group E5/E100 according to DIN classification was used as a prototype of diesel fuel. This motor fuel is a mixture of hydrocarbon petroleum fuel and organic raw material (ethanol), used as an oxidizer and density regulator.

As research [13] shows, ethanol in the hydrocarbon fuel solution is a solvent that reduces the lubricating ability of motor fuel.

The second criterion for the use of ethanol in fuel is a relatively lower calorific value, which reduces the calorific value of the main fuel. The use of pure ethanol in motor fuel, as a rule, involves the modification of diesel fuel equipment and some engine systems.

It is known from [14] that the use of triglyceride helps to change the contact conditions and increase (by 2 or more times) the carrying capacity of hydrocarbon fuels. However, in modern scientific literature, data on the use of this component (including as a component of an anti-caking additive) are not confirmed [15].

Hydrogen hydroxide is used to form a stable colloidal compound, a combustion stabilizer, and a fuel density regulator. The influence of which resource of precision pairs is currently also not investigated.

To obtain a stable solution of hydrocarbon motor fuel based on commercial diesel summer fuel with an anti-seize additive, the method of mixing fuel components with the help of ultrasonic influence was used.

Research results

The conducted resource tests of the plunger pairs of the high-pressure fuel pump showed that the use of commercial summer diesel fuel with an anti-seize additive reduces the intensity of the cyclic supply reduction. That increases the coefficient of stability by 35%, and this indicates an increase in the hydraulic density of the plunger pairs.

The error of approximation of experimental data curves does not exceed 5%, estimated by the method of least squares. The fuel supply at the starting revolutions allows you to determine the technical condition and predict the remaining life of the plunger pairs of the fuel pump. According to the recommendations, fuel supply by plunger pairs of HPFP brand UTN-5 at 100 min^{-1} should be at least 14.5 cm^3 [16].

The obtained experimental data show that when using commercial diesel summer fuel with an anti-seize additive, the resource of the plunger pairs of the fuel equipment increases from 1230 to 2214 motor hours.

Deviations in the resulting data do not exceed 5%, this indicates an accurate theoretical description of the operation of plungers. pairs of HPFP.

At the same time, the comparative resource during resource tests of plunger pairs was 2214 engine hours. when using commercial summer diesel fuel with an anti-seize additive and 1230 engine hours. when running on commercial summer diesel fuel. The data are presented in Fig. 1.

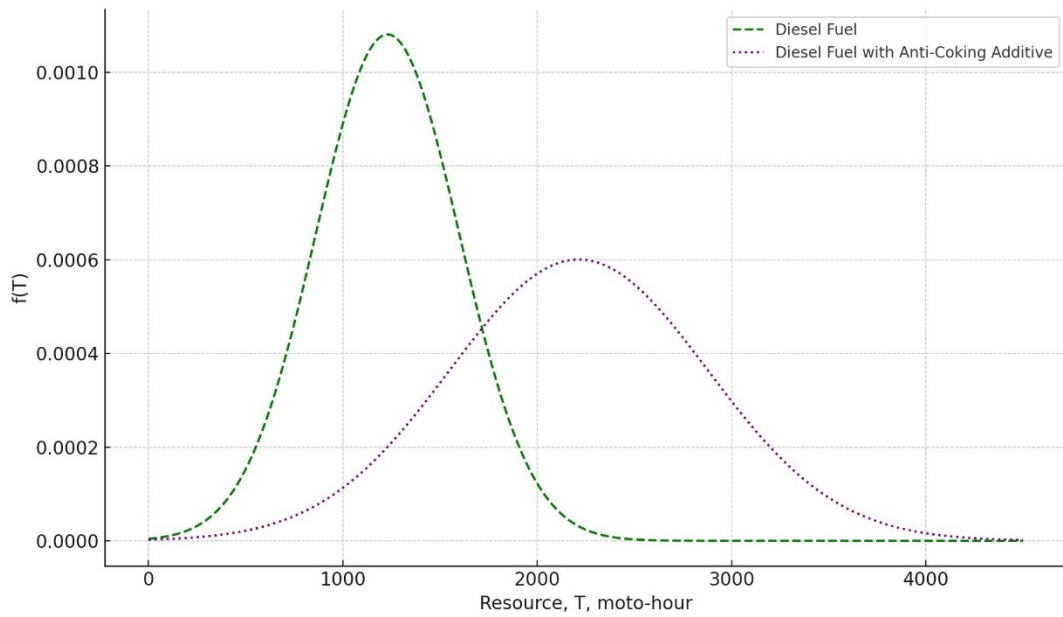


Fig. 1. The density function of the resource distribution of plunger pairs during resource tests

To determine the relationship between the factors, the correlation coefficient was determined. This coefficient was 0.8889 between the coefficient of kinematic viscosity and the density of fuels, -0.8796 between the kinematic viscosity and hydraulic density of piston pairs, -0.8851 between the density and hydraulic density of piston pairs, -0.99647 between the coefficient of friction and hydraulic density of plunger pairs. This indicates a close interrelation of factors.

In Fig. 2, 3 show graphs of changes in the hydraulic density of plunger pairs as a function of kinematic viscosity and friction coefficient.

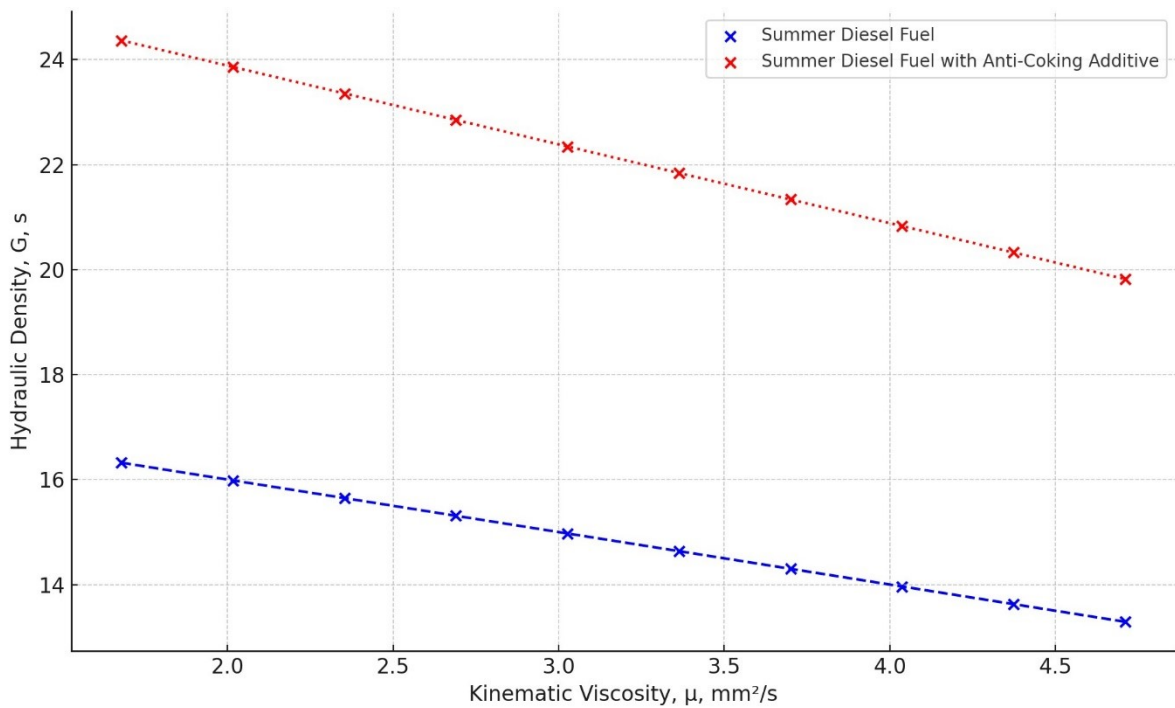


Fig. 2. Graph of changes in hydraulic density of plunger pairs from kinematic viscosity

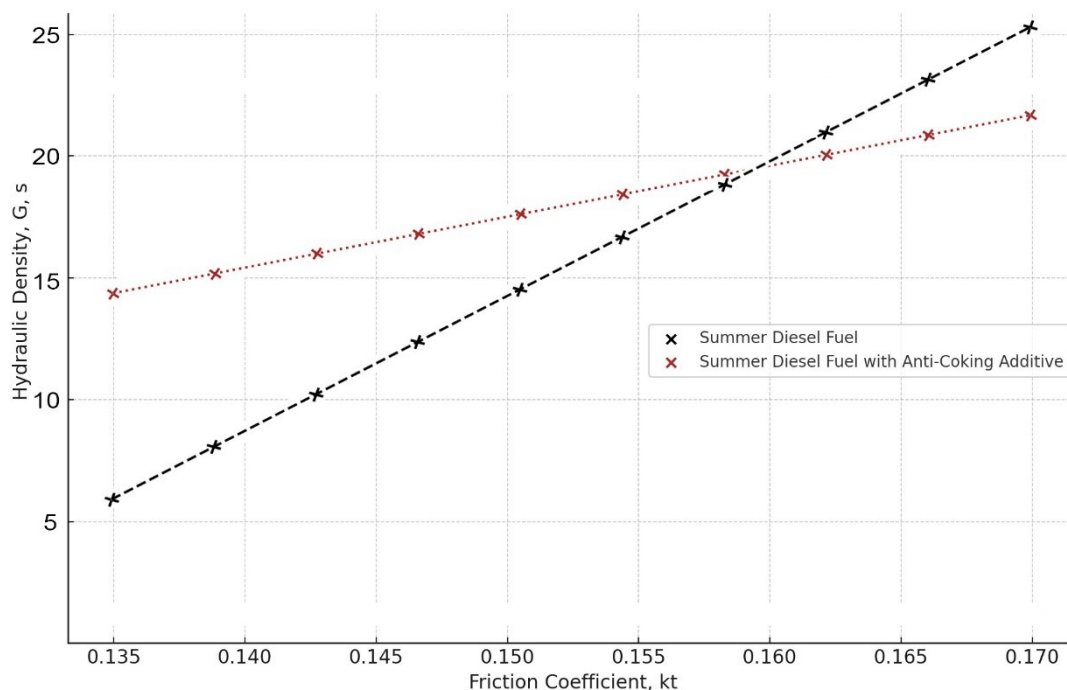


Fig. 3. Graph of changes in the hydraulic density of plunger pairs as a function of the friction coefficient

Fuel with an additive must have certain operational properties. In order to determine the possibility of operation of the plunger pairs of the high-pressure fuel pump on commercial summer diesel fuel with an anti-seize additive, the external speed characteristics of the D-240L diesel engine were determined when it was operating on commercial summer diesel fuel with an anti-seize additive and commercial summer diesel fuel. The obtained results show that when working on commercial summer diesel fuel with an anti-seize additive, the effective power of the engine decreases by 5.7% and the specific effective fuel consumption increases by 10.7%.

Based on the conducted theoretical and experimental studies, when transferring agricultural machinery from one type of fuel to another, no adjustments were made, then it is possible to operate on commercial summer diesel fuel with an anti-seize additive.

The work was carried out on MTZ-82 tractors. Commercial summer diesel fuel and commercial summer diesel fuel with an anti-seize additive were used. Summer diesel fuel (100% DP) was used on the control tractor. The tractors used in the study there are of the same year of production, with the same technical condition.

For the study of piston pairs of HPFP of internal combustion engines, corresponding to the technical requirements of the manufacturing plant were used. Before the test, the hydraulic density of the plunger pairs was determined.

At the HPFP of tractors on the stand, adjustments were made in accordance with the recommendations of the D-240 manufacturer (4Ch 11/12.5). At a frequency of 1100 revolutions per minute, the volumetric cyclic fuel supply in the nominal mode was $74 \pm 3\% \text{ cm}^3$ for 1000 cycles. After measuring the speed characteristics of HPFP on diesel fuel. In the tractor engine, when working on commercial summer diesel fuel with an anti-seize additive, the angle of the moment of fuel supply has been changed from 26 degrees. p.k.v. up to 28 degrees p.k.v. in accordance with the regulatory documentation of the D-240 diesel engine when operating on diesel fuel. Control of the working hours of the tractors was carried out using the used fuel collection card and the motor-hour counter. Motor fuel was supplied to the farm in the required amount based on the calculation of the variable working hours of the tractor [17]. The tractors used in the study performed the same field and transport work.

Determination of the characteristics of HPFP was carried out with a periodicity of 100 engine hours of operation in the conditions of a repair workshop according to the parameter of hydraulic density of plunger pairs. Cyclic feed measurements with the number of cycles of 1000 were performed at starting and nominal crankshaft revolutions. Experimental data show that during the operation of piston pairs on commercial diesel summer fuel with an anti-seize additive, the cyclic supply decreased on average from $V_{ts}=74 \pm 3\% \text{ mm}^3/\text{cycle}$ to $V_{ts}=55 \text{ mm}^3/\text{cycle}$ after observations, and on control piston pairs HPFP, working at the DP changed on average from $V_{ts}=59 \pm 3\% \text{ mm}^3/\text{cycle}$ to $V_{ts}=37 \text{ mm}^3/\text{cycle}$. Changes in the hydraulic density of the state from 24 to 17 from the operation of plunger pairs on commercial summer diesel fuel with an anti-seize additive and from 24 s to 6 s when operating on commercial summer diesel fuel.

Conclusions

1. Established:

- the main failure of HPFP of tractor engines is the failure of plunger pairs (about 65 - 80% of all high

pressure fuel pumps failures);

- the resource of HPFP plunger pairs under normal operation is generally absorbed in 50-60% of the resource declared by the manufacturer.

Failures of plunger pairs are caused by the seizing of their materials, which is a consequence of contact loads and the absence of an anti-seize additive in summer commercial diesel fuel. To ensure the working condition of the plunger pairs, it is necessary to develop the component composition of the anti-seize additive for commercial summer diesel fuel.

The component composition of the anti-seize additive commercial summer diesel fuel, which includes: ethanol, triglyceride, hydrogen hydroxide, is proposed. In this additive, ethanol is a regulator of the anti-seize density of the additive, triglyceride is a component that regulates the process of adhesion of the materials of the plunger pair parts, hydrogen hydroxide is a component that stabilizes the oxidation of triglyceride and the combustion of diesel fuel. The concentration of the additive components is substantiated: ethanol – 25%, triglyceride – 15%, hydrogen hydroxide – 5%, from the total volume of commercial summer diesel fuel. The concentration of components is determined based on the operational properties and calorific value of diesel fuel.

2. The indicator of the working condition of the plunger pair is theoretically substantiated. The functional dependence of the indicator of working condition (watertightness) was developed, taking into account the gap in the "sleeve-plunger" combination and the operational properties of commercial summer diesel fuel with an anti-seize additive.

3. Operational tests established that:

- the water tightness of plunger pairs when working on summer diesel fuel with an anti-seize additive is 17 - 24 s (with the normative value of the water tightness of new plunger pairs 18 - 24 s);
 - the hydraulic density of plunger pairs when working on commercial summer diesel fuel was - 6 - 12 s;
 - the friction coefficient is reduced from 0.005 to 0.001 during operation of piston pairs on summer diesel fuel with an anti-seize additive.

4. It was established during comparative bench resource tests that the resource of plunger pairs increases from 1230 to 2214 engine hours when working on summer diesel fuel with an anti-seize additive.

References

1. An experimental assessment on low temperature combustion using diesel/biodiesel/C2, C5 alcohol blends in a diesel engine / Qixin Ma, Quanchang Zhang, Zunqing Zheng // *Fuel*. 2021, Vol. 288. <https://doi.org/10.1016/j.fuel.2020.119832>.
2. Agarwal, A. K. Effect of Biodiesel Utilization of Wear of Vital Parts in Compression Ignition Engine / A. K. Agarwal, J. Bijwe, L. M. Das // *Transactions of 120 the ASME. Journal of Engineering for Gas Turbines and Power*. 2003, Vol. 125, No 2. P. 604-611.
3. Conversion of rapeseed cake into bio-fuel in a batch reactor: Effect of catalytic vapor upgrading / K. Giannakopoulou, M. Lukas, A. Vasiliev, Ch. Brunner, H. Schnitzer // *Microporous and Mesoporous Materials*. 2010, Vol. 128, Issues 1-3. P. 126-135. <https://doi.org/10.1016/j.micromeso.2009.08.022>.
4. Experimental investigation on performance, combustion and emission analysis of a direct injection diesel engine fuelled with rapeseed oil biodiesel / L. Anantha Raman, B. Deepanraj, S. Rajakumar, V. Sivasubramanian // *Fuel*. 2019, Vol. 246. P. 69-74. <https://doi.org/10.1016/j.fuel.2019.02.106>.
5. Knothe, G. Lubricity of components of biodiesel and petrodiesel: The origin of biodiesel lubricity / G. Knothe, K. Steidley // *Energy & Fuels*. 2005, № 19. P. 1192-1200.
6. LePera, M. Low-Sulfur and Diesel Fuel Lubricity / M. LePera // *Fuel Line Magazine*. 2000, № 4. P. 18-19.
7. Nagornov, S. A. Improving the three-component mixed motor fuel manufacturing process / S. A. Nagornov, A. Yu. Kornev, S. V. Romantzova // *Advanced Materials and Technologies*. 2020, № 2 (18). P. 57-65.
8. O. Lyman, D. Marchenko, "Prospects for the Application of Restoring Electric Arc Coatings in the Repair of Machines and Mechanisms", *Proceedings of the 2022 IEEE 4th International Conference on Modern Electrical and Energy System, MEES 2022*. <https://doi.org/10.1109/MEES58014.2022.10005709>.
9. Study of pressure and temperature influence on rapeseed biodiesel oxidation kinetics using PetroOXY method / Y. L. Machado, J. L. C. Fonseca, J. Q. Malveira, A. A. Dantas Neto, T. N. C. Dantas // *Fuel*. 2020, Vol. 282. <https://doi.org/10.1016/j.fuel.2020.118771>.
10. SuperLuBRisity, ALI ERDEMIR, ELSEVIER, Amsterdam, Netherlands. 2020. 560 p.
11. Marchenko, D., & Matvyeyeva, K. (2022). Increasing warning resistance of engine valves by gas nitrogenization method. *Problems of Tribology*, 27(2/104), 20-27. <https://doi.org/10.31891/2079-1372-2022-104-2-20-27>.
12. Review on the catalytic pyrolysis of waste oil for the production of renewable hydrocarbon fuels / Yunpu Wang, Qi Yang, Linyao Ke, Yujie Peng, Yuhuan Liu, Qiuhaio Wu, Xiaojie Tian, Leilei Dai, Roger Ruan, Li Jiang // *Fuel*. 2021, Vol. 283. <https://doi.org/10.1016/j.fuel.2020.119170>.

13. Marchenko, D., & Matvyeyeva, K. (2022). Study of the Stress-Strain State of the Surface Layer During the Strengthening Treatment of Parts. *Problems of Tribology*, 27(3/105), 82–88. <https://doi.org/10.31891/2079-1372-2022-105-3-82-88>.
14. Wedel, R. *Technical Handbook for Marine Biodiesel in recreational boats* / R. Wedel // CytoCulture international Inc. 1999. P. 35.
15. Dykha A.V., Marchenko D.D. Prediction the wear of sliding bearings. *International Journal of Engineering and Technology (UAE)*. India: "Sciencepubco–logo" Science Publishing Corporation. Publisher of International Academic Journals. 2018. Vol. 7, No 2.23 (2018). pp. 4–8. <https://doi.org/10.14419/ijet.v7i2.23.11872>.
16. Marchenko, D., & Matvyeyeva, K. (2023). Increasing the Wear Resistance of Restored Car Parts by Using Electrospark Coatings. *Problems of Tribology*, 28(1/107), 65–72. <https://doi.org/10.31891/2079-1372-2023-107-1-65-72>.
17. Marchenko, D., & Matvyeyeva, K. (2023). Research of Increase of the Wear Resistance of Machine Parts and Tools by Surface Alloying. *Problems of Tribology*, 28(3/109), 32–40. <https://doi.org/10.31891/2079-1372-2023-109-3-32-40>.

Марченко Д.Д., Матвєєва К.С., Курепін В.М. Підвищення зносостійкості плунжерних пар паливних насосів високого тиску за допомогою протизадирних присадок

У роботі наведено дослідження та обґрунтовано протизадирні присадки, які затребувані практично у всіх галузях, де працює важке обладнання та машини: у важкій промисловості, металургії та металообробці, верстатобудуванні, авіа- та суднобудуванні, автомобільному виробництві, будівництві, енергетиці. Разом з тим, розробка та застосування даного виду присадок в енергосферах агропромислового комплексу дуже скрутна через їхню відносну дорожнечу, а недостатність повного наукового дослідження проблеми не сприяє широкому використанню протизадирних присадок у двигунах сільськогосподарських тракторів. Тому виникла необхідність для проведення наукових досліджень щодо оцінки впливу протизадірної присадки на працездатність паливних насосів високого тиску та на базі отриманої інформації розробки виробничих рекомендацій. У ході досліджень отримано функціональну модель показника працездатного стану плунжерної пари з урахуванням експлуатаційних властивостей літнього дизельного палива з протизадірною присадкою. Наведено результати експериментальних досліджень з урахуванням експлуатаційних властивостей літнього дизельного палива з протизадірною присадкою. Отримано результати виробничих випробувань плунжерних пар паливних насосів високого тиску при використанні літнього дизельного палива з протизадірною присадкою. Використання літнього дизельного палива із протизадірною присадкою дозволяє збільшити ресурс плунжерних пар паливних насосів високого тиску з 1230 до 2214 годин; розроблені рекомендації щодо використання палива для двигунів тягового класу 14 кН. Коефіцієнт тертя знижується з 0,005 до 0,001 під час роботи плунжерних пар на літньому дизельному паливі з протизадірною присадкою. Отримано результати щодо підбору компонентного складу присадки у дизельне паливо та розроблено рекомендації щодо застосування протизадірної присадки у дизельне паливо.

Ключові слова: зносостійкість, коефіцієнт тертя, паливний насос, пара тертя, дизельне паливо, протизадирна присадка, ресурсні випробування



Wear resistance and lubricity of the spiral oil distribution profile of the valve guide sleeves of an internal combustion engine

O.V. Dykha^{*}, A.A. Vychavka, M.O. Dykha

Khmelnytskyi national University, Ukraine

**E-mail: tribosenator@gmail.com*

Received: 05 October 2024; Revised 02 November 2024; Accept 20 November 2024

Abstract

Valve guides are crucial for maintaining the correct alignment, positioning, and clearance of the valve stem as it moves in the cylinder head. When the guides are heavily worn, the engine begins to consume oil and the valve mechanism becomes noisy. Reliable lubrication of the inner surface of the guide bushing ensures the wear resistance of the valve-guide pair. This work proposes a special tool and technology for obtaining an oil-retaining profile on the inner surface of the valve guide, which increases the oil capacity of the surface, and therefore improves the lubrication conditions in the valve-guide friction pair. A gas labyrinth seal is created in the connection, which prevents oil from entering the combustion chamber. The surface of the bushing bore is strengthened due to the sealing of the surface. The results of wear tests of guide bushings with spiral oil-retaining grooves confirmed their effectiveness in terms of wear resistance. The wear rate of the bushings with grooves for the entire time range of the tests is on average 20% less than the wear rate of the bushings without grooves.

Keywords: internal combustion engine, valve guide, lubricity, wear resistance, oil-retaining spiral profile, tests

Introduction

One of the main reasons for repairing the cylinder head is the wear of the valve guide bushings. Bushings are constantly subjected to frictional loads. Lateral forces act on the valve stem, caused by a change in geometry in the valve mechanism, wear of the rocker cam or rocker arm. When the guides have a lot of wear, the engine begins to consume oil and there is an increased noise of the valve mechanism. This applies to both the intake tract (discharge in the cylinder) and the exhaust tract (Venturi effect). Oil in the catalytic converter exhaust system can cause it to overheat and fail. Oil in the intake system can "throw" spark plugs, contaminate exhaust gases, and also quickly accumulate as combustion products on the air surface of the valves and combustion chamber.

Guide bushings have the following defects: wear of the inner surface (58...96%), loosening of the fit (7...13%), cracks and fractures (3...10%). The amount of wear of the bushings has a pronounced uneven character. In the upper part of the bushing, the wear is small and has the shape of an oval, the major axis of which is perpendicular to the longitudinal axis of the engine. In the lower part, the bushings wear out more than in the upper part, while preserving the direction of wear. The greatest wear is observed at the point of impact of the valve stem on the sleeve with subsequent sliding at extreme friction. Greater wear of exhaust bushings compared to intake bushings is due to the additional heat load in combination with the valve.

Valve guides, which are critical to maintaining proper alignment, positioning, and clearance of the valve stem as it moves through the cylinder head, are typically made from materials that offer high wear resistance and improved thermal conductivity. The choice of material for guide valves largely depends on the operating conditions and requirements of the engine or mechanism. Manganese bronze is a group of high-strength, hard bronzes that are typically used in assemblies that require a combination of high strength, wear resistance, and corrosion resistance. Such alloys provide excellent durability and heat dissipation properties.

Review of literary sources



Research [1] was carried out on different failure modes of internal combustion engine valves. The closed valve is loaded by the force of the spring and the pressure inside the cylinder, which periodically changes during engine operation and reaches a peak value. This pressure inside the cylinder causes the valve cone to bend, resulting in slippage and improper contact between the valve face and seat insert, ultimately leading to wear. An analysis of exhaust valve failures was carried out in [2]. diesel engine. A visual inspection of the damaged engine parts showed that the fracture of the exhaust valve showed signs characteristic of fatigue failure. Additional observations of the crack initiation zones showed that the origin of the crack was not covered by material defects or corrosion products. Direct injection engines have a well-known propensity for intake valve deposits, regardless of operator maintenance, engine architecture, or cylinder configuration [3]. The process of deposit formation is not sufficiently studied and there is no standardized engine test to study the effect of variable fuel composition or lubricants. The article [4] analyzed the problems associated with the vibration diagnosis of the valve gap of the internal combustion piston engine, which is significant from the point of view of efficiency and durability. Classification methods are proposed for evaluating valve clearance. Experiments aimed at providing the information necessary for the development and verification of the proposed methods were conducted and described. In work [5] malfunctions of automobile valves were considered. Changes in the microstructure of the valves were studied and analyzed using a scanning electron microscope. The samples were made from failed engine valves, while new valves were also analyzed for comparison. The article [6] presents an analysis of elements of piston internal combustion engines that interact with the combustion chamber. An assessment of the condition of the tribological nodes: valve stem – valve guide and valve head – valve seat in random operating conditions was carried out. In the article [7], he proposed a device for determining wear for studying the tribological characteristics of the connections of the valve mechanism of the engine. The device uses a mechanical load system, which consists of a special eccentric wheel and disk springs that simulate the load from the engine combustion chamber, as well as simulate the contact loads of the valve mechanism elements. The test bench has three functions for different studies using specially designed instruments. Pairs of valves and valve seat inserts with the same material and structural properties, but with different operating conditions, were analyzed in [9] to study the wear process. The identified wear mechanisms were a combination of oxidation and adhesive wear, which was observed in the form of material transfer. The purpose of the research [10] is to study the dry sliding characteristics of GG25 cast iron with copper additives. It has been established that changes in load and sliding speed affect the wear characteristics is of primary importance. Loads were changed step by step, maintaining a constant speed.

Thus, increasing the wear resistance and lubricity of the parts of the valve mechanism of the internal combustion engine is an urgent task.

Causes of failure and deflection of guide bushings

Valve guide bushings are made of wear-resistant materials with fairly good thermal conductivity. These are special cast iron, metal ceramics, bronze and brass. Bronze and brass have a higher thermal conductivity, which is why they are used on most forced engines, for example, BMW, Audi, Volvo. To fix the sleeve in height, there is usually a support shoulder on the outer surface of the head of the cylinder block. Sometimes a split support ring is used instead. If the sleeve is smooth on the outside, then a special mandrel or remote sleeve will be needed to install it in the head.

The guide bushings of the intake valves should not protrude too much in the intake channel so as not to increase its aerodynamic resistance. But exhaust valve sleeves, on the contrary, should cover the valve stem for the maximum length to protect against heated exhaust gases and for better heat removal from the exhaust valve stem. If the guide bushings are made of bronze or brass, then they usually have the same length, since these alloys have high thermal conductivity.

The geometric dimensions and general appearance of the guide sleeve are shown in fig. 1.

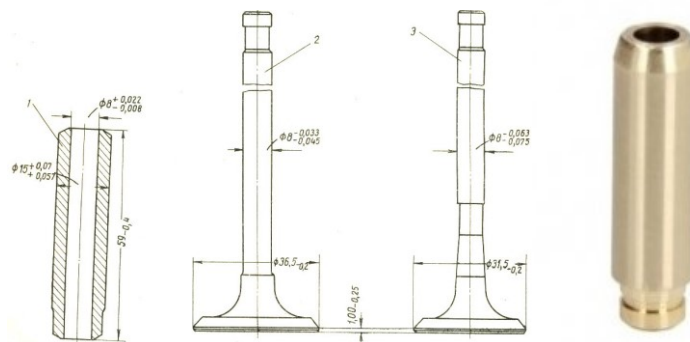


Fig. 1. The geometric dimensions and general appearance of the guide sleeve

Guide bushings have the following defects: wear of the inner surface (58...96%), loosening of the fit (7...13%), cracks and fractures (3...10%). The amount of wear of the bushings has a pronounced uneven character.

In the upper part of the bushing, the wear is small and has the shape of an oval, the major axis of which is perpendicular to the longitudinal axis of the engine. In the lower part, the bushings wear out more than in the upper part, while preserving the direction of wear. The greatest wear is observed at the point of impact of the valve stem on the sleeve with subsequent sliding at extreme friction. More wear of exhaust bushings compared to intake bushings is due to the additional heat load in combination with the valve. At the time of overhaul, wear of the valve bushings in the upper part is usually 0.06...0.08 mm, and in the middle part 0.04...0.07 mm. In the lower part, the wear of the bushings above reaches 0.24 mm or more. The coefficient of unevenness of wear along the length of the product is equal to: for intake valve bushings 3...4, for exhaust valve bushings 8...13. But in addition to natural wear, there are other reasons for the guide sleeve to fail. For example, if the timing belt breaks, the bushing can crack due to the bend of the valve. Improper installation or removal of oil caps can lead to deformation or breakage of the seat under the cap.

In engines receiving major repairs, clearances in the valve-sleeve combination are usually 1.5...3.5 times higher than the nominal ones. This leads to an increase in the consumption of oil for smoke through the valve-sleeve steam by 18...20%, and an increase in the smokiness of the processed gases - by 10...15%.

Operations for processing valve chamfers and seats are considered the most important in the technological process of repairing block heads. But there is an equally responsible operation – replacement (or restoration) of guide bushings, which are the technological basis for further processing of the saddle. Often, when repressing the bushings, the axis of the hole is shifted, which, with a large "skew", does not allow processing the working chamfer of the saddle of the same width all around. As a result, the heat dissipation is disturbed, and subsequently the seat or valve plate may burn out. In addition, the "skew" of the axis leads to accelerated wear of the valve stem and face.

Defecting guide bushings is a necessary condition for high-quality repair of the cylinder head. Due to the small hole, there are certain difficulties in controlling the dimensions of worn bushings. Defection of the bushings is carried out with the help of calipers or gauges (Fig. 2).



Fig. 2. Tool for measuring valve bushings.

The feeler gauge and cylindrical calipers allow for defecting of guide bushings with an accuracy of 0.01 mm. A micrometer is used to measure the valve stem. Measurements of the valve are necessary to determine the "sleeve-valve" gap.

In practice, most heads that come in for repair have bushings with wear that exceeds the allowable (usually 0.15 mm or more). As a rule, "exhaust" bushings are worn out more than "intake" bushings, which is explained by their increased thermal load. Traditionally, sleeve wear in a horizontal section has a pronounced ellipse with a larger axis in the plane of the rocker arm swing (rotation of the camshaft cam), and in a vertical section it resembles a "corset".

Technological methods of repairing valve guide bushings

The technology of replacing bushings by repressing is traditional. Aluminum heads are usually heated to a temperature of 1100C. They work with cast iron heads without their heating. Bushings must be pressed out using special mandrels and a pneumatic hammer or hydraulic press. This provides additional load along the axis of the bushing and minimizes damage to the hole (seat) of the bushing. When pressing the bushings, they are first cooled in liquid nitrogen, and then the block head is installed using special mandrels. After pressing, the opening of the sleeve must be processed to a size that provides the necessary thermal gap for the "sleeve-valve" connection.

In the presence of repair valves, the bushing is first deployed under the repair diameter of the valve stem, and then under the required gap between the bushing and the valve. The clearance is the same as for standard valves. When deploying the sleeve to obtain the correct geometry of the opening, it is necessary to start from the side of the removable cap, as this part of the sleeve is subject to less wear.

The bushing opening can be restored without pressing by using the method of plastic deformation of the metal. Using the tool set for the restoration of guide bushings from the company Neway (USA), it is possible to restore bushings with hole diameters from 6 to 12 mm. The degree of restoration of the worn hole in the sleeve is

determined by its material. For example, bushings made of non-ferrous materials with wear up to 0.5 mm can still be restored, and bushings made of strong cast iron or metal ceramics only with wear up to 0.15 mm.

The technology of restoring guide bushings by installing thin-walled sleeves made of special copper alloys is used. For the reliable application of this technology, it is not enough to have only a set of tools, and it is also necessary to observe the modes and sequence of operations. As a finishing operation, the hole is drawn with a ball.

Thus, the main advantage of bushing restoration technologies is maintaining maintainability due to the elimination of bushing repressing operations.

Restoring and increasing the wear resistance of guide bushings by knurling the oil-retaining profile

In this work, the use of a special knurling tool is proposed to restore and increase the wear resistance of guide bushings (Fig. 3).



Fig. 3. A special tool for restoring valve bushings.

The TOKAR (8.1) Knurling & Resizing arbors HSS tool is designed for restoring guide valves by rolling a spiral groove on the inner surface of the sleeve. This allows to reduce the internal diameter of the valve guide by deformation of the material. The material of the tool is HSS (High Speed Steel) – HRC 62±1. Restoration (knurling) of the valve guide must be carried out from a tool of smaller diameter with further increase to the stop of the valve guide rod, the entrance to the sleeve. The cone of the working part prevents the parts from cracking. Knurling reduces the size of the hole with an allowance of 0.04-0.06 mm, depending on the material. Example: The output size of a $\varnothing 8.02$ valve guide after rolling a $\varnothing 8.1$ bore will be $\varnothing 7.95-7.98$, depending on the material. After restoration (rolling), the inner hole is calibrated with a reamer of the required size.

The guides were processed on a lathe (Fig. 4). The sleeve was centered and fixed in the cam cartridge and rotated. The tool carried out a progressive axial feed movement.



Fig. 4. Treatment of the oil-retaining profile of the valve guide sleeve

After applying this technology, a spiral oil retaining profile remains on the surface of the sleeve opening, which:

- increases the oil capacity of the surface, and therefore improves the lubrication conditions in the "valve-guide" friction pair;
- a gas-labyrinth seal is created in the connection, which prevents oil from entering the combustion chamber;
- the surface of the sleeve opening is strengthened due to surface compaction (slender effect).

Since due to the spiral groove, the surface of the hole in the sleeve is reduced by only 10... 15%, its presence has almost no effect on the service life of the cylinder block, since the valve in the sleeve oscillates within the thermal gap and the valve stem never contacts the sleeve over the entire surface of the hole.

In fig. 5 shows the profile of the spiral oil retention grooves formed on the inner surface of the valve guide sleeve. The profile of the grooves, in accordance with the design of the tool, had a rounded shape.



Fig. 5. Spiral oil retaining grooves of the valve guide sleeve

In the process of plastic processing of the oil-retaining grooves in the opening of the guide bushing, the surface layer of the working surfaces is defamed, which also contributes to increasing the wear resistance of the bushings with grooves.

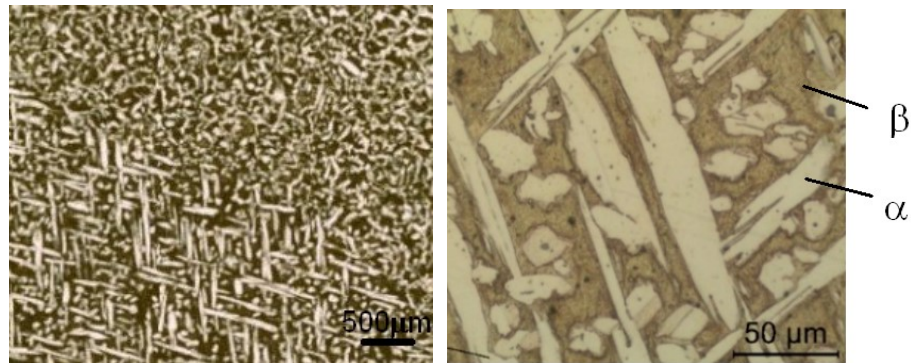


Fig. 6. Photomicrographs of the surface layer of bronze after plastic processing of the grooves

Optical microphotographs of the materials shown in fig. 6 show that the alloy consists of an α -phase and a β -phase, and that the α -phase has a long island shape typical of deformed bronze. In the microstructure, the light regions correspond to the α -phase, which has a face-centered cubic (fcc) lattice, while the dark regions correspond to the β -phase, which has a body-centered cubic (bcc) lattice. As a result of plastic deformation, the granular structure of the copper alloy is crushed.

Study of the wear resistance of the valve guide with oil retaining grooves

Tests for the wear of guide bushings were carried out on a special stand (Fig. 7).

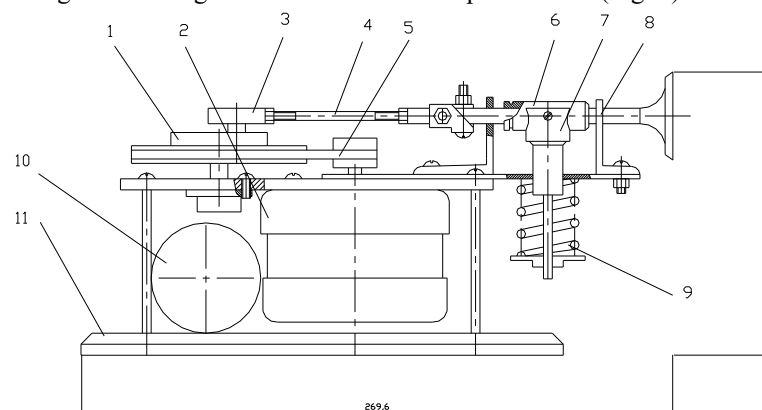


Fig. 7. Experimental stand for testing valve mechanism wear

The stand is mounted on the platform 11. The valve movement is driven by the DC motor 2, the shaft of which is located vertically and flanged to the intermediate plate. The engine shaft is equipped with a belt transmission pulley 5 to reduce the number of engine revolutions. On the driven pulley 1 there is a crank-sliding mechanism for converting rotary motion into translational motion. The valve moves in the guide sleeve 6 from the crank mechanism. The load on the coupling is carried out using a spring 9. A capacitor 10 is used to start the engine.

The tests were carried out under the following conditions. The load on the sleeve is 150 N. The number of double strokes of the valve is 100 strokes/min. Lubrication was carried out with engine oil M-8B.

The amount of wear of the guide bushing was periodically measured by an indirect method of measuring the chord L of the trace of wear on the ends of the bushing according to the diagram in Fig. 8 as the average value of two indicators.

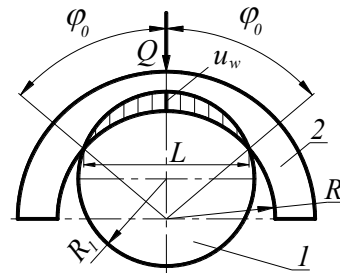


Fig. 8. Scheme for measuring the wear of the guide sleeve of the valve mechanism

The amount of linear wear was determined by the formula:

$$u_w(\varphi_0) = \Delta(\sec \varphi_0 - 1),$$

where Δ – the nominal gap between the valve and the sleeve;

φ_0 – the contact angle between the sleeve and the valve:

$$\phi_0 = \arcsin(L / 2R).$$

The tests were carried out for two versions of guide bushings: with a spiral groove and with a smooth hole. The results of tests and calculations are given in the table. 1.

Table 1

The results of determining the wear of the guide bushings of the valve mechanism

Number of cycles x103	2	4	6	8	10	12	14	16	18
Wear (K), μm	50	100	140	160	170	175	178	180	182
Wear (G), μm	70	120	160	185	200	210	220	230	235

In fig. 9 shows a graphical interpretation of the results of tests on the wear of guide bushings of the valve mechanism.

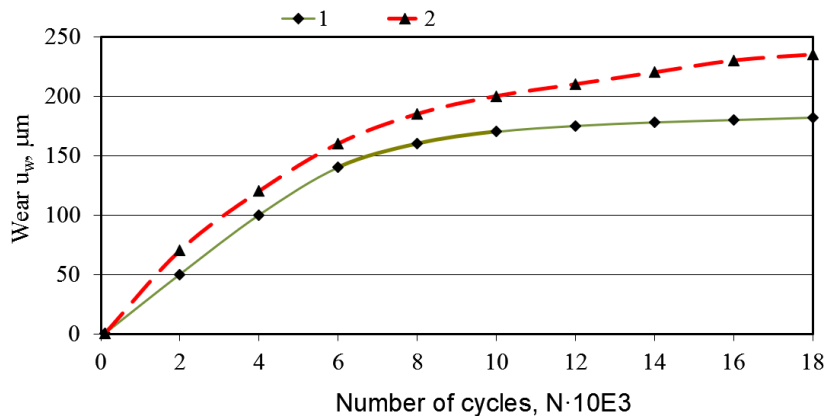


Fig. 9. The results of tests on the wear of valve mechanism bushings: 1- guide with grooves, 2- guide smooth.

Therefore, the results of the wear tests of guide bushings with spiral oil retention grooves confirmed their effectiveness according to the criterion of wear resistance. The value of wear of bushings with grooves for the entire time range of tests is on average 20% less than the value of wear of bushings without grooves.

Conclusions

1. A special tool and technology for obtaining an oil-retaining profile on the inner surface of the valve guide is proposed, which increases the oil capacity of the surface, and therefore improves the lubrication conditions in the "valve-guide" friction pair. A gas labyrinth seal is created in the connection, which prevents oil from entering the combustion chamber. The surface of the sleeve opening is strengthened due to surface sealing (slander effect).

2. The results of the wear tests of guide bushings with spiral oil retention grooves confirmed their effectiveness according to the criterion of wear resistance. The value of wear of bushings with grooves for the entire time range of tests is on average 20% less than the value of wear of bushings without grooves.

References

1. Raghuvanshi, NK, Pandey, A., & Mandloi, RK (2012). Failure analysis of internal combustion engine valves: a review. *International Journal of Innovative Research in Science, Engineering and Technology*, 1(2), 173-181. [failure-analysis-of-internal-combustion-enginevalves-a-review-libre.pdf \(d1wqtxts1xzle7.cloudfront.net\)](#).
2. Witek, L. (2016). Failure and thermo-mechanical stress analysis of the exhaust valve of diesel engine. *Engineering Failure Analysis*, 66, 154-165. <https://doi.org/10.1016/j.engfailanal.2016.04.022>
3. Guinther, G., & Smith, S. (2016). Formation of intake valve deposits in gasoline direct injection engines. *SAE International journal of fuels and lubricants*, 9(3), 558-566. <https://doi.org/10.4271/2016-01-2252>
4. Tabaszewski, M., & Szymański, GM (2020). Engine valve clearance diagnostics based on vibration signals and machine learning methods. *Exploatacja and Reliability*, 22(2), 331-339. <https://bibliotekanauki.pl/articles/1365185.pdf>
5. Pandey, A., & Mandloi, RK (2014). Effects of high temperature on the microstructure of automotive engine valves. *Journal of Engineering Research and Applications*, 4(3), 122-126. [X4301122126-libre.pdf \(d1wqtxts1xzle7.cloudfront.net\)](#)
6. Monieta, J. (2017). Analysis of the tribology processes of control valves of medium speed marine internal combustion engines. *Tribologia. Analysis of the tribology processes of control valves of medium speed marine internal combustion engines - Tribologia - Tom nr 4 (2017) - BazTech - Yadda (icm.edu.pl)*
7. Lai, F., Qu, S., Yin, L., Wang, G., Yang, Z., & Li, X. (2018). Design and operation of a new multifunctional wear apparatus for engine valve train components. *Proceedings of the Institution of Mechanical Engineers, Part J: Journal of Engineering Tribology*, 232(3), 259-276. <http://dx.doi.org/10.1016/j.wear.2015.08.017>
8. Rylski, A., & Siczek, K. (2013). Friction resistance between valve made of TiAl alloy and its guide made of phosphor bronze. *Applied Mechanics and Materials*, 404, 220-227. <https://doi.org/10.4028/www.scientific.net/AMM.404.220>
9. Forsberg, P., Hollman, P., & Jacobson, S. (2011). Wear mechanism study of exhaust valve system in modern heavy duty combustion engines. *Wear*, 271(9-10), 2477-2484. <https://doi.org/10.1016/j.wear.2010.11.039>.
10. Singh, B., Singh Grewal, J., Kumar, R., Sharma, S., Kumar, A., Mohammed, KA, ... & Ismail, EA (2024). Novel study on investigating the mechanical, microstructure morphological, and dry sliding wear characteristics of gray cast iron GG25 with copper additions for valve guides in internal combustion engines. *Frontiers in Materials*, 10, 1293254. <https://doi.org/10.3389/fmats.2023.1293254>

Диха О.В., Вичавка А.А., Диха М.О. Зносостійкість і мастильна здатність спірального маслорозподільного профілю напрямних втулок клапанів двигуна внутрішнього згорання

Направляючі клапанів мають вирішальне значення для підтримки правильного вирівнювання, позиціонування та зазору штока клапана під час його руху в головці блоку циліндрів. Коли напрямні мають велике зношування, то двигун починає витрачати масло і з'являється підвищений шум клапанного механізму. Надійне змащування внутрішньої поверхні напрямної втулки забезпечує зносостійкість пари «клапан-напрямна». В даній роботі запропонований спеціальний інструмент і технологія отримання маслоутримувального профілю на внутрішній поверхні напрямної клапана, який збільшує маслостійкість поверхні, а отже, покращуються умови змащення в парі тертя «клапан-напрямна». Створюється газолабіринтне ущільнення у сполученні, що запобігає потраплянню масла у камеру згорання. Зміцнюється поверхня отвору втулки за рахунок ущільнення поверхні. Результати випробувань на знос напрямних втулок із спіральними маслоутримувальними канавками підтвердили їх ефективність за критерієм зносостійкості. Величина зносу втулок із канавками для всього часового діапазону випробувань в середньому на 20% менша ніж величина зносу втулок без канавок.

Ключові слова: двигун внутрішнього згорання, напрямна клапана, мастильна здатність, зносостійкість, маслоутримувальний спіральний профіль, випробування



Dependence of wear intensity on the coating material of the hydraulic cylinder of the garbage truck's sealing plate

O.V. Bereziuk^{1*}, V.I. Savulyak¹, V.O. Kharzhevskiy², A.Ye. Alekseev¹

¹*Vinnitsia National Technical University, Ukraine*

²*Khmelnitskyi National University, Ukraine*

*E-mail: berezyukoleg@i.ua

Received: 10 October 2024; Revised 05 November 2024; Accept 25 November 2024

Abstract

The article is dedicated to the study of the influence of the coating material on the wear rate of the hydraulic cylinder of the mechanism of the garbage truck's sealing plate. By means of a first-order planning of experiment with first-order interaction effects using the Box-Wilson method, an adequate dependence of the wear rate of the hydraulic cylinder of the mechanism of the garbage truck's sealing plate on the coating material was determined. It is established that according to the Student's criterion, among the studied factors of influence, the intensity of wear of the hydraulic cylinder of the mechanism of the garbage truck's sealing plate is most affected by the iron content in the coating, the least – by the chromium content, and the nickel content affects only indirectly in interaction with the iron content. The response surfaces of the goal function – the intensity of wear of the hydraulic cylinder of the mechanism of the garbage truck's sealing plate and their two-dimensional sections in the planes of the influence parameters are shown, which allow to clearly illustrate the specified dependence of this goal function on individual influence factors. The expediency of conducting further research to determine ways to further improve the wear resistance of the hydraulic cylinder of the mechanism of the garbage truck's sealing plate is shown.

Keywords: wear, wear resistance, wear rate, hydraulic cylinder, mechanism, sealing plate, garbage truck, coating material, municipal solid waste, dependence, experiment planning.

Introduction

One of the important tasks of mechanical engineering is to increase the wear resistance and reliability of actuators of machines' mechanisms [1, 2], especially municipal ones, which mainly use hydraulic drive of working bodies. One of the main technologies for the primary processing of municipal solid waste (MSW) aimed at reducing transportation costs and reducing the negative impact on the environment is its compaction during the loading process into a garbage truck. Solid waste is compacted in a garbage truck using a compaction plate, the hydraulic cylinder of which is subject to intense wear due to the large number of operating cycles and significant pressing forces. This is due to the nonlinear compression characteristic of solid waste. Hydraulic cylinders are usually made of alloy steel, and wear-resistant coatings are widely used to increase their wear resistance. Therefore, it is an important task to determine the dependence of the wear rate of the hydraulic cylinder of the garbage truck's sealing plate mechanism depending on the coating material.

Analysis of recent research and publications

The scientific article [1] analyzes the disadvantages of using fluoropolymers in the friction unit "piston seal – car air conditioner compressor cylinder". Promising methods of modifying polytetrafluoroethylene and requirements for its fillers are considered. There was experimentally confirmed the advantages of antifriction composite fluoroplastic materials that were modified with combined fillers: carbon and glass fiber, carbon fiber and copper or lead oxide powder for the friction unit "piston seal – car air conditioner compressor cylinder"



In the paper [2] the effect of laser pretreatment on the nitriding intensity, structure, and wear characteristics of nitrided coatings on VT6 titanium alloy is considered. It is shown that pretreatment reduces the nitriding time, while increasing the thickness of the nitrided layer. It is established that the wear intensity is determined by the tribological structures of dissipative type arbitrarily formed in contact, which are formed from ultra-dispersed products of interaction of the components of the solid bodies of the friction pair and lubricants. The wear resistance of coatings obtained with pretreatment is 1.5-2 times higher than the wear resistance of coatings that are obtained by the traditional method.

In the scientific article [3], by means of the regression analysis it was established the power law that describes the dynamics of wear and tear of garbage trucks in the Khmelnytskyi region that allows its forecasting. This helps to plan the infrastructure of utility companies, including the composition and renewal of the garbage truck fleet, as well as the development of the base for their maintenance and repair, which is important for effective solid waste management. According to the forecast, the level of depreciation of garbage trucks in Khmelnytskyi region by 2030 will decrease to 51.9% if the current rate of renewal is maintained.

Among the main components of garbage trucks with side loading of MSW, the hydraulic system has the lowest mileage before failure, which, according to the research [4], significantly affects the increase in overall wear and tear of garbage trucks. In the paper [5] is shown that the structure and main causes of hydraulic equipment failures are: hydraulic cylinders – 34.92% (wear of seals, rod; rupture of the piston to rod fastening nut; rod bending; mechanical damage), hydraulic pumps – 16.40% (wear of the housing, gears, seals, cracks), pipelines and hoses – 15.34% (hose ruptures, pipeline wear), hydraulic distributors – 13.23% (wear of seals and spools; cracks in the housing).

An analysis of the causes of technical failures of garbage truck units [6] showed that a significant proportion of failures (about 45%) are associated with hydraulic drive failures. These failures are mostly caused by manufacturing defects arising from the use of low-quality components, as well as large fluctuations in the loads on the working mechanisms. The study of the causes of failures of working bodies showed that breakdowns are caused by defects in heat treatment and deviations from the design dimensions during machining (35%), as well as defects in the assembly, adjustment and tightening of threaded connectors (30%) and poor-quality welding (30%). It has been found that the vast majority of failures (80-90%) are caused by wear and corrosion of the working surfaces of machine parts. At the same time, failure does not occur immediately, but only when wear or corrosion reaches a certain critical level. It was also found that hydraulic cylinder failures caused by wear of the mating surfaces, deformation of the rod and cylinder during operation – up to 28% of all hydraulic drive component failures. Analysis of the durability results shows that the average operating time before failure of hydraulic actuator components, in particular the hydraulic cylinder, is approximately 1/3 of the maximum. That is, the manufacturer does not implement the planned service life by 45-55%. Most of the failures of hydraulic cylinder parts after the start of operation or repair are related to rods (31%) and sealing cuffs (42%). The analysis of failures of hydraulic system elements showed that the main faults are associated with the loss of external and internal tightness due to contamination of the working fluid, which leads to malfunctioning of the units.

These data are consistent with the results published in [7], which also indicates the main causes of failures of the hydraulic system of garbage trucks caused by wear: for a hydraulic pump – wear of gears; for hydraulic cylinders – wear of seals and rod; for a hydraulic distributor – wear of seals and spools; for hoses – wear of pipelines. Adequate dependencies of wear of garbage truck tires on the front and rear axles were determined according to the Fisher's criterion, which depend on the transported mass of MSW and the mileage of the garbage truck. According to the Student's criterion, it was found that the transported mass of MSW has the greatest impact on tire wear on both the front and rear axles, while the mileage of the garbage truck has the least impact. The dependencies of the number of garbage truck trips before the maximum permissible wear of tires on the front and rear axles were obtained.

The scientific paper [8] provides the causes of garbage truck failures, according to which the main causes of failures are external and internal leaks in hydraulic systems. External leakage was in 48% of all failures in the hydraulic system and occurs due to the destruction of hoses and pipelines, as well as due to the depressurization of seals in hydraulic cylinders and other units. Another significant cause of failure is internal leaks, which was in 36% of cases. Most of the failures caused by internal leaks are observed in such units as spool valves, safety and check valves, hydraulic cylinders and hydraulic pumps.

A study that was carried out in [9] showed that "tapered" wear of the hydraulic cylinder rod from 0.2 to 0.4 mm in length during the operation of the hydraulic cylinder before the first overhaul leads to a 7.2% decrease in pressure, an 11.4% increase in specific fuel consumption, and a 26% increase in the carbon monoxide content in exhaust gases. Increasing the wear of the rods in their working area by 0.6-0.7 mm causes a drop in pressure in the hydraulic system by 13.4%, an increase in specific fuel consumption by 21.3%, and a sharp increase in the toxicity of exhaust gases from 25% to 59%, which exceeds the maximum permissible standards. It is proposed to consider the wear of the geometric parameters of the hydraulic cylinder rod of the hydraulic drive of construction and road machines as the maximum permissible wear if its value does not exceed 0.4 mm. It was also found that rod wear worsens the physical and chemical properties of the working fluid, doubling the content of iron and impurities. This leads to the need for more frequent fluid changes and cost overruns, which significantly

reduces efficiency and durability, as well as shortens the service life of the hydraulic drive of construction and road machines.

The article [10] showed that the wear of sealing elements in hydraulic systems causes the gradual penetration of hydraulic fluid into non-working cavities of hydraulic machines. Although this process is not always visible, it leads to unproductive power losses of the hydraulic drive, which, in turn, increases fuel and lubricant consumption and reduces the power of the working bodies. The power loss due to the wear of sealing elements can cause non-optimal operating modes of the hydraulic motor, which negatively affects the efficiency of the hydraulic drive in general. The mechanical system "hydraulic cylinder – sealed piston – compressed hydraulic fluid" was researched. Thus, it was established the dependence of the efficiency of the hydraulic cylinder on the size of the leakage, and the results of the piston subsidence for the working fluid of the VMGZ type and the mechanism of fluid flow through the hydraulic cylinder seal are determined.

In the paper [11], the authors analyzed data from observations of garbage trucks and found that most failures are caused by wear and corrosion of the working surfaces of the equipment parts. Failures of hydraulic cylinders caused by wear of working surfaces, deformations of the rod and cylinder during operation account for 32% of all breakdowns of hydraulic drive parts. This is due to uneven loading of the body and abrasive wear of the working surfaces under conditions of intensive operation of the garbage truck. Studies of the cases of failures have shown that the main reason is the wear of the working surfaces of the main elements of the hydraulic drive, in particular spools and hydraulic distributor housings, hydraulic cylinder rods and other components. The main reason of the wear was found to be water-abrasive damage caused by untimely replacement of the hydraulic fluid and the use of low-quality or worn sealing elements, such as hydraulic cylinder seals. This causes that dust particles and wear products got into the sliding zone, which accelerates the wear of the working surfaces of the parts. One of the most promising methods for restoring worn parts is chromium plating in a cold self-regulating electrolyte, which produces chrome coatings with high quality deposits and ensures high performance of the process.

In the paper [12], the wear-resistant coatings alternative to galvanic chromium plating for the protection of hydraulic cylinders was analyzed and the optimal operating conditions under which each of them will be most effective were determined. It was also performed comparative studies of wear resistance in different working environments of protective multilayer vacuum-plasma coatings obtained by applying alternately thin layers of chromium and complex nitride (TiCr)N, α -Ti layers, titanium nitride - TiN and magnetron coating based on TiN, oxide ceramic coatings on aluminum electric arc coatings sprayed on a base of magnesium alloy MA-5, titanium alloy PTZV.

Paper [13] presents the results of studies on the effect of the pressing force on the wear rate of hydraulic press mechanism parts, in particular, on the hydraulic cylinder. Studies have shown that with an increase in the force applied during pressing, there is a decrease in the acceleration coefficient of the wear of the working cylinder. This indicates that higher forces do not always lead to faster wear, but rather that wear can slow down due to the peculiarities of the mechanism's operation under high loads. This result may be important for further optimization of hydraulic presses, as it allows to predict the service life of components depending on the operating conditions. In addition, the work showed the importance of developing effective measures for continuous automatic control of press operation parameters. This includes monitoring of the pressing force, hydraulic fluid temperature, and other critical indicators that may affect press operation. Preventing the hydraulic press from approaching emergency limits is a key factor for ensuring reliable and faultless operation of all its major components. The successful implementation of such control systems avoids situations where the system operates under conditions that can lead to breakdowns or premature wear. This is possible if the press is designed rationally, using high-quality materials and ensuring that all performance characteristics meet the specified requirements, which in turn can significantly increase the efficiency and durability of the equipment.

Paper [14] deals with the effect of the pressing force on the wear resistance of the working hydraulic cylinder of the garbage truck's sealing plate mechanism. An exponential dependence of changes in the rate of wear of the working hydraulic cylinder of the mechanism of the garbage truck's sealing plate depending on the pressing force was determined. It was established that for a Ukrainian-made garbage truck of the model KO-436, the wear rate of the working hydraulic cylinder of the mechanism of the garbage truck's sealing plate, according to the obtained dependence, will be 0.257 $\mu\text{m/h}$.

In the paper [15], it was researched the structure, hardness, and wear resistance of plasma coatings made of metals of the fourth row of the periodic table's fourth period: iron, nickel, and chromium, made from the mixtures of the corresponding powders to replace wear-resistant galvanic chromium coatings. Based on the determination of the intensity of molecular-mechanical and abrasive wear, the optimal composition of the plasma coating, which has advantages of galvanic chromium and free from its disadvantages, was proposed.

However, as a result of the analysis of known publications, it should be noticed that the authors did not find any specific mathematical dependencies in the intensity of wear of the hydraulic cylinder of the garbage truck's sealing plate mechanism on the coating material.

Aims of the article

Determination of the dependence of the wear intensity of the hydraulic cylinder of the mechanism of the garbage truck's sealing plate on the coating material.

Methods

The determination the dependence of changes in the intensity of wear of the hydraulic cylinder of the garbage truck's sealing plate mechanism from the coating material was carried out by planning a first-order experiment with first-order interaction effects using the Box-Wilson method. The coefficients of the regression equations were determined using the developed computer program "PlanExp", which is protected by a certificate of copyright law's registration.

Results

Preliminary processing of the results of experimental studies [15] showed that the wear rate of the hydraulic cylinder of the garbage truck's sealing plate mechanism is a function of the following three main parameters:

$$I_h = f(C_{Fe}, C_{Ni}, C_{Cr}), \quad (1)$$

where I_h – the intensity of abrasive wear, $\times 10^{10}$; C_{Fe} – the iron content in the coating of Fe-Cr-Ni composition, %; C_{Ni} – the nickel content in the coating of Fe-Cr-Ni composition, %, C_{Cr} – the chromium content in the coating of Fe-Cr-Ni composition, %.

The research of the influence of the above factors on the wear rate of the hydraulic cylinder of the mechanism of the garbage truck's sealing plate when processing the results of single-factor experiments by regression analysis is associated with significant difficulties and amount of work. Therefore, in our opinion, it is advisable to conduct a multifactorial experiment to obtain a regression equation for the response function – the wear rate of the hydraulic cylinder of the mechanism of the garbage truck's sealing plate by planning a multifactorial experiment using the Box-Wilson method.

The values of the wear intensity of the hydraulic cylinder of the mechanism of the garbage truck's sealing plate for different composition of the coating material are given in the Table 1 [15].

Table 1

Values of the intensity of wear of the hydraulic cylinder of the mechanism of the garbage truck's sealing plate for different composition of the coating material [15]

Abrasive wear intensity $I_h, \times 10^{10}$	Iron content in the coating $C_{Fe}, \%$	Nickel content in the coating $C_{Ni}, \%$	Chromium content in the coating $C_{Cr}, \%$
1.979	75	25	0
0.947	50	25	25
0.547	25	25	50
1.789	0	0	100

Based on the data in the Table 1, using a first-order experiment planning with first-order interaction effects, using the developed software protected by a copyright law's certificate, after rejecting insignificant factors and interaction effects by the Student's criterion, the dependence of the intensity of wear of the hydraulic cylinder of the mechanism of the garbage truck's sealing plate from the coating material was determined as follows:

$$I_h = 0,07343 C_{Cr} - 0,6671 C_{Fe} + 0,03053 C_{Fe} C_{Ni} - 5,554 [\times 10^{10}]. \quad (2)$$

Fig. 1 shows the response surfaces of the goal function – the wear intensity of the hydraulic cylinder of the mechanism of the sealing plate of the garbage truck I_h and their two-dimensional sections in the planes of the influence parameters, drawn using the equation (2), which allows to clearly illustrate this dependence.

It was found that according to Fisher's criterion, the hypothesis about the adequacy of the regression model (2) can be considered correct with 95% confidence. The coefficient of multiple correlation was determined as $R = 0.96513$, which indicates quite sufficient accuracy of the results.

According to the Student's criterion, it was established that among the studied factors of influence, the intensity of wear of the hydraulic cylinder of the mechanism of the garbage truck's sealing plate is most affected by the iron content in the coating, the least – by the chromium content, and the nickel content has an indirect effect only in interaction with the iron content.

The determination of the ways to further improve the wear resistance of the hydraulic cylinder of the garbage truck's sealing plate mechanism requires further research.

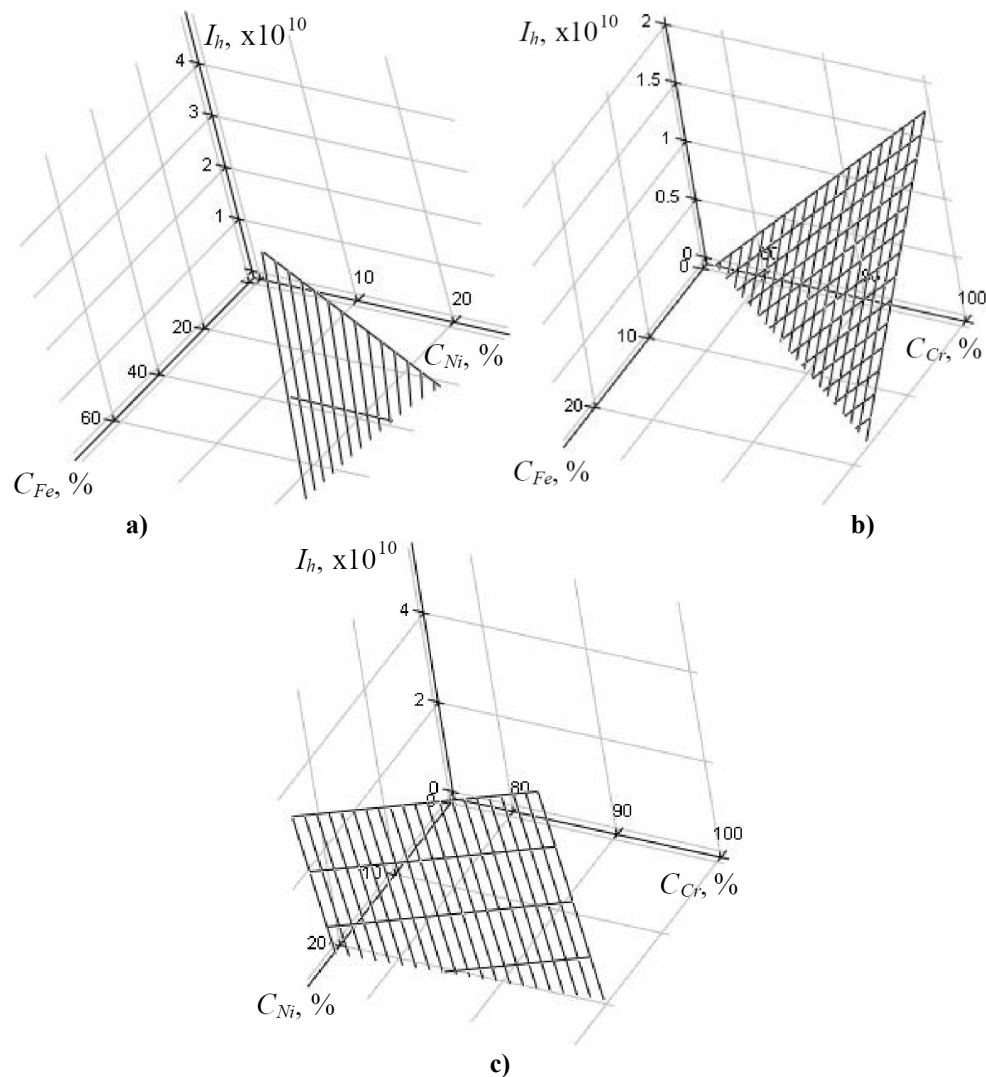


Fig. 1. Response surfaces of the goal function - wear intensity of the hydraulic cylinder of the mechanism of the garbage truck's sealing plate I_h in the planes of influence parameters: a) $I_h = f(C_{Fe}, C_{Ni})$; b) $I_h = f(C_{Fe}, C_{Cr})$; c) $I_h = f(C_{Ni}, C_{Cr})$

Conclusion

The adequate dependence of the intensity of wear of the hydraulic cylinder of the mechanism of the garbage truck's sealing plate on the coating material was determined according to the Fisher criterion. It is established that, according to the Student's criterion, among the studied factors of influence, the intensity of wear of the hydraulic cylinder of the mechanism of the garbage truck's sealing plate is most affected by the iron content in the coating, the least – by the chromium content, and the nickel content affects only indirectly in interaction with the iron content. The response surfaces of the goal function – the intensity of wear of the hydraulic cylinder of the mechanism of the garbage truck's sealing plate and their two-dimensional sections in the planes of the influence parameters are shown, which allow to clearly illustrate the specified dependence of this goal function on individual influence factors. The determination of the ways of improvement of the wear resistance of the hydraulic cylinder of the garbage truck's sealing plate mechanism requires further research.

References

1. Dykha O., Sviderskyi V., Holenko K. (2024) Pidvyshchennia antyfryktsiinykh kharakterystyk porshnevnykh ushchilnen kompresora kondytsionera avtomobilia [Increasing the anti-friction characteristics of car air conditioner compressor piston seals]. Herald of Khmelnytskyi National University. Technical sciences, 333(2), 314-321, <https://doi.org/10.31891/2307-5732-2024-333-2-50>.
2. Kharchenko V., Kindrachuk M., Marchuk V., Yurchuk A., Kostetskyi I. (2024) Kombinovana obrobka i mekhanizm znoshuvannia azotovanykh pokryttiv na tytanovomu splavi VT-6 [Combined treatment and wear mechanism of nitrided coatings on titanium alloy VT-6]. Problems of friction & wear, 103(2), 121-129, [https://doi.org/10.18372/0370-2197.2\(103\).18694](https://doi.org/10.18372/0370-2197.2(103).18694)

3. Bereziuk O.V., Savulyak V.I., Kharzhevskiy V.O. (2022) Dynamics of wear and tear of garbage trucks in Khmelnytskyi region. *Problems of Tribology*, 27(3/105), 70-75, <https://doi.org/10.31891/2079-1372-2022-105-3-70-75>
4. Nosenko A.S., Domnickij A.A., Altunina M.S., Zubov V.V. (2019) Theoretical and experimental research findings on batch-operation bin loader with hydraulically driven conveying element. *MIAB. Mining Informational and Analytical Bulletin*, 11, 119-130, <http://dx.doi.org/10.25018/0236-1493-2019-11-0-119-130>.
5. Lobov N.V., Maltsev D.V., Genson E.M. (2019) Improving the process of transport of solid municipal waste by automobile transport. *Proceedings of IOP Conference Series: Materials Science and Engineering*. IOP Publishing, 1(632), 012033, <https://doi.org/10.1088/1757-899X/632/1/012033>.
6. Kotomchin A.N., Lyakhov Yu.G. (2019) Analysis of failures of knots and units of construction, road, lifting and transport machines and specialized motor transport on the example of MUE "Communal service". *Engineering & Computer science*, 3, 174-178.
7. Bereziuk O.V., Savulyak V.I., Kharzhevskiy V.O. (2023) Establishing the peculiarities of tire wear of garbage trucks during the transportation of municipal solid waste. *Problems of Tribology*, 28(1/107), 59-64, <https://doi.org/10.31891/2079-1372-2023-107-1-59-64>
8. Kabashev R.A. (1997) Road and construction machines: abrasive wear of the working parts of earthmoving machines. Almaty: Gylym.
9. Nurakov S.N., Savinkin V.V. (2008) About development methods for calculating the wear of the rod cylinder interface of hydraulic machines. *Proceedings of the Karaganda State Technical University*, 3 (32), 96.
10. Shalapai VV, Machuga OS (2023) Vraty potuzhnosti u hidrotsylindri vnaslidok protikannia hidravlichnoi ridyny cherez neshchilnist [Power loss in a hydraulic cylinder due to hydraulic fluid leakage through a leak]. *Integrated quality assurance of technological processes and systems – 2023: materials of the XIII International Scientific and Practical Conference, May 25-26, 2023, Chernihiv. National University “Chernihiv Polytechnic”*, 287-289.
11. Kargin R.V., Yakovlev I.A., Shemshura E.A. (2017) Modeling of workflow in the grip-container-grip system of body garbage trucks. *Procedia Engineering*, 206, 1535-1539, <https://doi.org/10.1016/j.proeng.2017.10.727>.
12. Student MM, Gvozdetskyi VM, Kalahan OS, Posuvaylo VM, Shmirko VM, Sirak Ya (2015). Porivnialni kharakterystyky znosostiikosti oksydykh ta nitrydykh pokryttiv [Comparative characteristics of wear resistance of oxide and nitride coatings]. *Problems of Tribology*, 77(3), 54-59.
13. Korchak O.S., Bilenets K.E. (2019) Doslidzhennia trybotekhnichnykh vlastyvopei sylovykh tsylindriv hidravlichnykh presiv na bazi inzhenernoi metodyky otsinky yikh resursu bezvidmovnoi roboty [Investigation of tribotechnical properties of power cylinders of hydraulic presses based on an engineering methodology for assessing their uptime]. *Material Processing by Pressure*, 1, 186-192, [http://dx.doi.org/10.37142/2076-2151/2019-186\(48\)](http://dx.doi.org/10.37142/2076-2151/2019-186(48))
14. Bereziuk O.V., Savulyak V.I., Kharzhevskiy V.O., Alekseiev A.Ye. (2024) Determination of the regularity of the rate of wear of the working hydraulic cylinder of the mechanism of the sealing plate of the garbage truck from the pressing force. *Problems of Tribology*, 29(1/111), 38-44, <https://doi.org/10.31891/2079-1372-2024-111-1-38-44>
15. Mannapova O.V., Sokolov O.D. (2013). Vyznachennia skladu plazmovoho pokryttia za rivnem znoshuvannia [Determination of the plasma coating composition by the level of wear]. *Problems of friction and wear*, 2, 73-79.

Березюк О.В., Савуляк В.І., Харжевський В.О., Алексєєв А.Є. Залежність інтенсивності зносу від матеріалу покриття гідроциліндра ущільнюючої плити сміттевоза

Стаття присвячена дослідженню впливу матеріалу покриття на інтенсивність зносу гідроциліндра механізму ущільнюючої плити сміттевоза. За допомогою використання планування експерименту першого порядку з ефектами взаємодії першого порядку методом Бокса-Уїлсона визначено адекватну закономірність інтенсивності зносу гідроциліндра механізму ущільнюючої плити сміттевоза від матеріалу покриття. Встановлено, що за критерієм Стюдента серед досліджених факторів впливу найбільше на інтенсивність зносу гідроциліндра механізму ущільнюючої плити сміттевоза впливає вміст заліза у покритті, найменше – вміст хрому, а вміст нікелю впливає лише опосередковано у взаємодії із вмістом заліза. Показано поверхні відгуку цільової функції – інтенсивності зносу гідроциліндра механізму ущільнюючої плити сміттевоза та їхні двомірні перерізи в площинах параметрів впливу, які дозволяють наглядно проілюструвати вказану залежність даної цільової функції від окремих факторів впливу. Показано доцільність проведення наступних досліджень з визначення шляхів подальшого підвищення зносостійкості гідроциліндра механізму ущільнюючої плити сміттевоза.

Ключові слова: знос, зносостійкість, інтенсивність зносу, гідроциліндр, механізм, ущільнююча плита, сміттевоз, матеріал покриття, тверді побутові відходи, закономірність, планування експерименту.



Research on the wear resistance of the material cylinder of an automatic injection molding machine during plastics processing

V.A. Honchar

Khmelnytskyi National University, Ukraine

E-mail: rogervova@gmail.com

Received: 15 October 2024; Revised 10 November 2024; Accept 29 November 2024

Abstract

The article presents experimental studies of the pressure in the material cylinder of the D3328 automatic injection molding machine when processing various plastics, as well as experimental studies of wear along the length of the material cylinder of the DB3328 automatic injection molding machine after processing PS 68-30 fiberglass. Specially designed strain gauge pressure sensors were used. Signals from the sensors were output to an oscilloscope through the amplifying equipment and recorded on an oscillogram. The magnitude and distribution of pressure along the length of the material cylinder will significantly affect the amount of wear of both the screw and the cylinder. It was established that the pressure in the material cylinder of automatic injection molding machines is distributed unevenly along its length. The nature of the pressure distribution along the length of the material cylinder when processing various materials: during the injection period, the maximum pressure occurs in the melt zone with a subsequent sharp decrease in the middle zone and a slight increase in the loading zone. At the same time, the nature of the pressure change for all materials is similar at a diametrical gap between the screw and the cylinder $\delta=0.17$ mm. With an increase in the gap δ to 0.74 mm, the nature of the pressure distribution in the injection zone changes only when processing fiberglass, which is due to the partial ingress of glass fibers into the gap between the screw and the cylinder. Its magnitude and nature of the distribution along the length for different materials are different and depend on the physical, mechanical and rheological characteristics of these materials, the design of the screw and the technological modes of processing. The maximum pressure occurs in the melt zone during the period of material injection into the mold for 0.4-0.5 s.

Key words: wear, fiberglass, cylinder, pressure, sensor.

Introduction

In modern conditions of the development of society, plastics are increasingly used in the national economy and technology. Products made of plastics in the household and household in many cases exceed 50% of the total number of used items. The reason for such widespread use of plastic products is a number of their advantages over other materials related to economy and practicality. In connection with this, the equipment for processing plastics - extruders and thermoplastic machines - has received a great development. Extruders are continuous-acting machines, while thermo-plastic machines work cyclically, making products by casting into molds under a certain pressure [1-5]. Melting of plastics is achieved by heating them with special heaters and extrusion in the extrusion unit. The extrusion unit of thermoplastic machines includes a material cylinder and a screw with an injection system. The screw has a rotary and reciprocating movement, which it performs, respectively, during the period of collecting a portion of plastic and during the injection period.

Research Methodology

During the operation of the injection molding machine, a large pressure (up to 200MPa) occurs in the material cylinder, which affects both the strength of the material cylinder [5-7] and the wear resistance of the screw-cylinder pair [8]. The amount of pressure in the material cylinder of extruders and thermoplastic machines varies along its length and will be different when processing different materials. Therefore, the study of the



magnitude and distribution of pressure in the material cylinder of thermoplastic machines and extruders and the nature of wear of the screw and cylinder of this unit during the processing of various materials are relevant.

We have carried out research on the amount of wear along the length of the material cylinder of the DB-3328 thermoplastic machine after its operation during PS 68-30 fiberglass processing. Research has established that the amount of wear along the length is different and was from 0.5 to 2 mm per diameter. The maximum wear of 2 mm was in the injection zone at a distance of 80 mm from the end of the cylinder and in the fiberglass loading zone (1.85 mm) at a distance of 400 mm from the injection zone. In the space between these zones, the amount of wear decreased to 0.5 mm. It is known from literary sources that the intensity of wear depends on many factors (properties of the material of the friction pairs, specific load on the friction surface, properties of the environment, temperature, sliding speed, etc.), among which the pressure on the friction surface is of great importance. In extruders and thermoplastic machines, friction and wear of parts occurs as a result of their contact with the processed material and when the surfaces of the screw and cylinder are in direct contact. The amount and distribution of pressure along the length of the material cylinder will significantly affect the amount of wear of both the screw and the cylinder. The maximum pressure in the material cylinder depends on the design parameters of the screw and cylinder, the temperature, the viscosity of the processed mass, and the rotation frequency of the screw and is theoretically found according to the formulas [9-10]:

- for variable height of screw turns and variable material viscosity:

$$P_{\max} = \frac{\pi^2 D^2 n}{60} \left(\frac{\mu_1}{h_1^2} + \frac{\mu_2}{h_2^2} + \dots + \frac{\mu_z}{h_z^2} \right), \quad (1)$$

- for screws with a constant height of the turn and a constant viscosity:

$$P_{\max} = \frac{\pi^2 D^2 n \mu L}{60 h^2 \cdot H}, \quad (2)$$

where: D is the outer diameter of the screw;

n – rotation frequency of the screw;

H – screw pitch;

L – screw length;

h_1, h_2, h_z – the height of the screw turn;

μ_1, μ_2, μ_z – the viscosity of the material melt at the boundaries of each turn of the screw.

The injection pressure for thermoplastic machines can be determined by the formula:

$$P_{ip} = \frac{\rho_2 D_2^2 \eta}{d^2} K_1 K_2, \quad (3)$$

where P_{ip} – pressure in the hydraulic system of the injection molding machine;

D_2 – the diameter of the injection cylinder of the hydraulic system;

η – coefficient of useful action of the hydraulic cylinder;

K_1 – the coefficient that takes into account friction costs in the melt;

K_2 – the coefficient that takes into account the costs of hydraulic shocks.

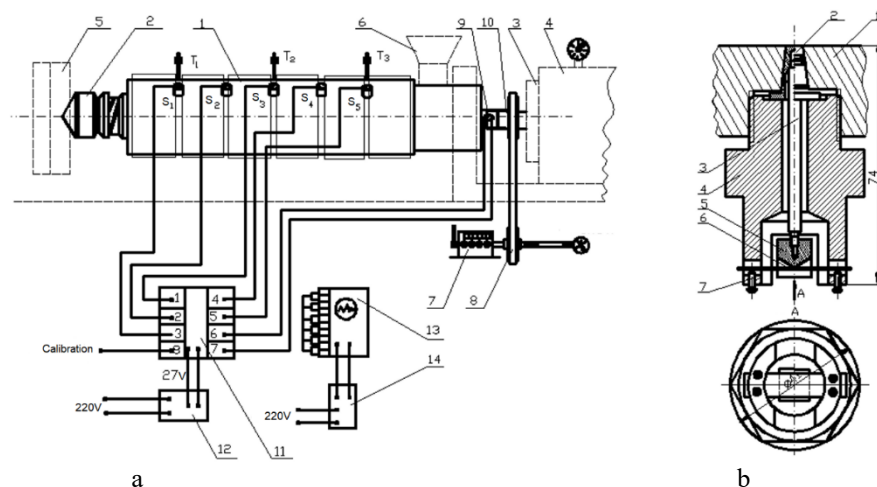


Fig. 1. a) Scheme of the experimental installation for determining the operational characteristics of thermoplastic machines and extruders: 1—material cylinder; 2—mouthpiece; 3—reducer; 4—hydraulic cylinder of the injection mechanism; 5—press form; 6—loading hopper; 7—screw rotation counter; 8—belt transmission; 9—strain gauges for torque measurement; 10—screw; 11—current amplifier; 12—amplifier power supply unit; 13—oscilloscope; 14—current rectifier; S_1, S_2, S_3, S_4, S_5 —pressure sensors; T_1, T_2, T_3 —thermocouples. b) Pressure sensor: 1—material cylinder; 2—tail; 3—rod; 4—sensor body; 5—prism; 6—beam; 7—adjusting screw.

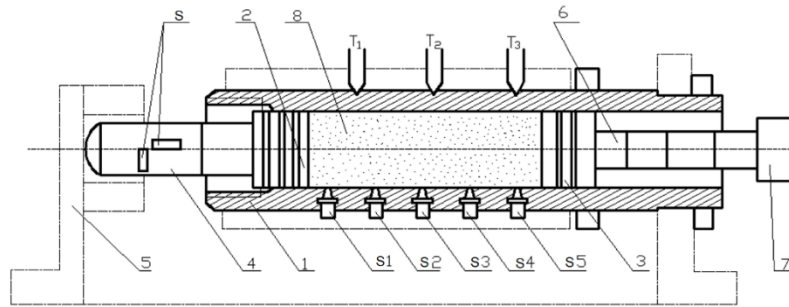


Fig. 2. Calibration scheme of pressure sensors: 1—material cylinder; 2—left plug; 3—right plug; 4—assembly rod; 5—mover; 6—rod of the right plug; 7—hydraulic cylinder rod; S1, S2, S3, S4, S5—pressure sensors; T1, T2, T3 — thermocouples; D is a strain gauge for measuring axial force.

Due to the fact that the pressure of the melt in the material cylinder of extruders and thermoplastic machines depends on many factors that are difficult to theoretically determine and take into account, there is a need to conduct experimental studies of the pressure in the material cylinder in different periods of the work cycle when processing different materials.

In order to study the pressure distribution along the length of the material cylinder from the injection molding machine during the processing of various plastics (high-pressure polyethylene, polystyrene, Kapron and fiberglass), an experimental installation (Fig. 1) was made on the basis of the injection molding machine D3328, in the material cylinder in which 5 pressure sensors were installed. The design of pressure sensors and the method of their installation in a material cylinder are shown in fig. 1. Signals from pressure sensors were output to the oscilloscope through the amplification equipment and recorded on the oscillogram. In the process of research, temperature in 3 zones, screw rotation frequency, torque and axial force on the screw were monitored.

The torque on the screw was measured by the tonometry method. The pressure in the hydraulic cylinder of the injection mechanism was measured by a standard pressure gauge and the tonometry method to record rapid pressure changes. The rotation frequency of the screw was fixed by a revolution counter.

Calibration of pressure sensors and strain gauges when measuring torque and axial force was carried out on a special device (Fig. 2) under conditions similar to the operating conditions of a thermoplastic molding machine with heating of plastic materials to 200-250°C. The auger was removed from the cylinder of the injection molding machine, the mouthpiece was unscrewed, and specially made plugs were inserted into it from both sides. The left plug 2 rested against the plate 5 through the collecting rod 4. The material cylinder was filled with plastic that melted as a result of heating by heaters. Through plug 3, with the help of rod 6 and the hydraulic injection cylinder of the hydraulic system, pressure was created when the "injection" button was turned on. The pressure in the material cylinder was recorded by sensors S1, S2, S3, S4 and S5, as well as a strain gauge glued on rod 4, which was previously tared and used as a dynamometer. Signals from sensors S1, S2, S3, S4 and S5 and the strain gauge on rod 4 were recorded through the amplifier on oscillograms, on the basis of which calibration graphs were built.

Experimental studies were carried out at the following constant values of the operational parameters of the installation: the inner diameter of the material cylinder is 40 mm, the injection pressure is 100 MPa, the pressure in the hydraulic cylinder is 50 MPa, and the pressure of the auger during loading is 0.4 MPa. Plastics with wide application in the national economy and a wide range of physical and mechanical characteristics were chosen as the tested materials, in particular: - high-pressure polyethylene, which is characterized by a wide range of material viscosity coefficient; polystyrene, which is easily processed and has high mechanical characteristics; kapron, which requires exact endurance of the technological mode of processing, a slight deviation from which leads to a sharp change in the viscosity and quality of the product; fiberglass, which is difficult to recycle, the basis of which is polyamide resin with properties that are close to those of kapron, and glass fiber sharply increases the viscosity of the material and, if it deviates from the technological mode of processing, leads to jamming of the auger.

In the process of research, the maximum was determined on the basis of recorded oscillograms P_{\max} and the average P_m pressures in the material cylinder in different periods of the work cycle. Average pressure value P_m was determined by the formula:

$$P_m = \frac{\int_0^t P(t) dt}{t} \quad (4)$$

and is the ratio of the waveform area $P = f(t)$ for a certain period t to the time spent on this period.

Results

Table 1 shows the results of experimental studies of the maximum and average values of pressures in the material cylinder, which occurred during the periods of injection and loading of the D 3328 thermoplastic machine, during the processing of various plastics.

Table 1

Results of experimental studies of pressures in the material cylinder during the processing of various plastics.

Material	Injection zone			Loading area			
	Injection time t, s	Pressure		Download time t, s	Quantity of revolutions auger n, rpm	Pressure	
		P_{max} , MPa	P_m , MPa			P_{max} , MPa	P_m , MPa
Polyethylene	1.5	125.0	91.2	13.5	25	70.0	47.0
Polystyrene	1.5	130.0	92.1	9.4	17.0	81.0	50.2
Kapron	1.6	120.0	83.0	19.8	35.6	80.5	45.1
Fiberglass	1.8	160.0	84.5	14.4	26.3	66.0	51.3

Table 1 shows that the maximum pressure in the material cylinder occurs in the melt zone at the end of the screw (injection zone) during the injection period during the processing of all the studied materials. The highest pressure occurs during the processing of fiberglass (160MPa). Its value reaches 183 MPa in extreme cases (jamming moment). When processing polyethylene, polystyrene and capron, the maximum value of pressure in this period is within 120-130 MPa. The injection time is the largest when processing fiberglass and is 1.8s, for other materials it is 1.5-1.6 s.

In fig. 3 shows samples of oscillograms of pressure changes during the injection period for various materials, from which it can be seen that in the initial period, the pressure during the processing of all materials is small and amounts to 45-50 MPa, and then reaches a maximum within 0.15-0.2 s. The maximum pressure is maintained for 0.4-0.5 s, after which it gradually decreases to a minimum value of 10-20 MPa, and remains so during the exposure period.

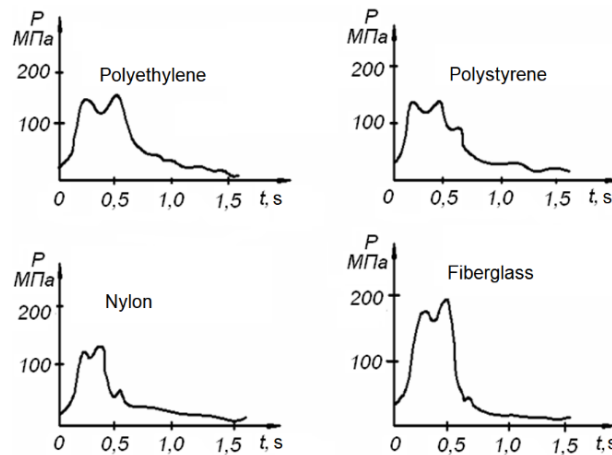


Fig. 3. Pressure oscillograms during the injection period of the D3328 injection molding machine during the processing of various plastics, with a diametral gap between the screw and the cylinder $\delta=0.17$ mm.

During the loading period, the pressure in the loading zone is different for different materials. The maximum value (Table 1) occurs during the processing of kapron and polystyrene (91-92 MPa) in the area where the S5 sensor is located, with a gradual decrease in the direction of the S2 sensor to a value of 40 MPa. At the same time, the average value of the P_m pressure is 47-50 MPa. When processing fiberglass, the pressure difference in the loading zone between sensors S5 and S3 decreases, and the average value of pressure P_m is 51.3 MPa. The maximum time and number of revolutions of the auger during the loading period occurs when processing kapron, which is related to the physical and mechanical properties of this material and their sensitivity to temperature changes.

The nature of the pressure distribution along the length of the material cylinder during the processing of various materials is shown in fig. 4, from which it can be seen that during the injection period, the maximum pressure occurs in the melt zone (S1 sensor) with a subsequent sharp decrease in the middle zone (S3 and S4 sensors) and a slight increase in the S5 sensor zone (loading zone). At the same time, the nature of the pressure change for all materials is similar for the diametrical gap between the screw and the cylinder $\delta = 0.17$ mm (Fig. 4a). With an increase in the gap δ up to 0.74 mm (Fig. 4b), the nature of the pressure distribution in the injection zone changes only during the processing of fiberglass, in particular in the area of effect of the S4 sensor, which is caused by the partial penetration of glass fibers into the gap between the screw and the cylinder.

During the loading period (Fig. 5), the nature of the pressure distribution along the length of the cylinder for all materials is similar to the injection period (Fig. 4a), but with the difference that the absolute value of the pressure in this period is 1.7-2 times smaller.

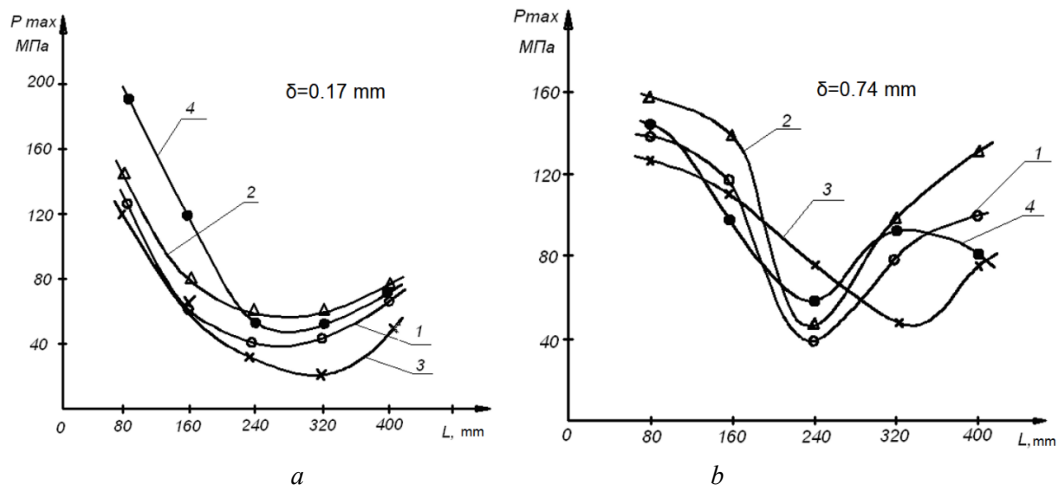


Fig. 4. Distribution of the maximum pressure along the length of the material cylinder during the injection period of the D3328 thermoplastic machine during processing:
1—polyethylene; 2—polystyrene; 3—capron; 4—fiberglass.

The analysis of the time t and the number of revolutions n of the screw during the loading period (Table 1), which are necessary for taking a portion of plastic, shows that the thermoplastic machine has the highest productivity when processing polystyrene, and the lowest - when processing kapron.

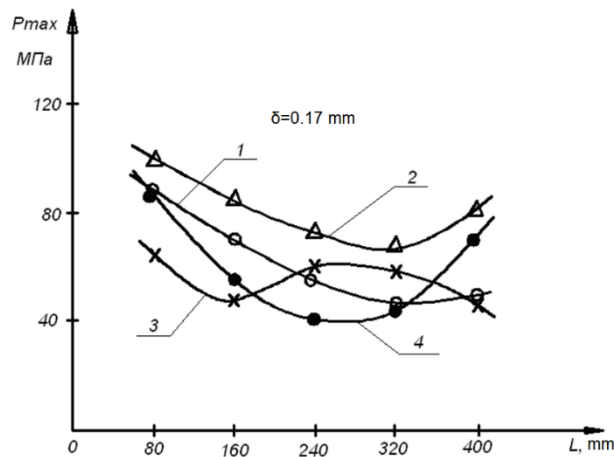


Fig. 5. Distribution of the maximum pressure along the length of the material cylinder during the loading period of the D3328 thermoplastic machine during processing:
1—polyethylene; 2—polystyrene; 3—capron; 4—fiberglass.

This is explained by the physico-mechanical and rheological properties of processed materials, which largely depend on the processing temperature.

Conclusions

The following conclusions can be drawn on the basis of the conducted research:

1. The pressure in the material cylinder of thermoplastic machines is distributed unevenly along its length. Its size and the nature of the distribution along the length for different materials are different and depend on the physical, mechanical and rheological characteristics of these materials, the design of the screw and the technological modes of processing.

2. The maximum pressure occurs in the melt zone during the injection of the material into the mold for 0.4-0.5s, and its value when processing fiberglass reached 183 MPa.

3. Research on the wear of the material cylinder of the DB3328 thermoplastic machine after processing fiberglass showed that there is a complete correlation between the amount of wear and the amount of pressure along the length of the cylinder.

References

1 Park, J. C., & Kim, B. H. (2000). Automated molding design methodology to optimize multiple defects in injection molded parts. *International Journal of Precision Engineering and Manufacturing*, 1(1), 133-145. <https://koreascience.kr/article/JAKO200011920329191.pdf>

- 2 David, Z., Walter, F., & Andreas, B. (2023, May). Wear phenomenon in injection molding. In AIP Conference Proceedings (Vol. 2607, No. 1). AIP Publishing. <https://pubs.aip.org/aip/acp/article-abstract/2607/1/040003/2892409/Wear-phenomenon-in-injection-molding>
- 3 Milan, J. C., Machado, A. R., Tomaz, Í. V., da Silva, L. R., Barbosa, C. A., Mia, M., & Pimenov, D. Y. (2021). Effects of calcium-treatment of a plastic injection mold steel on the tool wear and power consumption in slot milling. *Journal of Materials Research and Technology*, 13, 1103-1114. <https://www.sciencedirect.com/science/article/pii/S2238785421004609>
- 4 Silva, F., Martinho, R., Andrade, M., Baptista, A., & Alexandre, R. (2017). Improving the wear resistance of moulds for the injection of glass fibre-reinforced plastics using PVD coatings: A comparative study. *Coatings*, 7(2), 28. <https://www.mdpi.com/2079-6412/7/2/28>
- 5 Jiang, X., & Kong, F. (2023). Understanding mold wear mechanisms and optimizing performance through nico coating: An In-Depth analysis. *Metals*, 13(12), 1933. <https://www.mdpi.com/2075-4701/13/12/1933>
- 6 Levytskyi V.E., Masyuk A.S., Katruk D.S. (2021). Technological features of obtaining extruded products from polylactide. *Chemistry, Technology and Application of Substances*. Vol. 4. No. 2, 179–187. DOI:10.23939/ctas2021.02.179
- 7 Bobzin, K., Brögelmann, T., Grundmeier, G., de Los Arcos, T., Wiesing, M., & Kruppe, N. C. (2017). A Contribution to explain the Mechanisms of Adhesive Wear in Plastics Processing by example of Polycarbonate. *Surface and Coatings Technology*, 332, 464-473. <https://doi.org/10.1016/j.surfcoat.2017.07.080>
- 8 Blutmager, A., Spahn, T., Varga, M., Friesenbichler, W., Riedl, H., & Mayrhofer, P. H. (2020). Processing Fiber-Reinforced Polymers: Specific Wear Phenomena Caused by Filler Materials. *Polymer Engineering & Science*, 60(1), 78-85. <https://doi.org/10.1002/pen.25261>
9. Shved M. P., Shved D. M., Velikoivanenko S. P. (2018) New resource-energy-saving process of polymer extrusion. *Young scientist*, No. 1, 447–449. <https://doi.org/10.1016/j.rser.2021.111219>
- 10 Polishchuk, O., Zozulia, P., Polishchuk, A., Maidan, P., Skyba, M., Kostyuk, N., ... & Kravchuk, O. (2020). Development and research of equipment for processing of granulated polymeric materials via 3d printing for the needs of light industry. *Fibres and Textiles* (4), 70, 80. http://vat.ft.tul.cz/2020/4/VaT_2020_4_10.pdf

Гончар В.А. Дослідження зносостійкості матеріального циліндра термопластавтомата при переробці пластмас

В статті приведені експериментальні дослідження тиску в матеріальному циліндрі термопластавтомата Д3328 при переробці різних пластмас, а також експериментальні дослідження зносу по довжині матеріального циліндра термопластавтомата ДБ3328 після переробки склопластику ПС 68-30. Застосовано спеціально розроблені тензометричні датчики тиску. Сигнали від датчиків через підсилювальну апаратуру виводилися на осцилограф і записувалися на осцилограму. Величина та розподіл тиску по довжині матеріального циліндра буде суттєво впливати на величину зносу як шнека, так і циліндра. Встановлено тиск в матеріальному циліндрі термопластавтоматів розподіляється нерівномірно по його довжині. Характер розподілу тиску по довжині матеріального циліндра при переробці різних матеріалів: в період вприску максимальний тиск виникає в зоні розплаву з послідуєчим різким зменшенням в середній зоні та незначним збільшенням в зоні завантаження. При цьому характер зміни тиску для всіх матеріалів подібний при діаметральному зазорі між шнеком і циліндром $\delta=0,17\text{мм}$. Зі збільшенням зазору δ до $0,74\text{мм}$ характер розподілу тиску в зоні вприску змінюється лише при переробці склопластику, що зумовлено частковим попаданням скловолокон в зазор між шнеком і циліндром. Його величина і характер розподілу по довжині для різних матеріалів різні і залежать від фізико-механічних і реологічних характеристик цих матеріалів, конструкції шнека та технологічних режимів переробки. Максимальний тиск виникає в зоні розплаву в період вприскування матеріалу в пресформу на протязі $0,4-0,5\text{с}$.

Ключові слова: знос, скловолокно, циліндр, тиск, датчик



Modeling of contact stresses and evaluation of wear life of a valve mechanism guide with lubricating grooves

K.E. Holenko, A.A. Vychavka, M.O. Dykha*, V.O. Dytyniuk

Khmelnytskyi national University, Ukraine

**E-mail: tribosenator@gmail.com*

Received: 25 October 2024; Revised 25 November 2024; Accept 10 December 2024

Abstract

Valve guides are crucial for maintaining proper alignment, positioning, and valve stem clearance as it moves in the cylinder head. Valve bushings are subjected to load and sliding friction; with excessive wear of the guides, the engine begins to consume oil and the valve mechanism becomes noisy. This paper proposes the use of a special knurling to restore and increase the wear resistance of guide bushings. The profile tool is designed to restore valve guides by rolling a spiral groove on the inner surface of the sleeve. After applying this technology, a spiral oil-retaining profile remains on the surface of the sleeve bore. Using the Solid model, the effect of changing the geometry of the guide bore by the lubricating grooves on the maximum and average stress indices in the guide-valve contact was analyzed. It was found that the maximum stresses of the model with grooves are lower than those of the model with a smooth guide surface. Based on the finite element model, the durability of the valve-guide pair with oil-retaining grooves was analyzed and it was determined how many cycles the contact surface of the guide can withstand. It was established that by reducing the contact pressure, the actual resource of the guide with grooves increased.

Keywords: guide bushing, valve, lubricating grooves, finite element analysis, contact pressure, resource.

Introduction

Valve guides, which are critical for maintaining proper alignment, positioning, and clearance of the valve stem as it travels within the cylinder head, are typically made of materials that provide high wear resistance and improved thermal conductivity. Valve bushings are subject to friction loads. Lateral forces act on the valve stem caused by changes in geometry in the valve mechanism, wear of the rocker cam or rocker arm. When the guides are heavily worn, the engine begins to consume oil and increased noise of the valve mechanism appears. This applies to both the intake tract (vacuum in the cylinder) and the exhaust tract (Venturi effect).

In this work, the use of a special knurling tool is proposed to restore and increase the wear resistance of guide bushings. The tool is designed to restore valve guides by rolling a spiral groove on the inner surface of the sleeve. After applying this technology, a spiral oil-retaining profile remains on the surface of the sleeve hole, which:

- increases the oil capacity of the surface, and therefore, improves the lubrication conditions in the friction pair "valve-guide";
- creates a gas labyrinth seal in the connection, which prevents oil from entering the combustion chamber;
- strengthens the surface of the sleeve hole due to surface sealing (hardening effect).

The creation and study of the tribological properties of the lubricating profile on the inner surface of cylindrical sliding guides has been given attention in scientific papers [1-9].

In this work, computer modeling of the performance of a valve guide with spiral grooves was carried out using the lubricity criterion.

The geometry of the oil retaining profile and the lubricity of the profile



Let's analyze the effect of changing the geometry with lubrication grooves of the guide hole on the indicators and . Using the method of extrusion of the body of the solid model, we draw a channel with a width of 1.5 mm and a depth of 0.05 mm in steps of 3 mm (Fig. 1). σ_{max} σ_{ave}

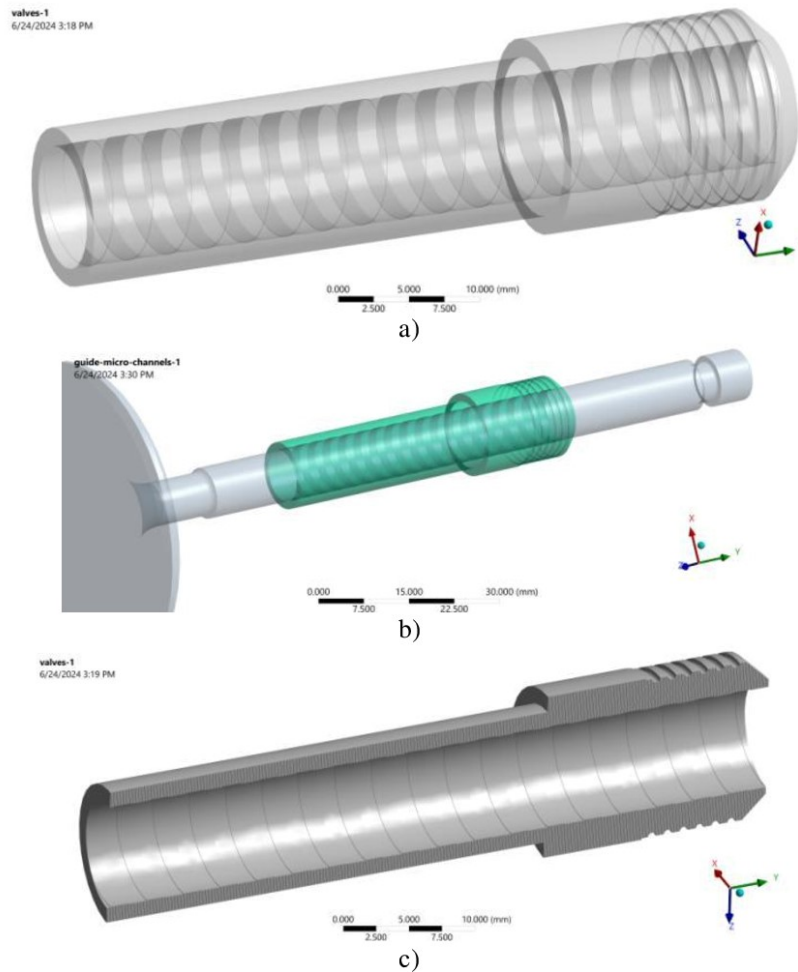


Fig. 1. Solid model of a guide with channels: a, b) guide separately and assembled with a valve; d) cross section of the guide

The gap between the valve flap and the guide remains uniform and unchanged relative to the boundary conditions of the previous modes: 0.03358 mm in the lower points of the spiral (protrusions) and increased by 0.05 mm in the upper ones (channel depressions).

Consider the hypothesis that the presence of channels in the valve guide improves the lubrication regime, thereby reducing the coefficient of friction between the valve stem and the guide. μ_v

Factors of the lubricity of the oil-retaining profile of the grooves:

- Improved oil flow: channels in the guide can improve oil distribution and flow, increasing the formation of a lubricating film between surfaces.

- Hydrodynamic lubrication: Improved oil flow can change the lubrication regime from marginal or mixed lubrication to hydrodynamic lubrication, where a full film of lubricant separates the contact surfaces, greatly reducing friction.

- Reduced metal-to-metal contact: Channels help maintain a continuous oil film by reducing direct metal-to-metal contact, thus reducing the coefficient of friction.

The Reynolds equation describes the pressure distribution in a thin film of oil between two surfaces. For a simplified one-dimensional flow in the presence of channels, this can be expressed as:

$$\frac{\partial}{\partial x} \left(h^3 \frac{\partial p}{\partial x} \right) = 6\mu U \frac{\partial h}{\partial x},$$

where: h – film thickness, mm; p – pressure in the film, Pa; μ – dynamic oil viscosity, Pa·s; U – relative speed between surfaces, m/s; x – spatial coordinate along the length of the contact, mm.

The force of friction (F_f) in the hydrodynamic mode of lubrication can be estimated using:

$$F_f = \tau A = \frac{\mu U A}{h},$$

where: τ – shear stress in oil, Pa; A – contact area, m^2 ; F_f

The coefficient of friction is determined by the ratio of the force of friction to the normal load (F_N):

$$\mu_f = \frac{F_f}{F_N} = \frac{\mu UA}{h F_N}$$

For a typical guide without channels, the film thickness can be less uniform and thinner, resulting in more friction due to more frequent metal-to-metal contact.

For a guide with channels, the film thickness is more uniform and thicker due to improved oil flow, resulting in reduced friction.

Assuming that the channels increase the effective thickness of the film by a factor (α): $\alpha > 1$

$$h_c = \alpha h,$$

the coefficient of friction with channels can be expressed as:

$$\mu_{fc} = \frac{\mu UA}{\alpha h F_N}$$

Due to the increase in the thickness of the lubricating film and the homogeneity through the channels, the effective coefficient of friction decreases by the value of α , confirming that the presence of channels can lead to a decrease in the coefficient of friction. In the modes studied below with a profiled guide (with channels), the value of the coefficient of friction is set. $\mu_v = 0.05$

Analysis of the stress state of the guide and valve with an oil-retaining profile

Taking into account the increase in the volume of space in the contact pair, it was empirically established that for similar constructions of the guide with channels, the value of convection heat transfer increases to 400-600 $W/(m^2 \cdot ^\circ C)$. Let's apply the value of convection equal to 450 $W/(m^2 \cdot ^\circ C)$.

The difference in the boundary conditions between the previous and the current studied regime is only in growth of convection from 300 to 450 $W/(m^2 \cdot ^\circ C)$, which is the result of modification of the geometry of the contact surface of the guide (adding channels according to Fig. 1)

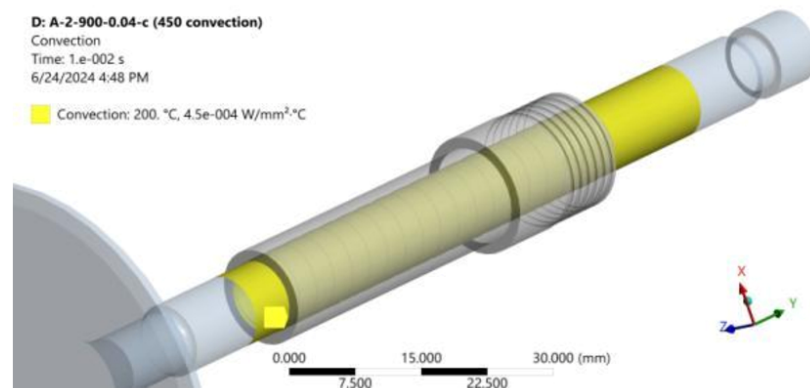


Fig. 2. Application of convection 450 $W/(m^2 \cdot ^\circ C)$ to the guide-valve contact pair

Let's analyze the influence of the channels in the guide on the resulting valve stresses (Fig. 2):

- the contact surface of the valve was subjected to 23.5% lower maximum stresses in the channel model σ_{max} compared to mode (smooth guide hole). The extremum is fixed at a moment in time $t_m = 0.002$ s. The graph has a jumpy character, which is caused by the relief surface of the guide during the beginning of the contact. Unlike the "smooth" mode, where growth is recorded σ_{max} to 21.67 MPa followed by a decrease to 13.19 MPa at the end of the experiment (blue curve at 4.32), the uniformity of the curve (red curve) clearly favors the surface of the valve. Tensions range from: 14.27 MPa as of $t_m = 0.0072$ s (Fig. 4.23 b), 14.84 MPa ($t_m = 0.0145$ s - fig. 4.23 c) and 13.6 MPa ($t_m = 0.0244$ with);

- the average stress value is 4.24 MPa, which is 6.27% higher than σ_{ave} mode without grooves. The explanation for this result lies in the "point-likeness" of stress transfer from the protrusions of the guide to the smooth surface of the valve. Both extremes occur at the end of the experiment $t_{v0} = 0.04$ s.

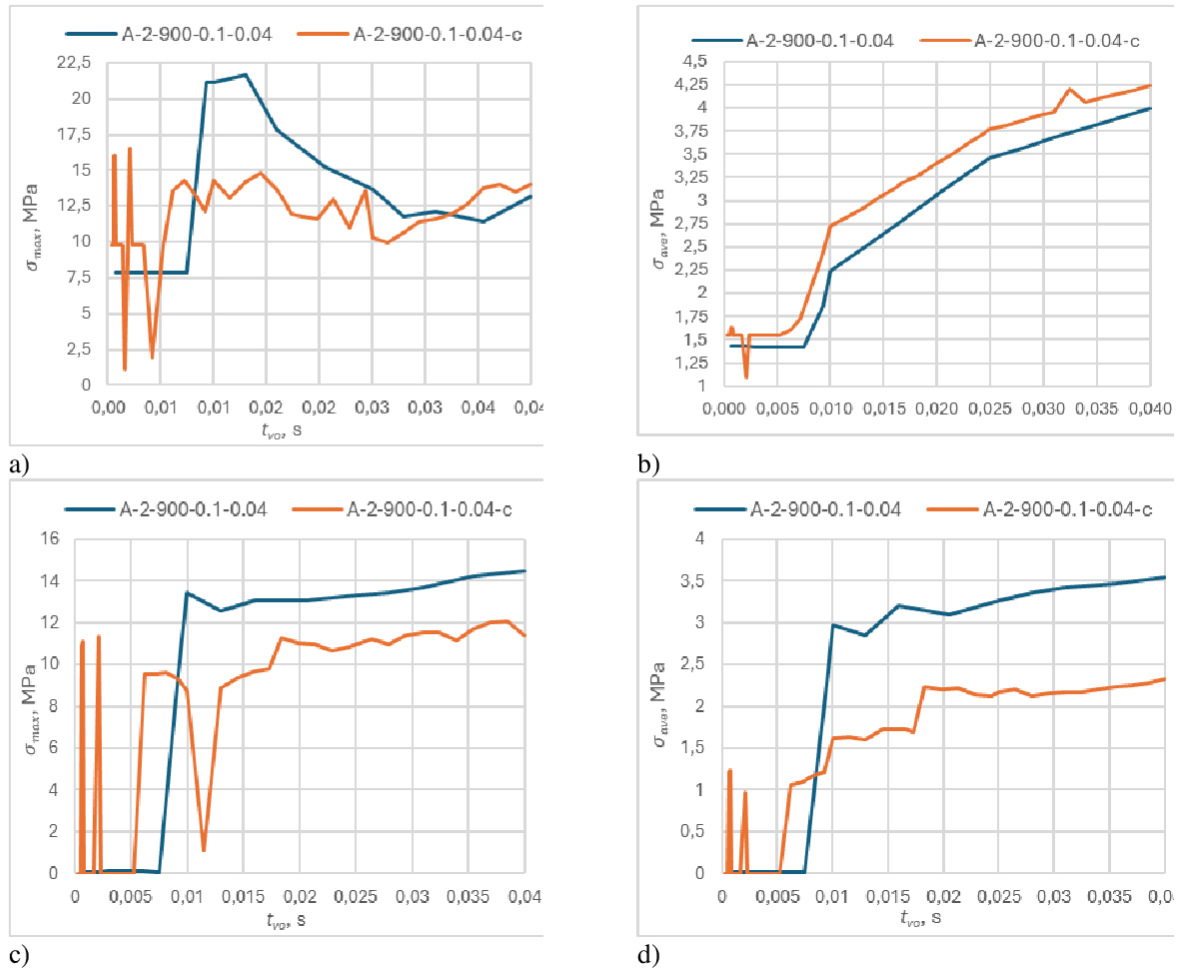


Fig. 3. The effect of the presence of channels on the stress during: a, b) and on the contact surface of the valve; c, d) and on the contact surface of the guide, respectively t_{vo} , σ_{max} , σ_{ave} , σ_{max} , σ_{ave}

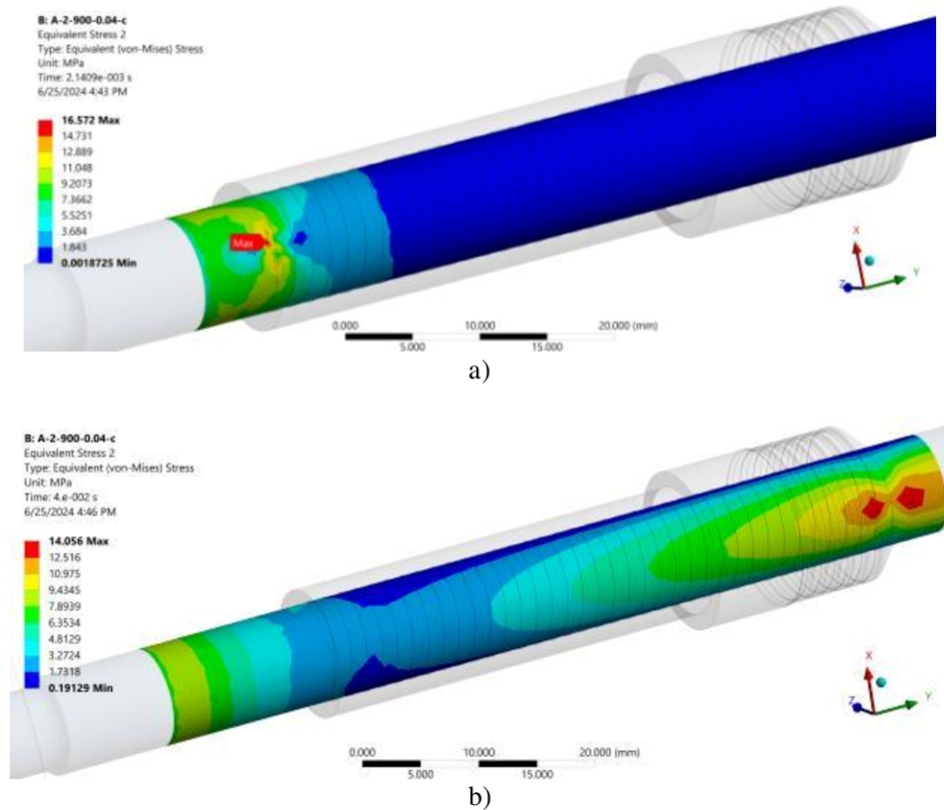


Fig. 4. Mises stress map of the valve surface at different time points t_m : a) 0.0021 s; b) 0.04 s

The results on the contact surface of the guide are as follows:

- maximum stresses of the model with the channel σ_{\max} are 12.08 MPa, which is 16.7% lower than the mode with a smooth guide surface. Value σ_{\max} achieved at the moment of time $=t_m 0.0385$ s (Fig. 4.34 a). Location σ_{\max} changes during the duration of the experiment, for example, as of $=t_m 0.00214$ s (Fig. 4.34 b) σ_{\max} is 11.34 MPa and is observed at the edge of the opposite opening of the guide, and then shifts towards the center of the guide: $=9.54$ MPa at the moment of time $=\sigma_{\max} \sigma_{\max} t_m 0.00621$ s (Fig. 4.34 c) and 11.29 MPa in $t_m = 0.0183$ s. During the first 0.012 s, oscillations were recorded until the contact between the valve and the guide was stabilized. Further, the stress curve is roughly parallel, but lower by 2.0-2.5 MPa. Thus, throughout the experiment, the value σ_{\max} in the first mode with the channel is lower, which positively affects the wear of the guide surface;
- unlike the smooth surface of the guide, the Mises stress map has clear contours within the spiral of the channel. This effect is of practical benefit - by selecting the desired geometric parameters of the channel, for example, the step, it is possible to control the distribution of stresses on the surface of the guide;
- the average stress value is 2.32 MPa, which is $\sigma_{\text{ave}} - 34.5\%$ lower than the first mode without grooves. The explanation for this result lies in the transfer of stresses from the guide to the smooth surface of the valve. σ_{ave} By analogy with σ_{\max} average stresses also exhibited fluctuations during the first milliseconds of contact. Both extremes σ_{ave} come at the end of the experiment $t_{v0} = 0.04$ s.

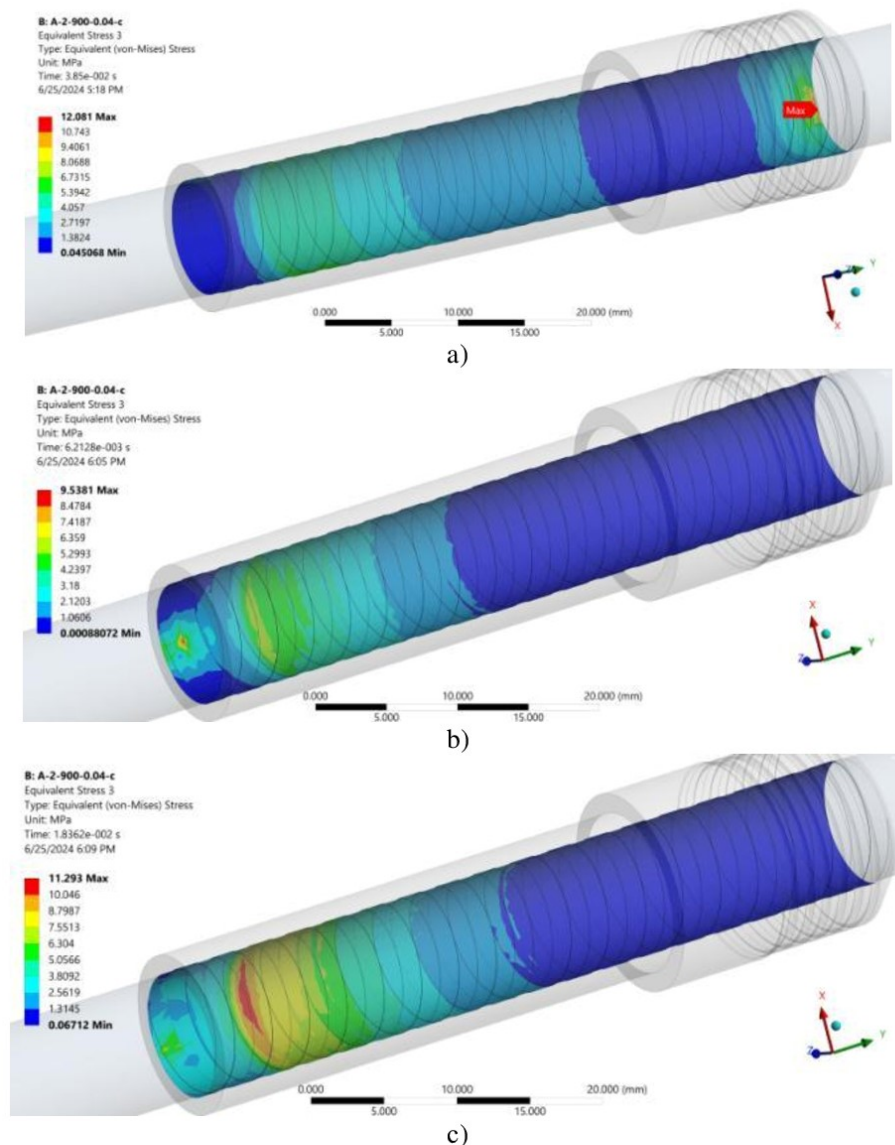


Fig. 5. Mises stress map of the guide surface at different time points t_m : a) 0.0385 s; b) 0.0062 s; c) 0.0183 s

Study of the thickness of the lubricating layer (gap) in the "valve-guide" pair

To confirm that there is no contact between the valve and the recesses of the guide channels, use the Contact Tool > Gap tool. In fig. Figure 4.35 shows the value of Gap at different moments of time - the gap in the depressions remains throughout the experiment, as evidenced by the blue color of the scale.

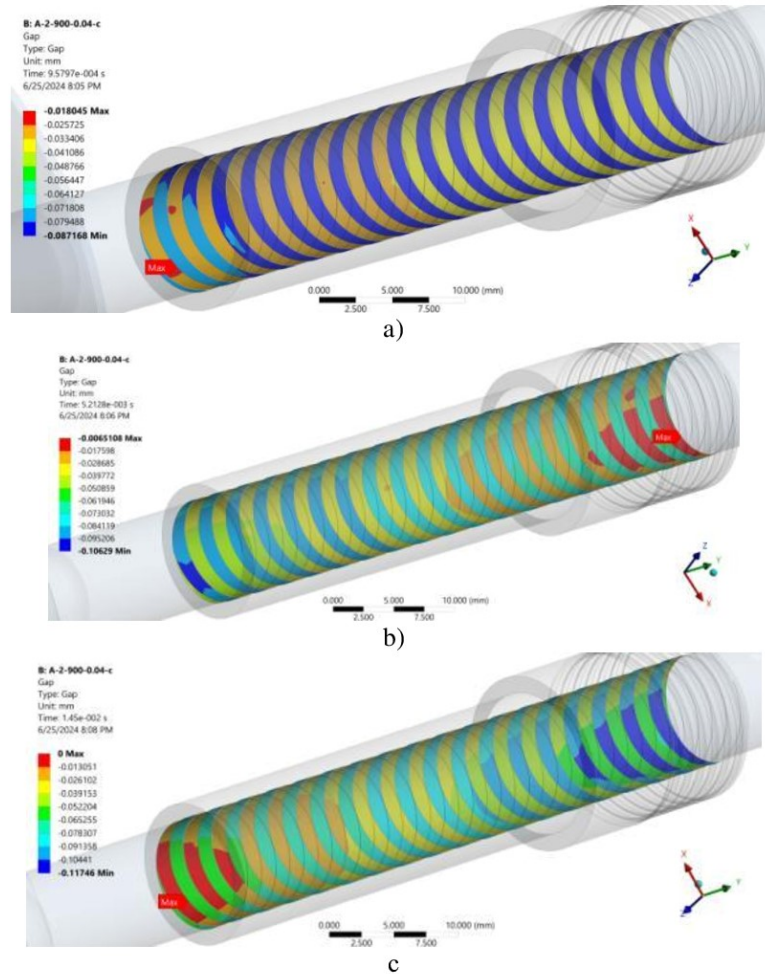


Fig. 6. Map of the gap (gap) in the contact area at the moment of time: a) 0.00096 s; b) 0.0051 s; c) 0.0145 s

Let's investigate the situation with stresses on the surface of channel protrusions, comparing the results with the entire surface (valves together with protrusions). The curves of the maximum stresses coincide throughout the experiment (Fig. 6a), except for the period 0.018–0.021 s, where it is even higher for the entire surface (together with depressions). This is quite unexpected, because the protrusions are always the first to perceive contact, which was confirmed based on the evaluation of the size of the gap (gap). The situation with average stresses is more unambiguous - it is lower by 2-3% in the case of only the surface of the protrusions during the entire experiment = 0.04 s (Fig. 6b). This indicates that the depressions concentrate higher stresses on themselves. As a rule, they appear in the corners of depressions, where theoretically the greatest bending moment occurs (the protrusion acts as a cantilever beam).

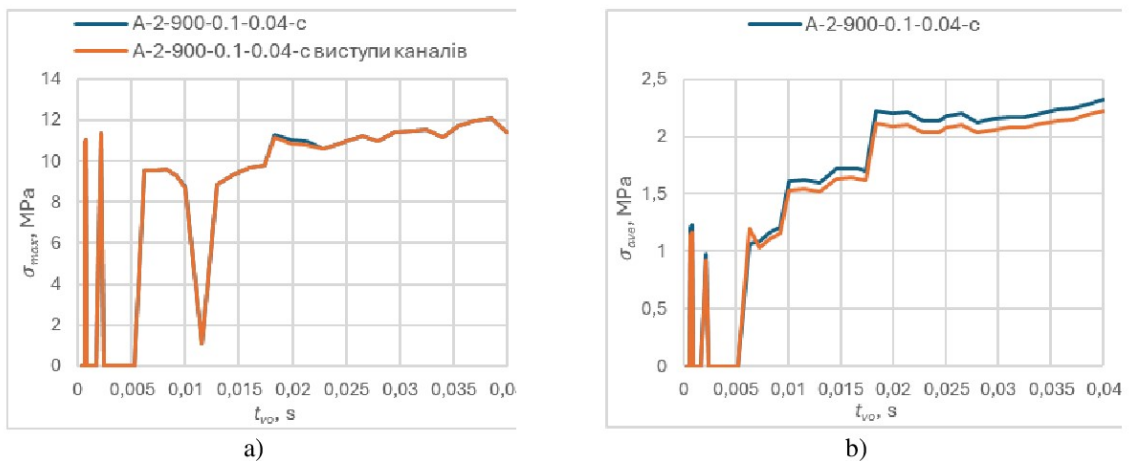
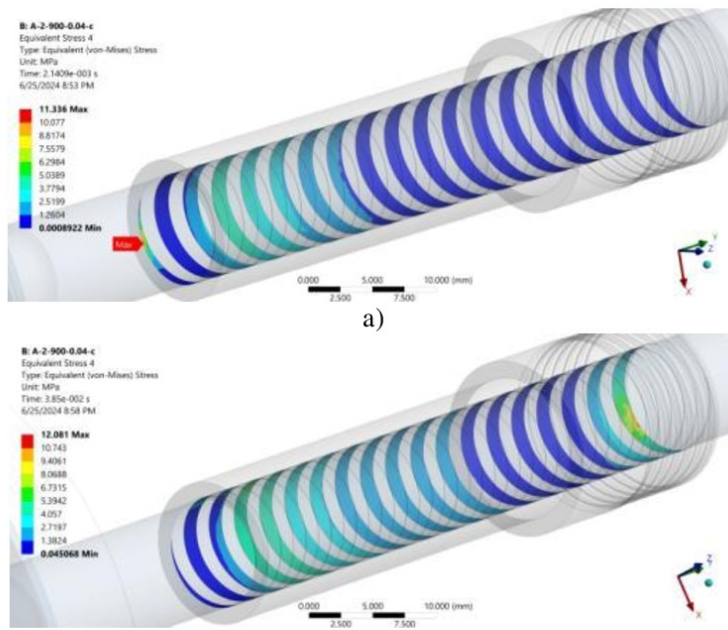


Fig. 7. Comparison of stresses on the surface of channel protrusions with the entire surface of the guide hole: a) σ_{max} ; b) σ_{ave}

Intermediate stress states exclusively on the surface of the protrusions are shown in Fig. 8. Consolidated stress data are summarized in table. 1.



b) Fig. 8. Mises map of stresses exclusively on the surface of the protrusions of the guide at different moments of time t_m : a) 0.0021 with; b) 0.0385 s

Table 1

Summary results for stresses and for Ansys model modes σ_{max} σ_{ave}

Contact surface of the valve						
Regime	σ_{max} , Mpa	$\Delta\sigma_{max}$, %	$t_{\sigma_{max}}$, p	σ_{ave} , Mpa	$\Delta\sigma_{ave}$, %	$t_{\sigma_{ave}}$, p
A-2-900-0.1-0.04	21.67	+50.3	0.013	3.99	+15.0	0.04
A-2-900-0.05-0.04-c	16.57	-23.5	0.002	4.24	+6.27	0.04
The contact surface of the guide						
Regime	σ_{max} , Mpa	$\Delta\sigma_{max}$, %	$t_{\sigma_{max}}$, p	σ_{ave} , Mpa	$\Delta\sigma_{ave}$, %	$t_{\sigma_{ave}}$, p
A-2-900-0.1-0.04	14.50	+3.4	0.04	3.54	+24.2	0.04
A-2-900-0.05-0.04-c	12.08	-16.7%	0.0385	2.32	-34.5%	0.04
A-2-900-0.05-0.04-c*	12.08	0%	0.0385	2.23	-3.9%	0.04

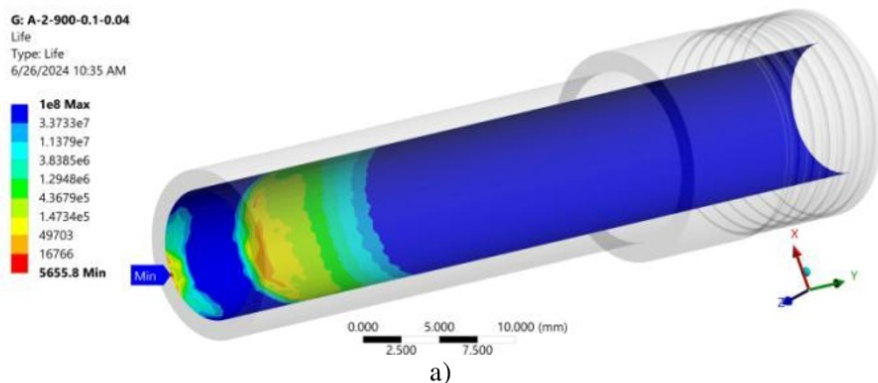
* the results of channel protrusion stresses

Durability of the "valve-guide" pair with oil retaining grooves

Let's set the "Scale Factor" value to 25 and measure how many cycles (Fatigue Tool > Life) the contact surface of the guide can withstand with a 25-fold increase in each of the modes: $N_c \sigma_{max}$

mode A-2-900-0.1-0.04 received σ_{max} at a point in time $t_m = 0.04$ s and demonstrated $=5655.8$ cycles (Fig. 9 a); N_c

mode A-2-900-0.1-0.04-c showed $=34620$ cycles (Fig. 9 b) according to at the moment of time $N_c \sigma_{max}$ $t_m = 0.0385$.



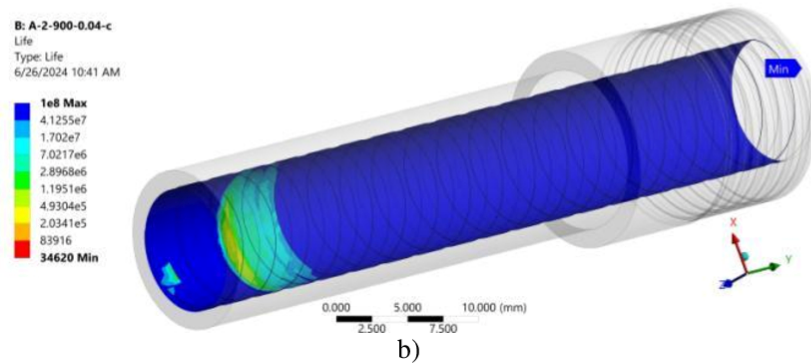


Fig. 9. Maps of wear resistance based on the tool4 Tool Fatigue Tool > Life: a) regime A-2-900-0.1-0.04 $int_m=0.04$ s; b) regime A-2-900-0.1-0.04-c $int_m=0.0385$ s

Thus, by reducing the value σ_{max} on 16.7% (table 4.3), the actual resource of the guide with channels increased by more than 6 times.

Conclusions

1. Using the Solid model, the effect of changing the geometry with lubrication grooves of the guide hole on the indicators of maximum and average stresses in the "guide-valve" contact was analyzed. It was established that the maximum stresses of the model with grooves are 12.08 MPa, which is 16.7% lower than the mode with a smooth guide surface.

2. Based on the finite-element model, the durability of the "valve-guide" pair with oil retaining grooves was analyzed. It was determined how many cycles the contact surface of the guide can withstand with a 25-fold increase in each of the modes. It was found that due to the reduction of the value by 16.7%, the actual resource of the guide with grooves increased by more than 6 times.

References

1. Buscaglia GC, Ausas RF, Jai M (2006) Optimization tools in the analysis of micro-textured lubricated devices. *Inverse Prob Sci Eng* 14(4):365–378. <https://doi.org/10.1080/17415970600573452>
2. Nikam MD, Shimpi D, Bhole K, Mastud SA (2019) Design and development of surface texture for tribological application. *Key Eng Mater* 4834:55–59. <https://doi.org/10.4028/www.scientific.net/KEM.803.55>
3. Wang HT, Zhu H (2015) Tribology properties of textured surface with ring-shape pits. *Lubr Eng* 40(01):49–53. <https://doi.org/10.3969/j.issn.0254-0150.2015.01.011>
4. Rahmani R, Mirzaee I, Shirvani A, Shirvani H (2010) An analytical approach for analysis and optimisation of slider bearings with infinite width parallel textures. *Tribol Int* 43(8):1551–1565. <https://doi.org/10.1016/j.triboint.2010.02.016>
5. Fu Y, Ji J and Bi Q. The influence of partially textured slider with oriented parabolic grooves on the behaviors of hydrodynamic lubrication. *Tribol Trans* 2012; 55: 210–217.
6. Feng, H.; Peng, L. Numerical analysis of water-lubricated thrust bearing with groove texture considering turbulence and cavitation. *Ind. Lubr. Tribol.* 2018, 70, 1127–1136. [CrossRef]
7. Brito FP, Miranda AS, Claro JCP, Fillon M. Experimental comparison of the performance of a journal bearing with a single and a twin axial groove configuration. *Tribology International* 2012; 54:1–8.
8. Brito FP, Miranda AS, Claro JCP, Fillon M. Experimental comparison of the performance of a journal bearing with a single and a twin axial groove configuration. *Tribology International* 2012; 54:1–8.
9. S. B. Malanoski, C. H. T. Pan, The Static and Dynamic Characteristics of the Spiral-Grooved Thrust Bearing, *Journal of Basic Engineering* 320 87 (3) (1965) 547–555. doi:10.1115/1.3650603.

Голенко К.Е., Вичавка А.А., Диха М.О., Дитинюк В.О. Моделювання напружень в контакті і оцінка ресурсу по зносу напрямної клапанного механізму із змащувальними канавками

Направляючі клапанів мають вирішальне значення для підтримки правильного вирівнювання, позиціонування та формування зазору штока клапана під час його руху в головці блоку циліндрів. Втулки клапанів піддаються навантаженню і тертю ковзання, при великому зносі направляючих двигун починає витрачати масло і з'являється підвищений шум клапанного механізму. У даній роботі запропоновано використання спеціальної накатки для відновлення та підвищення зносостійкості напрямних втулок. Профільний інструмент призначений для відновлення напрямних клапанів шляхом накочування спіральної канавки на внутрішній поверхні гільзи. Після застосування цієї технології на поверхні отвору гільзи залишається спіральний маслоутримуючий профіль. За допомогою моделі Solid проаналізовано вплив зміни геометрії мастильних канавками направляючого отвору на показники максимального та середнього напружень у контакті «направляюча-клапан». Встановлено, що максимальні напруження моделі з канавками нижче, ніж у моделі з гладкою прямою поверхнею. На основі кінцево-елементної моделі проаналізовано довговічність пари «клапан-направляюча» з маслоутримувальними канавками і визначено, скільки циклів витримує контактна поверхня напрямної. Встановлено, що за рахунок зменшення значення контактного тиску фактичний ресурс направляючої з канавками збільшився.

Ключові слова: напрямна втулка, клапан, мастильні канавки, скінчено-елементний аналіз, контактний тиск, ресурс



Cavitation-erosion resistance of eutectic coatings in sodium chloride solution

M. Pashechko^{1*}, V. Holubets², J. Zubrzycki¹, O. Tisov³

¹Lublin University of Technology, Poland

²Ukrainian National Forestry University, Ukraine

³Xi'an Jiaotong University, China

*E-mail: mpashechko@hotmail.com

Received: 30 October 2024: Revised 30 November 2024: Accept 15 December 2024

Abstract

The paper presents original research results related to the resistance of proprietary eutectic coatings applied to C45 structural steel to cavitation-erosion wear. This type of wear is encountered in devices operating in the chemical, petrochemical, heat and power industry and other industries. The research was conducted on a unique measuring stand developed by the authors. The research was conducted in a highly corrosive environment, i.e. sodium chloride solution. As a result of the research work, curves of the change in the electrode potential of C45 steel with different surface conditions and its polarization curves were obtained. Thanks to these curves, it was possible to determine the optimal method of protecting the tested steel against cavitation-erosion wear.

Keywords: eutectic coatings, structural steel, cavitation-erosion wear, sodium chloride, test bench

Introduction

To the most dangerous types of corrosive destruction of devices operating in the chemical, petrochemical, heat and power industry and other industries include destruction under the influence of stress corrosion. The interaction of corrosive environments with metal working under mechanical load leads to irreversible chemical processes and phenomena at the metal - environment boundary and reduces the durability and reliability of responsible parts of machines, devices and building structures[1–3].

In the literature, the results of numerous studies show that when the environment has a micro-impact effect on the metal, corrosion processes increase rapidly. This is due to a number of reasons [4–6]. The first reason can be indicated that during micro-impact, the diffusion of oxidants to the working surface of the part increases with simultaneous outflow of dissolved metal ions from it. Another reason is that the adsorption layers of secondary structures - corrosion products - are subject to intensive destruction. Thirdly, during micro-impact load, a mechano-chemical effect is observed. Depending on the degree of micro-impact impact, the role and significance of each of the above factors changes significantly [7–9]. It can be seen that at a low intensity of micro-impact loading, the destruction of metal during cavitation-erosion fatigue is explained by the influence of the first two factors. With the increase of external influences, i.e. with deformation and hardening of the surface layer of the part, the third factor appears [10,11]. In order to increase the resistance to cavitation-erosion wear of metal surfaces operating in a corrosive environment, eutectic coatings are applied.

The nature of cavitation-erosion fatigue changes significantly depending on the simultaneous impact of such factors as the intensity of micro-impact load and corrosive activity of the environment. In the case of low corrosive activity of the environment and high intensity of micro-impact impact, the mechanical factor dominates. In the case of low external impact and high corrosive activity of the environment, on the contrary, the corrosive factor dominates. In the conditions of medium intensity of micro-impact load and high or medium corrosive activity of the environment, the intensity of corrosive processes increases. In this case, both mechanical and corrosive factors appear, the role of which was confirmed by the following research results.

In the case of cavitation-erosion wear process in a corrosive environment, hydrogenation processes can have a significant impact [12]. The negative influence of hydrogen on plasticity, fatigue strength and other



mechanical properties of metals is known. As a result of high pressures and temperatures at the point of contact of the metal with the liquid, intensive plastic deformation of the surface layer of the metal, destruction of passive layers, it is possible to occur cathodic reactions with the release of hydrogen, the influence of which on the process of cavitation-erosion wear process is different [13–15]. In the initial phase of wear and at low hydrogen concentration, it increases microhardness and abrasion resistance. When the process duration and hydrogen amount increase, wear resistance decreases. However, in relation to this work, such a conclusion requires further research [16].

The possibilities of increasing the durability of machine parts subject to intensive cavitation-erosion wear in corrosive environments by applying protective coatings with eutectic composition and structure are presented below. Moreover, the study of electrochemical processes during cavitation-erosion fatigue in various environments using the potentiostatic method confirms that the micro-impact interaction of liquids has a significant effect on the nature and intensity of electrode reactions.

Experimental

The tests were carried out on two different eutectic coatings developed by the authors of the work and on a sample made without a eutectic coating. The cavitation-erosion resistance of the developed coatings was tested taking into account the mutual interaction of mechanical and corrosive factors [5,17,18]. The experiment consisted of two stages: determination of electrochemical characteristics, which were used for theoretical prediction of coating resistance. In the next step, wear tests were performed. The cavitation-erosion resistance of C45 steel with eutectic coatings was tested in a 3% aqueous solution of NaCl on a specially designed measuring station (Fig. 1) using potentiostatic method.

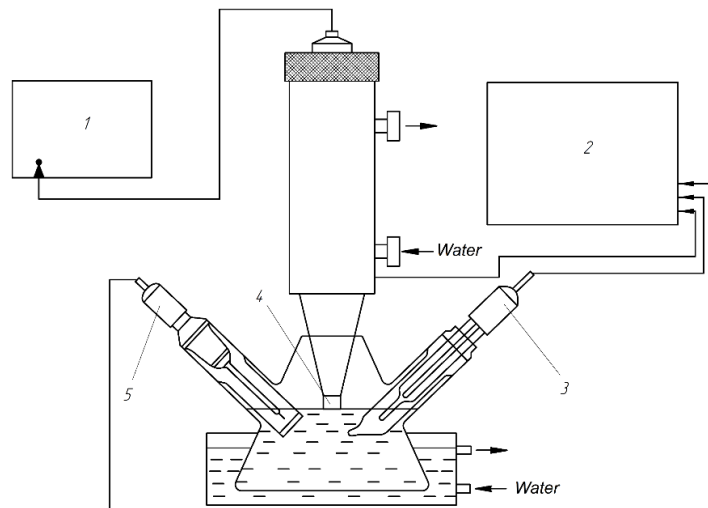


**Fig. 1. Schematic diagram of the device for cavitation-erosion wear of coatings with simultaneous study of electrochemical processes:
1-ultrasonic vibration generator with magnetostrictive vibrator, 2-potentiostat, 3-saturated calomel electrode, 4-working electrode (test sample), 5-reference electrode (platinum) [12]**

The experimental device consists of three main parts (Fig. 1): an ultrasonic vibration generator 1 with a magnetostrictive vibrator, an electrochemical cell 4, in which a working electrode (sample) is placed, attached by means of a thread to the magnetostrictive vibrator, and a potentiostat 2 model P-5827M. The diameter of the samples, which also serve as working electrodes, is 0.01 m. Before connecting to the magnetostrictive vibrator, the samples were pre-grinded using M20 sandpaper.

Results and Discussion

Based on the results of measurements of the general electrode potentials of the tested 45 steel samples in the corrosive-erosive wear process in a 3% NaCl aqueous solution (Fig. 2), it can be seen that the eutectic coatings of the powder mixtures used in the tests are of the cathode type.

The potential values almost do not change with time. Comparing the results of measurements of electrode potentials of some eutectic coatings during cavitation-erosion wear in a 3% aqueous solution of NaCl and in this environment in static conditions, one can notice differences in their kinetics when using ultrasonic vibrations from ordinary corrosion. This difference is due to the fact that in the conditions of cavitation-erosion wear, diffusion processes are present, intensified by acoustic currents in turbulent flows.

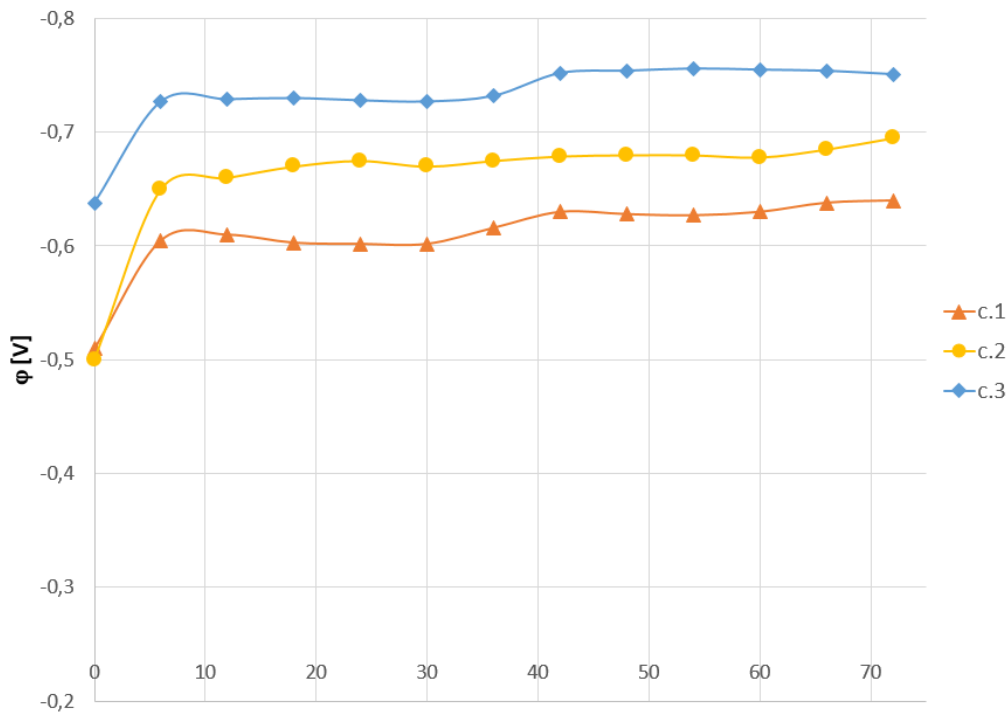


Fig. 2. Change in the electrode potential of C45 steel without coating (c.1) with eutectic coatings from mixtures No. 1 (c.2) and No. 2 (c.3) during cavitation-erosion wear in a 3% aqueous NaCl solution

The destruction of the forming adsorption layers, corrosion products, mechanical destruction of the forming micro irregularities and other phenomena are observed.

Conclusions

The high resistance of the coating of the mixture No. 1 is confirmed by the test results (Table 1). The cavitation-erosion resistance of this coating in a 3% aqueous solution of NaCl is the highest and shows good compliance with the anticorrosive and electrochemical properties of the coating in this environment under static test conditions. High protective properties occur due to the structure and phase composition, represented by solid solutions of chromium in α -iron, nickel and manganese in γ -iron, as well as insignificant amounts of the $Fe_{0,4}Mn_{3,6}C$ phase.

Table 1

Cavitation and erosion resistance of steel 45 in various environments

Coating type	$\Delta M \cdot 10^{-6}, \text{ kg}$		
	Distilled water	3% NaCl*	3% NaCl**
Without coating	3.2	6.2	12.9
Eutectic from the mixture			
No. 1	0.7	13.1	29.8
No. 2	1.7	10.8	25.1
		*Research time $36 \cdot 10^2 \text{ s}$	**Research time $72 \cdot 10^2 \text{ s}$

Since the hardness of the eutectic coating of the No. 2 mixture is higher than that of the No. 2 mixture, the resistance characteristics of the coating of the base mixture are higher than those compared. This agrees well with the data [12] regarding the wear resistance of eutectic coatings. When exposed to a corrosive environment (3% NaCl solution), the mechanism of cavitation-erosion wear changes significantly. In this case, both the corrosive and mechanical factors play the main role, with the corrosive factor dominating (it is known that as a result of the micro-impact impact of the aggressive environment, the intensity of the corrosive factor may be proportional, smaller or larger in comparison to the intensity of the mechanical impact). In connection with this, the described electrochemical processes during cavitation-erosion wear of coatings are confirmed, which explain the resistance characteristics of the tested coatings.

It is worth mentioning the corrosion-fatigue nature of the destruction of the tested coatings, which in the case of uncoated steel is visible in the increased occurrence of surface defects such as pores, cracks and others. In contrast to eutectic coatings, where the uniform destruction of the hardened layer takes place over the entire surface, in the boronized coating the destruction starts from the pores and then runs along the grain boundary of the diffusion layer towards the ferrite or pearlite that make up the matrix with further splitting of the coating zone.

In conclusion, it can be noted that during the cavitation effect of a liquid environment on the surface of the sample, intense short-term pressures develop, the duration of which is 10^{-5} s. Only the surface layer of the metal takes part in resisting the dynamic effect of the environment, the depth of which, depending on the intensity of the effect and the properties of the metal, can range from several micrometers to several millimeters [11,19]. Therefore, applying coatings of relatively large thickness and high hardness, continuity and plasticity to the metal surface can be an effective means of increasing the durability of steel products under contact loading. The results of tests of cavitation-erosion resistance of eutectic coatings with these properties confirm the validity of their use for these purposes.

Thus, the factor responsible for long-term operation of machine parts under contact load in cavitation conditions is not the high mechanical properties of steel with a coating, but its strength. This can be explained by the fact that it is not the macroscopic characteristics of this coating, but the ability of the microvolume of its surface layer to resist the influence of the surrounding environment, which can provide the resistance of the part under similar load conditions. At the same time, it is necessary to ensure the structural uniformity of the surface layer of the produced coating.

References

- [1] AlHazaan AN, Sherif E-SM. Corrosion Behavior of Al7075, Ti-6Al-4V, and Sn-3.6Ag-1Cu Alloys in 3.0 wt.% Sodium Chloride Solutions Using Potentiodynamic Polarization Measurements. *Int J Electrochem Sci* 2015;10:4193–207.
- [2] Chen L, Li M, Wang S, Guo Z, Liang B, Xue J, et al. Microstructure and Corrosion Resistance of Ni-Al Coating Prepared by Plasma Transferred Arc Technology. *J Mater Eng Perform* 2024;33:1596–614. <https://doi.org/10.1007/s11665-023-08084-0>.
- [3] Cruz JR, Henke SL, Pukasiewicz AGM, d'Oliveira ASCM. The effect of boron on cavitation resistance of FeCrMnSiB austenitic stainless steels. *WEAR* 2019;436:203041. <https://doi.org/10.1016/j.wear.2019.203041>.
- [4] Ciubotariu CR, Frunzaverde D, Marginean G. Investigations of Cavitation Erosion and Corrosion Behavior of Flame-Sprayed NiCrBSi/WC-12Co Composite Coatings. *Materials* 2022;15. <https://doi.org/10.3390/ma15082943>.
- [5] Hoi KC, Lei WH, Liu Y, Shek CH, Ferreira JTG, Cortez NFT, et al. Cavitation erosion of the CoCrFeNi high entropy alloy having elemental segregation. *Wear* 2023;530–531. <https://doi.org/10.1016/j.wear.2023.204990>.
- [6] Holubets' VM, Pashechko MI, Borec J, Barszcz M. Micromechanical Characteristics of the Surface Layer of 45 Steel After Electric-Spark Treatment. *Mater Sci* 2019;55:409–16. <https://doi.org/10.1007/s11003-019-00318-8>.
- [7] Cao S, Zhao X, Wei Z, Ji C, Zhang C, Zhu Q, et al. Effect of Si addition on the microstructure and liquid lead-bismuth eutectic cavitation erosion behaviors of AlCrFeMoTi laser clade coatings. *Mater TODAY Commun* 2024;39:108798. <https://doi.org/10.1016/j.mtcomm.2024.108798>.
- [8] Jiang H, Zhao X, Cao S, Wang D, Zhu Q, Lei Y. Effect of Y₂O₃ addition on the microstructure and liquid LBE cavitation erosion behaviors of Fe-Cr-Al-Ti-C-xY₂O₃ laser clade coatings. *J Nucl Mater* 2022;572:154030. <https://doi.org/10.1016/j.jnucmat.2022.154030>.
- [9] Lentz J, Roettger A, Theisen W. Mechanism of the Fe₃(B,C) and Fe₂₃(C,B)₆ solid-state transformation in the hypoeutectic region of the Fe-CB system. *ACTA Mater* 2016;119:80–91. <https://doi.org/10.1016/j.actamat.2016.08.009>.
- [10] Pashechko M, Dziedzic K, Stukhliak P, Barszcz M, Borec J, Jozwik J. Wear Resistance of Eutectic Welding Coatings of Iron-Based Fe-Mn-C-B-Si-Ni-Cr at Increased Temperature. *J Frict Wear* 2022;43:90–4. <https://doi.org/10.3103/S106836662201010X>.
- [11] Tisov O, Pashechko M, Yurchuk A, Chocyk D, Zubrzycki J, Prus A, et al. Microstructure and Friction Response of a Novel Eutectic Alloy Based on the Fe-C-Mn-B System. *MATERIALS* 2022;15:9031. <https://doi.org/10.3390/ma15249031>.
- [12] Golubets VM. RESISTANCE OF EUTECTIC COATINGS TO CAVITATION-EROSION. *WEAR. Sov J Frict Wear Engl Transl Trenie Iznos* 1985;6:99–103.
- [13] Zhang CH, Wu CL, Zhang S, Jia YF, Guan M, Tan JZ, et al. Laser cladding of NiCrSiB on Monel 400 to enhance cavitation erosion and corrosion resistance. *RARE Met* 2022;41:4257–65. <https://doi.org/10.1007/s12598-016-0814-4>.
- [14] Wu YP, Zhang JF, Li GY, Hong S, He ZH. Cavitation erosion characteristics of TiC reinforced metal matrix composite layer fabricated by plasma cladding. *Mater Technol* 2011;26:251–6. <https://doi.org/10.1179/175355511X13110717549396>.

- [15] Wang W, Wang M, Sun F, Zheng Y, Jiao J. Microstructure and cavitation erosion characteristics of Al-Si alloy coating prepared by electrospark deposition. *Surf Coat Technol* 2008;202:5116–21. <https://doi.org/10.1016/j.surfcoat.2008.05.013>.
- [16] Nowakowska M, Łatka L, Sokołowski P, Szala M, Toma FL, Walczak M. Investigation into microstructure and mechanical properties effects on sliding wear and cavitation erosion of Al₂O₃-TiO₂ coatings sprayed by APS, SPS and S-HVOF. *Wear* 2022;508–509. <https://doi.org/10.1016/j.wear.2022.204462>.
- [17] Taillon G, Pougoum F, Lavigne S, Ton-That L, Schulz R, Bousser E, et al. Cavitation erosion mechanisms in stainless steels and in composite metal-ceramic HVOF coatings. *Wear* 2016;364–365:201–10. <https://doi.org/10.1016/j.wear.2016.07.015>.
- [18] Tian Y, Yang R, Gu Z, Zhao H, Wu X, Dehaghani ST, et al. Ultrahigh cavitation erosion resistant metal-matrix composites with biomimetic hierarchical structure. *Compos PART B-Eng* 2022;234:109730. <https://doi.org/10.1016/j.compositesb.2022.109730>.
- [19] Szala M, Hejwowski T, Lenart I. CAVITATION EROSION RESISTANCE OF Ni-Co BASED COATINGS. *Adv Sci Technol-Res J* 2014;8:36–42. <https://doi.org/10.12913/22998624.1091876>.

Пашечко М., Голубець В., Зубжицький Я., Тісов О. Кавітаційно-ерозійна стійкість евтектичних покриттів в розчині хлориду натрію

У статті наведено оригінальні результати досліджень щодо стійкості запатентованих евтектичних покриттів, нанесених на конструкційну сталь С45 до кавітаційно-ерозійного зношування. Цей вид зносу зустрічається в пристроях, що працюють в хімічній, нафтохімічній, теплоенергетичній та інших галузях промисловості. Дослідження проводились на унікальному вимірювальному стенді, розробленому авторами. Дослідження проводили у високорозійному середовищі, тобто розчині хлориду натрію. В результаті проведених досліджень отримано криві зміни електродного потенціалу сталі С45 з різними умовами поверхні та її поляризаційні криві. Завдяки цим кривим вдалося визначити оптимальний спосіб захисту досліджуваної сталі від кавітаційно-ерозійного зношування.

Ключові слова: евтектичні покриття, конструкційна сталь, кавітаційно-ерозійне зношування, хлорид натрію, випробувальний стенд